UNIVERSITY OF CAPE TOWN
IYUNIVESITHI YASEKAPA • UNIVERSITEIT VAN KAAPSTAD

Medical Biotechnology & Immunotherapy Group
Institute for Infectious Disease & Molecular Medicine
South African Research Chair in Cancer Biotechnology
Department of Integrative Biomedical Sciences
Faculty of Health Sciences
University of Cape Town

Masters Thesis

Generation of Glioblastoma specific SNAP based antibody fusion proteins for future radiolabelling application

Grace Mayuni

September 2022

Supervisor:
Prof. Dr. Dr. Stefan Barth

Co-supervisor:
Dr. Dharanidharan Ramamurthy

Plagiarism Declaration

1. This thesis/dissertation has been submitted to the Turnitin module (or equivalent similarity and originality checking software) and I confirm that my supervisor has seen my report and any concerns revealed by such have been resolved with my supervisor.

2. I know that Plagiarism is wrong. Plagiarism is to use another's work and pretend that it is one's own.

3. I have used the Vancouver referencing style for citation and referencing. Each significant contribution to, and quotation in, this research project proposal obtained from the work or works, of other people has been attributed, cited and referenced.

4. This research project proposal is my own work.

5. I have not allowed and will not allow anyone to copy my work with the intention of passing it off as his or her own work.

Signed: Signed by candidate

Date: 8th September 2022

Acknowledgments

First and foremost, I would like to thank God for granting me the ability and grace to see this work through to completion.

I am extremely grateful to Prof. Dr. Dr. Stefan Barth for his support as my supervisor and mentor during the completion of my master's research. Thank you for having faith in me since my first day as an honours student at the MB&I unit. You have taught me a great deal about the cutting-edge approaches for employing biotechnology to cure cancer. I have learned substantially from your extensive knowledge and experience.

I am also grateful to Dr. Ramamurthy, my co-supervisor. I appreciate your help and willingness to support me at all times. I value all the information and wisdom you provided me to apply during my research.

I would like to thank the MB&I team for being exceptional lab mates. I want to thank Maryam Karaan and Dr. Alex Akrinimade in particular for their invaluable help with my experimental work. Also, I would just like to express my gratitude to Salizwa Malindi and Liyabona Mpondo for being my friends and encouraging me throughout this journey.

I could not have undertaken this journey without my family and friends. Their unwavering love and support kept me going. Dad and Mom, I can never compensate you for all the sacrifices you made throughout the years; without you, I would not be here.

I would like to extend my sincere thanks to Dirk Lang, Viantha Naidoo, and Carla van Nierkiek for their assistance with my imaging work at the UCT Confocal Microscopy unit.

Thanks should also go to the Sturrock Lab for its aid with resources and lab equipment.

Finally, I would like to thank the National Research Fund(NRF) and UCT for helping to make my pursuit of postgraduate education possible through their financial support.

Table of Contents

Index of Figures and Tables

Figures

Tables

List of Abbreviations

ADC	Antibody-Drug Conjugate
AGT	O^6-Alkylguanine-DNA Alkyltransferase
AKT	Protein kinase B
AMP	Ampicillin
AMP^R	Ampicillin resistance
AURIF	Monomethyl auristatin F
BBB	Blood Brain Barrier
BG	Benzyl guanine
BG-Alexa 488	BG-modified SNAP-Surface® Alexa Fluor® 488
BG-Alexa 647	BG-modified SNAP-Surface® Alexa Fluor® 647
BSA	Bovine Serum Albumin
CAF	Cancer Associated Fibroblast
CAR	Chimeric Antigen Receptor
CDR	Complementary determining region
CNS	Central Nervous System
DAR	Drug to Antibody Ratio
dH_2O	deionized H_2O
DMEM	Dulbecco's Modified Eagle's Medium
DMSO	Dimethyl Sulphoxide
DNA	deoxyribonucleic acid
ECM	Extracellular matrix
eGFP	Enhanced Green Fluorescent Protein
EGFR	Epidermal Growth Factor Receptor
EMT	Epithelial to mesenchymal transition

FAPα	Fibroblast Activation Protein Alpha
FBS	Fetal Bovine Serum
FDA	Food and Drug Administration (United States)
FR	Framework Regions
GBM	Gliobastoma Multiforme
GSC	GBM Stem Cell
HEK293T	Human Embryonic Kidney cells
IC_{50}	Inhibitory concentration resulting in 50% inhibition
IDH	Isocitrate dehydrogenase
IMAC	Immobilized Metal Affinity Chromatography
mAb	monoclonal antibody
MB&I	Medical Biotechnology and Immunotherapy Research Group
MGMT	O-6-Methylguanine-DNA Methyltransferase
MMAF	Monomethyl Auristatin F
mTOR	Mammalian target of rapamycin
ORF	open reading frame
PI3K	Phosphoinositide 3-Kinase
PS	Penicillin Streptomycin
PTEN	Phosphate and Tensin Homolog
PVDF	Polyvinylidene Fluoride
rcf	Relative centrifugal force
RE	Restriction Enzyme
RMT	Receptor mediated transcytosis
rpm	Revolutions per minute of rotor
RPMI	Roswell Park Memorial Institute

Commented [MK1]: Include AURIF as well

RT	room temperature
RTK	Receptor Tyrosine Kinase
scFv	Single chain variable fragment
SDS-PAGE	Sodium Dodecylsulphate Polyacrylamide Gel Electrophoresis
SOC	Super Optimal Broth with Catabolite repression
TAA	Tumour Associated Antigen
TAE	Tris-acetate EDTA buffer
TKI	Tyrosine Kinase Inhibitor
TME	Tumour microenvironment
UI	Uncertainty Interval
UV	Ultraviolet
w/v	Weight per volume
XTT	2,3-bis-(2-methoxy-4-nitro-5-sulfophenyl)-2H-tetrazolium-5-carboxanilide

Abstract

Each year, Central Nervous System (CNS) cancers affect about 300,000 individuals globally, accounting for 1-2% of all adult cancer cases. Despite being rare, CNS cancers reportedly have disproportionately high morbidity and mortality rates compared to their incidence.

Globally, Glioblastoma Multiforme (GBM) is the most aggressive CNS malignancy, accounting for 45% of brain tumours, with less than 5% of patients surviving for more than 5 years. To date, complete surgical resection followed by adjuvant chemotherapy and/or radiotherapy has been the standard of care treatment. This has been shown to not be curative, as it can only slightly improve prognosis and increase patient survival from 3–4 months to 14–16 months after diagnosis. However, it has been noted that early diagnosis increases the chance of patients going into complete remission following early treatment. Unfortunately, current methods of diagnosing GBM are very invasive and imprecise, necessitating more targeted, and more reliable diagnostic techniques.

The use of antibody-based targeted agents in GBM treatment is being advanced due to their ability to specifically differentiate tumour masses from healthy tissue. The success of antibody-based targeted approaches lies in the selection of biomarkers that are selectively found in tumour cell populations. One type of biomarker is known as tumour-associated antigens (TAAs), which are antigenic substances present at a much relatively lower incidence on normal cells but highly correlated with certain tumour cells. The focus of this study was on two TAAs that have been established as being overexpressed in GBM: (i) the transmembrane protein epidermal growth factor receptor (EGFR), which is associated with tumour cell proliferation, and (ii) Fibroblast Activation Protein alpha (FAPα), an active protease in the stromal tissue of the GBM tumour microenvironment.

SNAP-tag® fusion antibodies against the abovementioned TAAs were employed in this study. The fusion antibody is a recombinant antibody-based fusion protein created by fusing the SNAP-tag®, a modified version of the DNA repair enzyme O^6-alkylguanine DNA alkyltransferase (hAGT), to a single chain variable fragment (scFv) region of an antibody, thereby providing a tool that can detect and label TAAs. The SNAP-tag® element is engineered to irreversibly react with any benzylguanine (BG) substrates, including labelling dyes or toxins, with a controlled 1:1

stoichiometry. According to previous studies, SNAP-tag fusion proteins have exhibited strong cytotoxic profiles as an immunotherapeutic tool as well as good imaging profiles as an immunodiagnostic tool.

In this study, the recombinant SNAP fusion proteins, anti-FAPα (scFv)-SNAP and anti-EGFR (scFv)-SNAP were transiently expressed in mammalian cell culture. The recombinant protein was purified from harvested cell culture supernatant using immobilized metal ion affinity chromatography (IMAC). The enzymatic activity of the SNAP-tag element was tested using BG-modified fluorophores. To characterize highly specific *in vitro* labelling, the SNAP-tag-based fusion proteins were conjugated to BG-Alexa Fluor 647 to generate an immunofluorescent protein that can label TAAs in live tumour cells. To characterize the immunotherapeutic activity, the SNAP-tag fusion proteins were conjugated to the small molecule toxin, BG-Auristatin F, to generate an ADC that can kill TAA-expressing cells *in vitro*.

Anti-FAPα (scFv)-SNAP and anti-EGFR (scFv)-SNAP fusion proteins were successfully expressed in this study with sufficient yields for small-scale purification. Through a series of self-labelling experiments with the BG-modified fluorophores, BG-Alexa Fluor 488 and BG-Alexa Fluor 647, the enzymatic activity of the SNAP-tag element of each construct was confirmed. The optimal binding ratio of fusion protein: BG-substrate conjugate for downstream experiments was determined to be 1:1. Using live cell imaging, the biological functionality of the fusion protein construct through site-specific labelling on antigen-expressing cell lines was demonstrated. Finally, this study investigated the cytotoxicity of SNAP-fusion proteins conjugated to toxic payloads. Using a cell proliferation assay, the next-generation ADC, anti-EGFR (scFv) SNAP-AURIF, was tested and validated for its cell-killing activity. This ADC was able to elicit high rates of killing, exhibiting IC50 values in nanomolar ranges in three different antigen-positive tumour cell lines, with no cytotoxicity observed in the antigen-negative tumour cell lines. The targeted activity of this recombinant SNAP fusion protein format validates its biological function, making it suitable for further preclinical investigation.

This study aimed to characterize SNAP fusion proteins that can target GBM-specific TAAs. It successfully demonstrated the optimal conjugation efficiencies and validated the site-specific targeted activity of the scFv SNAP fusion antibody format. This work serves as a proof-of-concept

towards investigating the use of radio-labelled SNAP-tag-based antibody fusion proteins in GBM tumour detection and patient stratification to offer personalized therapeutics.

Chapter 1: Literature review

1.1. Background - Central Nervous System (CNS) cancers

1.1.1. Worldwide statistics of CNS cancers

Globally, over 300,000 people were diagnosed with either primary brain or spinal cord tumours in 2020 (1). CNS cancers are currently the 10th leading cause of cancer mortality in both men and women worldwide, with 251,329 deaths in 2020 (1). Tumours can be localised in any region of the CNS, but 85-90% are in the brain (2,3) and the others are found in the spinal cord, cranial nerves and meninges (2). There are no established causes for CNS cancers, but ionising radiation and lifestyle choices might increase the risk of tumour development (4). A 2016 study stated the CNS tumour incidence rate to be 4.63 per 100,000 persons, representing a 17.3% increase since 1990 (5). However, the global statistics do not accurately depict the true incidence and mortality. This is because the accurate diagnosis of CNS tumours requires all those affected to have access to appropriate medical imaging and surgery facilities and the availability of experts.

Signs and symptoms of CNS cancers depend on two factors- tumour location and growth rate (6). General signs of CNS tumours localized in the brain include headaches, seizures, nausea, drowsiness, confusion, cognitive impairment, and paralysis- which all indicate increased intracranial pressure (2,6). Symptoms are non-localising and focal (reflecting the impact of the tumour on specific brain structures) (2).

The diagnosis and treatment of CNS tumours require intricate diagnostic and therapeutic technologies. Due to associated high mortality rates, the impact of CNS tumours on hospitals and health care systems has been disproportionate concerning the incidence rate (2). As long-term management and diagnosis need highly specialized medical and surgical care, incidence rates are probably underreported. This is especially true in developing nations like those in Africa and other regions with significant rural populations. The unavailability of advanced imaging and radiologists, neurologists, oncologists, and neurosurgeons in many locations in Africa affects diagnostic accuracy, thus influencing the registry and death certificate data. The epidemiology of brain tumours is unknown in South Africa (SA) as it lacks a national registry for brain tumours. According to a 2016 study by Patel *et al.*, brain cancer incidence rates in SA are among the highest in the African continent. A total of 1177 (982 to 1317 95% UI) deaths were recorded in sub-

Commented [MK2]: This should maybe be in your abbreviation list if it's not already

Saharan Africa, with 822 (687 to 915 95% UI) of those SA cases. The study also reported 967 incidences (804 to 1049 95% UI) out of 1292 (1083 to 1388 95% UI) sub-Saharan Africa cases, representing a 26% increase from 1990 (2). Given the projected substantial increase in cancer rates in South Africa (Figure 1), the rise in brain cancer incidences cannot be overlooked and must be addressed (7).

Commented [MK3]: Figure 1 is difficult too actually see unless you zoom in really closely. Is there a way to make this bigger or have a different figure? Alternatively you could redraw the figures on Excel

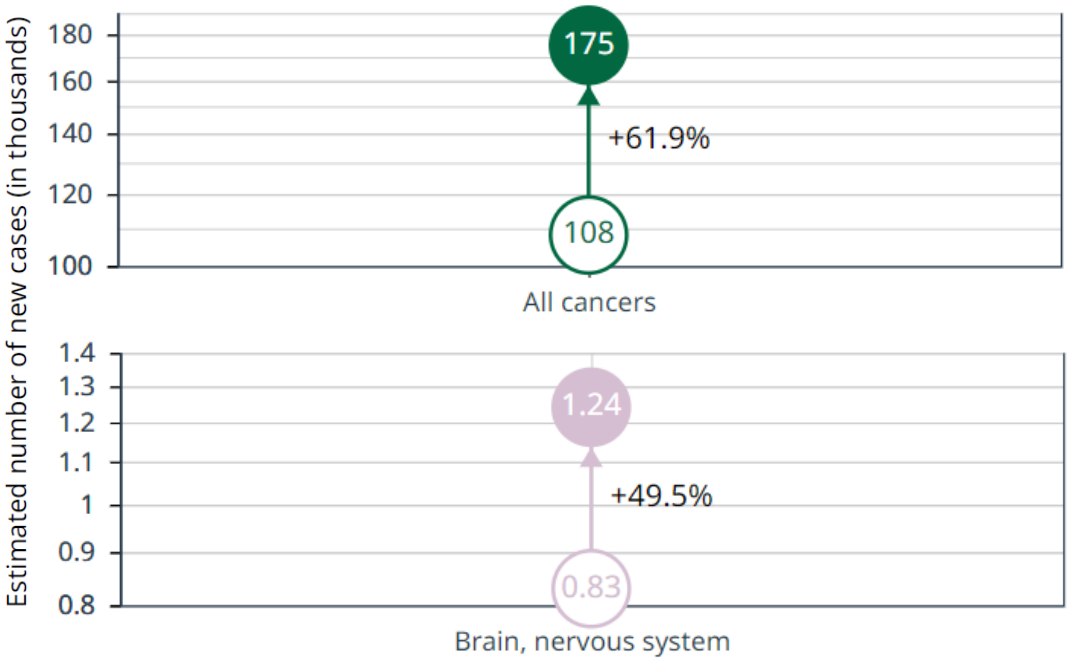

Figure 1. Predicted rise in cancer incidences in South Africa from 2020(○) to 2040(●). (A) Total number of cancer cases are predicted to rise from 108 000 to 175 000, indicating a 61.9% increase (B) Total number of CNS cancer cases are predicted to rise from 830 to 1240, indicating a 49.5% increase. Source: World Health Organisation; Global Cancer Obervatory; https://gco.iarc.fr/tomorrow

1.1.2. Biology of CNS cancers and Glioblastoma Multiforme

CNS cancers develop at any age but are most common in adults aged 55-65 (8). Incidentally, brain cancers are the leading cause of cancer-related deaths in individuals younger than 35 years (9). Gliomas, which are CNS tumours originating from glia cells, are categorized by the World Health Organization (WHO) into four classes (I, II, III, and IV) based on increasing degree of malignancy. (3). Of the subgroups, Glioblastoma Multiforme (GBM) (WHO IV) is the most common primary CNS tumour that develops in the brain or spinal cord, formed from astrocytes (star-shaped cells that support nerve cells) (10). About 75% of adult cases of brain tumours are glioblastomas (11). GBM has been defined as being highly malignant, characterized by fast progression, angiogenesis, high genomic instability, therapeutic resistance, and high relapse frequency (12). GBM is deadly, with the median survival time being less than 1 year from the time of diagnosis (10,13).

Understanding the molecular mechanisms that cause GBM development (also known as glioma genesis) is crucial for combating the disease. It has been demonstrated that malignant transformation in GBM is brought on by chromosomal abnormalities, nucleotide substitutions, and epigenetic changes (14). In 2008, The Cancer Genome Atlas (TCGA) studied 206 Glioblastoma cases and conducted an integrative analysis of DNA copy numbers, gene expression and DNA methylation aberrations and nucleotide sequence aberrations in 91 GBMs (14). Twenty years of research have identified three core signalling events altered in human Glioblastoma development, which include: dysregulation of growth factor signalling via the amplification and mutational activation of receptor tyrosine kinase (RTK) genes, activation of the phosphatidylinositol 3-kinase (PI3K) pathway and inactivation of the p53 and retinoblastoma tumour suppressor pathways (12). However, Genome-Wide Associated Studies (GWAS) profiling studies have shown remarkable genomic heterogeneity among Glioblastoma patients. A few studies have discovered the existence of molecular subclasses within Glioblastoma, that when fully defined, may allow for the precise stratification of patients (15,16).

The tumour microenvironment (TME) of GBM is characterized by a heterogeneous population of malignant cells as well as a diverse, non-transformed cell population which includes microglia, macrophages, endothelial cells, and astrocytes (10,17). Several studies have identified GBM stem cells (GSCs), a subpopulation of tumorigenic stem-like cells that might be responsible for the development and aggressive nature of glioblastoma (18). Like stem cells, GSCs are self-renewing,

pluripotent, and highly proliferative. Unlike normal stem cells, GSCs express a plethora of proteins that promote cell survival, allowing GSCs to evade quiescence after DNA damage – allowing them to initiate, sustain/maintain and spread neoplasms (18).

However, due to the observed intertumoral and intratumoral heterogeneity, some researchers argue against a single cell origin of GBM and theorise that glioma genesis is a result of the transformation of multiple cell types (19).

1.2. Summary of current GBM diagnosis and treatment landscape

1.2.1. Diagnosis methods of GBM

Currently, imaging techniques like magnetic resonance imaging (MRI), computed tomography, and positron emission tomography (PET), are used to localize tumour masses and for image-guided biopsy. MRI is currently the standard technique used for the diagnosis and monitoring of gliomas. MRI provides valuable information that aids clinicians in pre-treatment characterization and determining therapy responsiveness (20). Limitations with conventional MRI include: (i) inaccurate differentiation of primary tumours from metastatic masses and brain lymphomas and (ii) inaccurate measure of disease progression (21).

Another established form of GBM diagnosis is a histopathological examination of a brain tissue biopsy. The histological assessment looks for increased cell density, regions of necrosis, abnormal cell types and angiogenesis (19).

Although these techniques have allowed for general glioma classification, molecular profiling provides the advantage of determining the unique biomarker expression profiles for each patient – allowing for tailor-made therapy options that target pivotal oncogenic processes (20). Since 2016, the WHO classification of CNS cancers has changed from formerly focusing on histological analysis to genetic and molecular analysis (22). TCGA genetically classified glioblastoma has been able to establish aberrantly expressed genes for each subtype. Some of the aberrant signalling and genetic alterations that have been identified as key players in gliomagenesis include: (i) IDH mutations, (ii) MGMT methylation, (iii) 1p/19q deletions, (iii) PI3K dysregulation, (iv) p53 pathway dysregulation, and (iv) amplification in EGFR (23). Even though these classifications cannot indicate intra-tumoral heterogeneity or clonal tumour evolution during disease prognosis -

they remain a useful means of stratifying patients (24). Improving the precision of tumour diagnosis would allow for early-stage GBM diagnosis, resulting in early treatment, which would prevent disease progression and thereby enhance patient survival rates. It is also providing a basis for developing personalized therapies (19).

Through molecular profiling, it has also been observed that copy number alterations (CNAs) vary at various stages of glioma genesis (25). Investigating changes in the genomic profile during the course of glioma genesis could lead to the identification of disease biomarkers at various stages of tumour growth, resulting in improved disease diagnosis (according to stages) (20). Additionally, this might make it possible to apply the most effective therapies for each stage.

Commented [MK4]: Is this one or two words. Previously referred to as two words. Just make sure

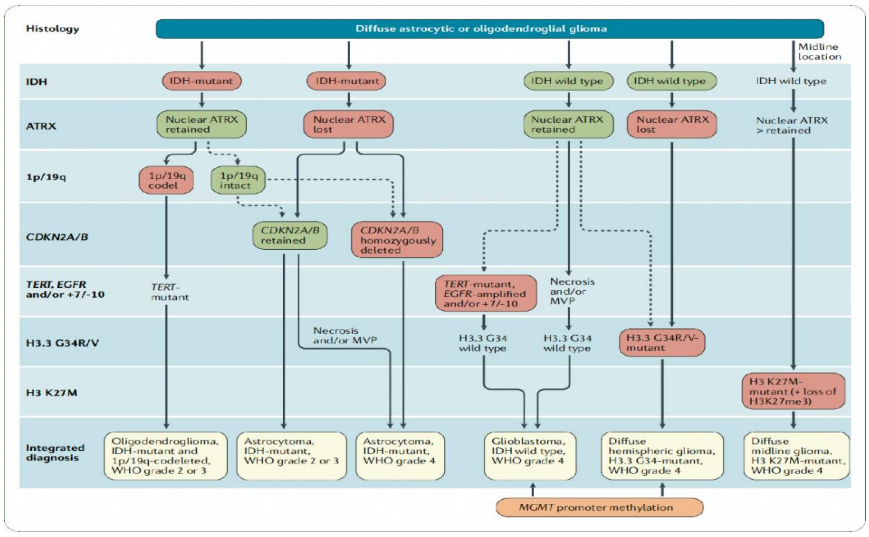

Figure 2. **Key pathological markers in molecular classification of Gliomas** (Source: www.atlasantibodies.com)

1.2.2. Standard therapy of GBM and prevailing challenges

CNS cancers have been described as complex, which makes devising effective treatments a challenge. To effectively treat CNS cancer, experts suggest a multimodal approach as the ideal option for the best clinical outcome.

Currently, the standard of care treatment for GBM is maximum surgical resection, followed by adjuvant chemotherapy and/or radiotherapy (26). This only provides a short-term prognostic advantage of extending survival time by a few months, with >90% of treated patients dying 5 years post-diagnosis (27). The reasons for the poor treatment responses will be discussed further below.

In the 1960s, radiotherapy was increasingly employed to treat brain tumours. (9). The principle of this form of therapy is to non-specifically target cells undergoing rapid division. It proved to increase survival for malignant glioma patients by doubling the average survival period post diagnosis from 6 months to 12 months (28). However, the use of whole brain radiotherapy has been limited by the sensitivity or tolerance of the CNS elements to radiation. This led to research and development into administration that targets specific brain regions in a fractionated manner which allows for high dose administration in a specific region, consequently minimizing toxicity to healthy brain tissue (9).

Research into the use of chemotherapeutic agents became popular in the 1990s (29). Temozolomide (TMZ), an alkylating agent, has been the most popular drug in chemotherapy research for gliomas to date (30,31). The first ever TMZ clinical trial was in 1993, where 5 out of 10 patients of adjuvant therapy were significantly responsive to the therapy (32). TMZ became FDA-approved for brain cancer treatment in 2005 (33). Oral administration of TMZ has displayed anti-tumour effects as a monotherapy in treating recurrent glioma (33). When used in combination with radiotherapy, TMZ showed statistical significance in improving patient survival with low levels of associated toxicity in primary glioblastoma (33). Two years of this combination treatment was able to increase the survival rate from 10% to 27% (33).

These discussed treatments are not curative and often lead to tumour progression and patient mortality. Minimal advancements have been made in GBM treatment in the past three decades, except for TMZ chemotherapy in combination with radiotherapy, which has achieved limited survival prolongation (34). The mean survival time remains 14-16 months (18). TMZ therapy also displays associated toxicity, limiting prolonged administration (35). This treatment is also limited by poor drug delivery, exhibiting insolubility in physiological conditions, and can cause off-target effects such as DNA damage (36).

Despite the increasing scientific understanding of GBM (behaviour, molecular features and heterogeneous genetic landscape) as well as research advances and clinical trials, the prognosis

remains poor (37). Different factors may have an impact on the lack of progress in the development of new GBM treatments. The three main hypothesized factors are complex tumour biology, drug delivery across the blood-brain barrier (BBB), and treatment resistance. (37).

First off, brain tumours rarely spread outside the central nervous system (CNS); instead, it has been established that they infiltrate deeply into brain tissue, disrupting blood vessels and brain circuits. This is one of the main contributing elements to the complicated biology of GBM tumours. (9). Complete surgical resection is, therefore, impossible and impairs the effective delivery of treatments to these cell populations without harming healthy brain tissue (38). Such that this has presented another clinical challenge of a high morbidity rate associated with surgery (39).

Next, the BBB, which is protective of the brain, prevents chemotherapeutic agents from accumulating at the tumour site, making adequate distribution of treatment in the region of interest impossible (27).

Finally, research has demonstrated that Glioblastoma often develops chemotherapeutic resistance, but the underlying molecular mechanisms are not known (17,40). It is postulated that GSCs might drive and maintain this therapeutic resistance (41).

1.2.3. Overcoming the challenge of BBB

The BBB is made of a single layer of endothelial, tanycytic and ependymal cells woven together by tight junctions (42). This barrier presents an interface between brain and body - and allows for nutrient transport, homeostasis, brain-body communication, and protection from foreign materials. The permeability of the BBB is a vital factor in developing molecular therapeutic agents. The BBB restricts small molecule transportation and actively clears foreign substances that interact with the protective layer (19). *In vivo* testing of therapeutic agents in CNS tumours extensively reveals that most exhibit low BBB penetration and cannot reach the concentration required for therapeutic effect at the target brain tissue (43). Several invasive methods have been used to bypass the BBB and deliver drugs to the brain, including the injection of a drug into CNS tissue, brain cerebrospinal fluid, or the spinal cord (44). Transient BBB disruption, such as intracarotid arterial infusion of hyperosmotic saccharide solutions, biochemical BBB opening by vasodilatory compounds, or MRI-guided ultrasound, can also be used to increase BBB permeability (44). To some extent, these

methods are effective in increasing access to the BBB, but they are unsuitable for widespread application due to their high cost, and associated discomfort. Invasive approaches also pose risks of toxicity or infection, as well as damage to healthy brain tissue. To overcome the difficulties associated with invasive methods of transient BBB disruption, non-invasive approaches to directly target the BBB and deliver drugs into the CNS have been created (45). Various macromolecules and nanocarriers have been shown to be efficiently transported using receptor-mediated transcytosis (RMT) which provides selective and active targeting via BBB endothelial cell-expressed transport receptors (46). Among the targeted receptors are the transferrin receptor (TfR), insulin receptor, insulin-like growth factor receptor, low-density lipoprotein receptor (LDLR), and low-density lipoprotein receptor-related proteins 1 (LRP1) and 2 (LRP2) (47).

Researchers are currently investigating RMT-based BBB targeting strategies using antibodies, recombinant fusion proteins, and peptides as vectors (45). Non-invasive vector-based delivery strategies hold promise for delivering novel therapeutic agents into the CNS *in vivo*.

1.2.4. Novel approaches in GBM therapy

Improving the quality of life of Glioblastoma patients depends on the discovery and development of novel efficacious therapies as well as having ideal systems for testing and developing these therapies. To overcome the challenges of standard GBM treatment, several alternative therapy strategies are being explored such as tyrosine kinase inhibitors (TKIs), immunotherapy, antibody-based therapy, and RNA therapies (48).

Tyrosine Kinase Inhibitors (TKIs)

Human Receptor Tyrosine Kinases (RTKs) are grouped in 20 subfamilies, but all share similar structural architecture - which includes: (i) an extracellular ligand-binding region, (ii) a transmembrane helix, (iii) a cytoplasmic protein tyrosine kinase domain - which contains a carboxyl terminal and regulatory regions (49). The activation of RTKs is induced by ligand binding, resulting in receptor dimerization or oligomerization, which activates the cytoplasmic kinase, triggering a series of phosphorylation reactions, and resulting in the activation of transcription factors (50). The consequence of this signalling is the activation of target gene

expression in response to ligand binding (50,51). RTK signalling pathways are complex and control several biochemical processes, which are tightly regulated (52).

It has been established that dysregulation and aberrant expression of protein kinases are implicated in cancer growth and metastasis (53). Receptor Tyrosine Kinase inhibitors (TKIs) are pharmacological agents that block transmembrane protein kinase modulated signal transduction pathways (54). TKIs are considered potent treatment options for GBM because they inhibit key cell signalling pathways implicated in gliomagenesis (55). To date, there are 62 FDA-approved TKIs such as Gefitinib, Lapatinib and Cobimetinib used for Non-small cell lung cancer (NSCLC), breast cancers and melanomas (54,56,57). While TKIs have successfully relieved the disease burden in other cancers, ongoing hurdles in GBM clinical trials include resistance, inter- and intra-tumoural heterogeneity, and off-target toxicity (58).

Immunotherapy

Immunotherapy is the manipulation or supplementation of the immune system in order to elicit a desired response in a disease state. Due to the reported clinical success, immunotherapy is currently a prominent focus in cancer research (59). Several immunotherapies that have been proven to increase patient survival are currently authorized for use in clinical settings. (60). Some forms of immunotherapies include vaccines, immune-regulatory antibodies, oncolytic viruses and adoptive cell therapy (59). A type of adoptive cell therapy known as chimeric antigen receptors (CAR) T cell therapy is a growing area of research in GBM (61). CARs are synthesised receptors, which combine an artificial antibody fragment (for target cell identification) and a T cell activation and co-stimulation domain (62). CAR T cell therapy has been demonstrated to be highly effective in treating B cell cancers, with two CD19-specific CAR T cells being FDA approved for B cell malignancies (63). However, several factors have limited the potency of CAR T cells against solid tumours like GBM. These include the immunosuppressive TME, poor CAR T cell penetration and trafficking through the BBB into the TME, and their reduction in persistence and activity over time (64).

RNA Therapies

RNA therapy involves the use of antisense oligonucleotides or small-interfering RNA (siRNAs) which are complementary to DNA regions that have pathology significance and result in inhibition of mRNA translation - a gene silencing technique (65). This therapy type has shown promising results in prostate cancer and NSCLC (66,67). One drawback of RNA therapy is the biochemical properties of these oligonucleotides – the molecules are hydrophilic and anionic. As a result, these molecules cannot pass the cell membrane by passive diffusion to penetrate the BBB (68). Thus, creating miRNA-based therapies for GBM is more complex as it requires a drug delivery system (68).

1.2.5. Targeted antibody-based therapy

One important thing to consider when developing targeted therapies is precision medicine. The principle of a precision medicine approach firstly identifies common biomarkers and then stratifies patients to receive personalized targeted therapy. It is important to identify which therapeutic agents are the best fit for a patient, based on their biomarker expression profile.

Molecular target therapy has the potential to improve the care of patients with malignant diseases. Targeted therapies have proven to be successful in several cancers such as melanoma, breast cancer, lung cancer, and leukaemia; therefore, this strategy is promising for treating glioblastomas (69). In the past two decades, research advances have been made with molecular target therapies in glioblastoma. In 2009, Bevacizumab, a monoclonal antibody (mAb) against vascular endothelial growth factor (VEGF), received FDA approval (70). Even though Bevacizumab increased progression-free survival (PFS), it does not benefit overall survival (OS) in newly diagnosed or recurrent glioblastoma (71). One other mAb-associated drawback comes with the form of administration (local vs systemic). This might be because the size of the mAb format (~150kDa) makes it a challenge for the large mAb to be transported across the BBB without the aid of a transport vector (68,72).

Antibody-Drug Conjugates (ADCs), which combine selective targeting of monoclonal antibodies (mAbs) with cytotoxic drug action, have become a prominent focus the cancer treatment (73,74). Because the drug is specifically directed at the desired antigen, ADCs have made the use of highly

toxic chemotherapeutic agents acceptable. (73-75). The inherent shortcomings of conventional ADCs, however, include poor antigen specificity and low specific cytotoxicity as a result of random drug to mAb conjugation. Additionally, heterogeneous ADC populations exhibit variation in pharmacokinetics, efficacy, and toxicity profiles (76).

Despite its associated challenges, targeted therapy presents a potential alternative to the standard of care GBM therapy as it has the ability to reduce unwanted toxicity and demonstrate higher efficacy. As of 2022, there are still no approved target therapies for glioblastoma (77). Even when primary tumours initially respond to first-line therapy, the probability of recurrence is high and tumour resistance is usually observed with second-line treatment (21). There is an urgent need for discovering targeted therapies that can overcome the limitations of current glioblastoma treatment modalities as a step forward in countering the high morbidity and mortality associated with this disease.

1.2.6. Recombinant SNAP-tag fusion proteins

The SNAP-tag is a 20kDa modified version of the human DNA repair enzyme- human O^6-alkylguanine-DNA-alkyltransferase (hAGT); it undergoes covalent self-labelling reactions with benzyl guanine (BG) modified substrates such as fluorophores and reporter compounds (78). SNAP-tag labelling is both irreversible and quantitative, this makes it perfect for the accurate detection and quantification of target protein (79). Moreover, SNAP-tag offers a high reaction rate and label specificity, high labelling efficiency, photostability and a versatile range of commercial substrates (80).

A unique antibody format has been generated by genetically fusing an antibody fragment to the SNAP-tag, which benefits from all of the characteristics of both components (Figure 3). This format, known as the SNAP fusion protein, has been shown to be functional in the *in vitro*, *in vivo* as well as *ex vivo* detection of TAAs (80,81). The fusion protein provides an adaptable tool that can serve a dual function, either as an immunodiagnostic or as an immunotherapeutic, owing to the SNAP-tag's diverse range of substrates (Table 1) (81). SNAP fusion proteins have now been studied as a potential next-generation class of ADCs. (74). The novelty is brought about by the use of genetic linkers which introduce enhanced stability when compared to the unstable chemical linkers in conventional ADCs (74).

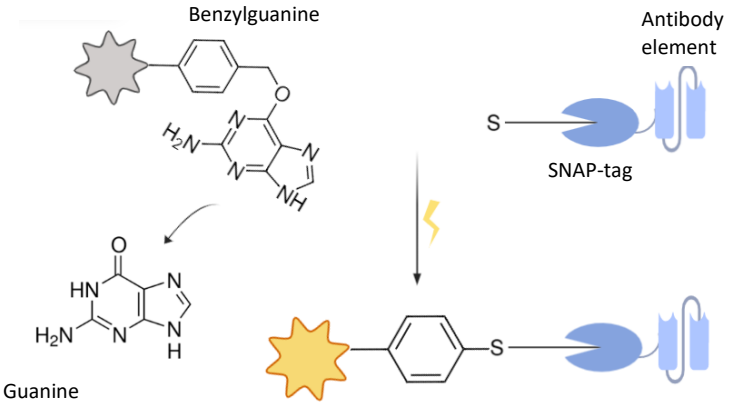

Figure 3. Site-specific enzymatic conjugation of the SNAP-tag. An illustration of the covalent reaction between the enzymatic element of the SNAP fusion protein with a BG-modified substrate (star). Image generated with https://biorender.com/

Single chain variable fragments (scFv) are antibody derivatives generated from full-length immunoglobulin G (IgG) (82). They are a recombinant version of IgG antigen-binding domain, which is composed of the variable regions of the light (VL) and heavy chains(VH) connected by a peptide linker (Figure 4). These features can be manipulated to optimize binding affinity and stability. Fragmenting the full-length mAb alters its physiochemistry. The smaller sized fragment(~25kDa) allows for enhanced penetration into tissues that mAbs(150 kDa) cannot access. Moreover, the relatively small size also makes the production process simpler and less expensive than full-length mAb production (82). Due to their highly efficient antigen targeting capacity, ScFv-based SNAP fusion proteins have been used in numerous targeted therapy studies.

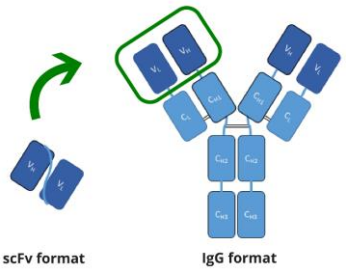

Figure 4. scFv antibody fragment architecture .Schematic overview of the scFv antibody format used to generate TAA targeting motif of the recombinant SNAP fusion protein. Left: scFv antibody fragment(~25kDa), right: full-length IgG antibody(150kDa). (Source: http://tropicalpharmacology.com)

In comparison to current ADC strategies, SNAP fusion proteins provide a variety of advantages. These include: (ii) improved site specificity for chemical conjugation, (ii) high stability , and (iii) controlled stoichiometry (74,79). Since the SNAP-tag's specificity allows drug toxicity to be directed toward the intended target, relative small doses are necessary to produce the desired therapeutic response. This aids in minimizing the unwanted side effects associated with the use of chemotherapeutic drugs (83). Furthermore, because the SNAP-tag is human-derived, it may possess little or no immunogenicity in human tissue—the key differentiating factor between it and other directed conjugation approaches (76). This is supported by the fact that no hAGT-related autoimmune diseases have been described to date.

Table 1. Studies illustrating the use of SNAP fusion protein for immunodiagnostic or immunotherapeutic purposes

Commented [MK5]: I really like this ☺

Construct	Label	Substrate(s)	Application	Biological Model	Advantages	References
425(scFv)SNAP	Fluorescent dye	BG-747	Optical imaging	Tumour cells (*in vitro*) Xenograft tumour (*ex vivo*)	• Rapid and specific accumulation at tumour site • Efficient renal clearance • High tumour to background ratio	(84)
425(scFv)-SNAP	Photosensitizer	BG-PEG24-Ce6	Phototoxicity	Tumour cells (*in vitro*)	• High efficacy and sensitivity • No off-side toxicity	(76)
SNAPf-ADRβ2	Fluorescent dye	BG-800	Optical imaging	Cell lysate Tumour cells (*in vitro*) Xenograft tumour	• High sensitivity •	(85)
425(scFv)-SNAP	Photosensitizer	BG-IR700	Phototoxicity Optical imaging(*in vitro* and *ex vivo*)	Tumour cells(*in vitro*) Human tumour tissue(*ex vivo*)	• High specificity and efficacy	(86,87)
SCF-SNAP	Fluorescent dye	BG-Alexa Fluor 647	Optical imaging	Peripheral blood sample(*in vitro*) Tumour tissue(*ex vivo*)	• High sensitivity	(80)
SNAP-EGFR	Fluorescent dye	BG-Dy549 BG-CF633	Live cell imaging	Tumour cells(*in vitro*)	• High photostability • Low non-specific staining	(88)

1.3. Tumour associated antigens in Glioblastoma therapy and diagnosis

Great progress has already been made in the understanding of the molecular pathways in glioma genesis as well mechanisms that maintain malignant phenotype - which has led to the research and development of novel targeted therapies. There is still a pending need for establishing biomarkers for glioblastoma that would ideally be useful in tumour subtyping and determining patient response to therapies. An ideal biomarker should be able to overcome the challenge of the complex nature of the disease as well being able to detect tumour masses in a minimally invasive way (20).

1.3.1. Targeting cellular pathways - EGFR

EGFR is a 170 kDa transmembrane glycoprotein belonging to the ErbB family of tyrosine kinase receptors - which include EGFR, HER2/ErbB2, HER3/ErbB3 and HER4/ErbB4. The extracellular membrane, transmembrane domain, and intracellular tyrosine kinase domain of each ErbB family member are flanked by regulatory regions. The ErbB family is known to be regulated by twelve different growth factors. Epidermal growth factor (EGF), transforming growth factor (TGF), and neuregulins are among them (89). EGF receptor (EGFR) dimerizes in response to growth factor binding, followed by receptor internalization. Internalization causes trans-auto phosphorylation of tyrosine residues on the C-terminal domain, which triggers signal transducers and activates intracellular substrates such as Rat Sarcoma (RAS) (Figure 5) (90). RAS activation triggers downstream signalling cascades such as (Mitogen-activated protein kinase) MAPK and (phosphatidylinositol 3' kinase) PI3K/AKT pathways. Translocation of effectors of these pathways to the nucleus results in transcriptional activation of regulatory genes of cellular growth. For example, AKT activation promotes the activation of the mTOR protein- which has two different complexes. Complex 1- mTORC1, upon activation, promotes cellular growth through biosynthesis of lipids, proteins, and organelles, as well as inhibition of catabolic reactions. Complex 2- mTORC2 is known to promote phosphorylation and activation of different molecules involved in cell survival, metabolism, and proliferation (91). EGFR signalling is tightly regulated in normal and controlled physiological conditions, and its dysregulation has been linked to cancers such as NSCLC, pancreatic, breast, head, neck, gastrointestinal, and brain cancers (92). EGFR is now an established oncogene which exhibits amplification, overexpression, and triggering mutations in the mentioned cancer types. Aberrant EGFR phosphorylation results in downstream signalling that

Commented [MK6]: Add a reference

activates cellular proliferation, angiogenesis, resistance to apoptosis and increased local tissue invasion (23). EGFR expression has also been shown to have a strong influence on clinical outcomes in cancer cases (23,92).

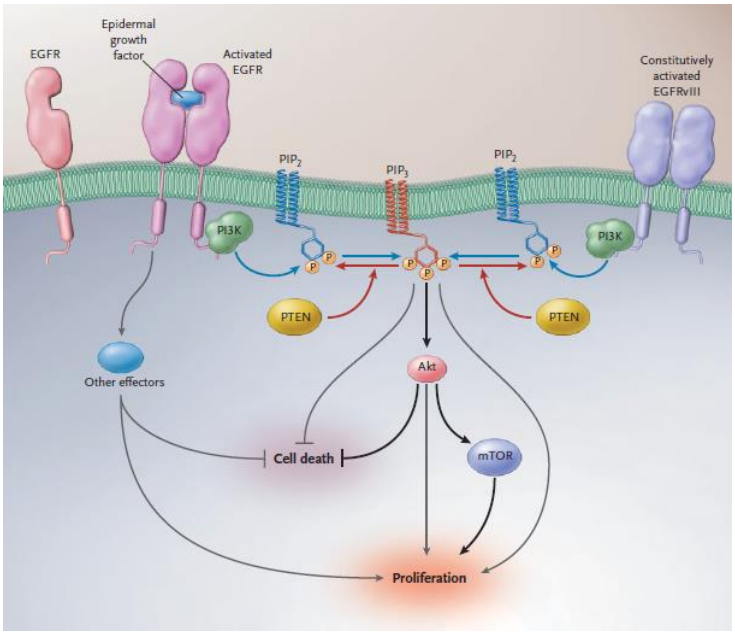

Figure 5. EGFR regulated PI3K–Akt Signalling. A schematic diagram exhibiting EGFR signalling PI3K-Akt pathway that promotes cancer progression. (Source: www.nejm.org, 2005)

EGFR in GBM

All ErbB members are associated with neural development in feotuses. EGFR has been shown to affect neural progenitor cell migration and proliferation. It was found that in an EGFR knock-out model - phenotype included neurodegeneration and defect in cortical astrocytes (92). In an EGFR knock-in model (mice modified to express EGFR), it was involved in signalling in cortical astrocytes, as it induces the anti-apoptotic AKT pathway (93). From these observations, EGFR might play a role in the differentiation/proliferation of astrocytes.

Commented [MK7]: In foetuses?

In healthy adult human tissues, including adult brain tissues, there is minimal to no EGFR protein expression. On the other hand, gliomas and other solid tumours have a high but variable expression of this gene (94). In GBM, EGFR modifications such as amplifications, deletions, and single nucleotide polymorphisms (SNPs) have been observed (95). Over 40 per cent amplification and up to 60 per cent overexpression of EGFR have been identified in GBM (96). A study by TCGA found a total of 41/91 EGFR alterations in human GBM biopsies (14). Verhaak *et al*. showed that in the classic subtype of GBM, EGFR amplification was found in 97% of cases (24). In 24% to 67% of GBMs, overexpression of EGFRvIII, a constitutively active truncated mutant of EGFR, has been observed (2). EGFRvIII constantly activates the PI3K signalling pathway (2). All these findings make EGFR a relevant TAA in GBM development. However, it is important to note that primary GBM is highly associated with EGFR amplification when compared to secondary GBM (97).

The frequency of EGFR aberrations observed in primary GBM has led to the research and development of many EGFR-target therapies, some of which are in clinical trials (98).

Examples of EGFR targeting agents being developed include small-molecule/tyrosine kinase inhibitors (TKIs) and antibody-based therapies, intending to disrupt EGFR signalling pathways. EGFR's response to various therapies has been studied at both the preclinical and clinical levels. TKIs have been shown to cause tumour cell death by disrupting the PI3K signalling pathway (99). Treatment with EGFR kinase inhibitors led to significant tumour shrinkage in malignant glioma (100). However, only 10–20% of patients with glioblastoma have shown to react to the FDA-approved EGFR kinase inhibitors, Erlotinib and Gefitinib (101,102). For patients with the EGFRvIII mutation, clinical trials with an anti-EGFR (vIII) targeting ADC, AMG595, have been ongoing (103). ABT-414 is an ADC shown to selectively bind cancer cells with EGFR(wt) amplification - was able to get internalized to release Monomethyl Auristatin F (MMAF). Results showed a 6-month progression-free survival (PFS) of 28.8% and 6-month overall survival (OS) of 72.5%. However, clinical trials with ABT414 had to be discontinued due to associated ocular toxicity that was more aggressive than the benefit of the treatment (104,105). Different pathogenetic hypotheses could explain ABT-414's corneal toxicity. It has been hypothesised that ABT-414 could release its cytotoxic effect into the cornea by binding the EGFR in the corneal basal epithelial layer, primarily affecting the corneal tissue and the sub-basal nerve plexus (106).

An alternative hypothesis states that ABT-414 could theoretically cause ocular toxicity through an off-target mechanism: it is assumed that the unconjugated cytotoxin is directly taken up by corneal tissue with a specific tropism for it (107).

1.3.2. Targeting cancer-associated fibroblasts – FAPα

It has been established that tumours consist of heterogeneous cell populations, including endothelial cells, inflammatory and immune cells, pericytes, smooth muscle cells and cancer-associated fibroblasts (CAFs) (108,109). CAFs are phenotypically distinct from normal fibroblasts and have been shown to shape the tumour microenvironment (TME) by promoting tumorigenesis, cancer evolution and therapeutic resistance (110). CAFs are believed to support tumour growth in numerous ways - produce tumour mitogenic factors, stimulate angiogenesis and promote the deposition of the extracellular matrix (ECM) (111). Given their influence on TME, selectively targeting CAFs is an ideal strategy for complementing anti-cancer therapy.

Fibroblast activation protein alpha (FAPα) is a 170 kDa glycosylated surface membrane serine protease that exhibits proteolytic activity against extracellular matrix proteins such as collagen (112). FAPα is overexpressed on the surface of cell membranes as well as the cytoplasm of CAFs (113,114). Its expression is rare in healthy tissues and benign epithelial tumours (115). However, high expression is seen in stromal cells such as fibroblasts, myofibroblasts, and areas of tissue remodelling such as sites of wound healing and chronic inflammation (116). FAPα has also been found to be highly expressed in more than 90% of human carcinomas (breast, colorectal and lung) (108,115,117). In a lung cancer model, it was demonstrated that knocking out FAPα resulted in decreased tumour burden, lower tumour proliferation and increased survival (117). A recent meta-analysis of 15 studies looking at FAPα expression in 11 solid tumours, concluded, by immunohistochemistry that FAPα positivity was found between 50-100% of patients and that overexpression was linked to more aggressive tumour invasion, increased metastasis, and lower survival- especially when FAPα was detected in malignant cells (118).

A study by Yang *et al.* showed that FAPα promotes the growth of stromal fibroblasts and induces their transformation to CAFs (119). Knock out of FAPα in oral cancer mouse model exhibited decreased activity of PI3K/AKT and Ras-ERK pathways- which resulted in decreased tumour cell proliferation, migration, and invasiveness (120). To date, the true role of FAPα in these various

biochemical processes has yet to be elucidated (116). However, it has been suggested that FAPα might play a role in extracellular matrix remodelling (121).

Despite the limitations in our understanding of the biology of FAPα, several factors make it an attractive biomarker. Firstly, as a surface membrane protein with no soluble cleavage products in circulation, targeting can easily be enriched at the tumour site. Secondly, $FAP\alpha^{+}$ stromal tissue can account for more than 90% of the gross tumour mass, making a targeted approach very likely to be efficacious. Thirdly, FAPα expression in CAFs has been shown to be more stable than in malignant cells. Lastly, what makes FAPα an attractive target is its broad applicability to several common cancer types which are difficult to treat due to poor prognosis (122,123).

FAPα - a potential GBM target

There is currently limited data on the presence of CAFs in brain tumours, but several studies have reported the presence of stromal non-malignant mesenchymal cells, which are suggested to be recruited or activated in response to tumour growth. It has been observed that these non-malignant stromal cells contribute to the upregulation of FAPα expression in high-grade gliomas (13,40).

Substantial FAPα expression has been seen in both malignant glial cells and stromal cells (13). A study by Busek *et al.* reported that over 70% of mesenchymal tumours had 2-fold upregulated expression of FAPα protein compared to non-tumorous tissue (40). It has also been observed that higher levels of FAPα expression in glioblastoma tissue are correlated with a poorer prognosis (10,124). Interestingly, FAPα expression is grade-dependent, representing a suitable marker to develop a diagnostic tool that can differentiate between glioblastoma subtypes (40).

The expression of FAPα in the Glioblastoma microenvironment together with restricted expression in healthy adult brain tissue makes it a target for the specific delivery of diagnostic and therapeutic agents. If highly specific FAPα-targeted therapies can be developed for Glioblastoma patients with high FAPα protein expression, this could aid in overcoming the challenge of therapeutic resistance.

1.4 SNAP fusion proteins as radio-immunoconjugates in GBM

The field of molecular imaging is advancing and has enhanced the degree to which mouse tumour models can be studied. Targeted imaging of tumours involves the use of imaging probes conjugated to antibodies or antibody-derived fragments for specific TAAs (125,126).

The design and development of targeted radioisotope labelled ligands have enabled the use of Single-photon emission computed tomography (SPECT) and PET technology to advance the non-invasive imaging of *in vivo* tumour biology (127). Researchers can also non-invasively measure tumour-related parameters to monitor the impact of radiolabelled cancer therapeutics at the cellular and molecular level (85,128)**.** PET imaging has been incorporated in addition to MRI, to aid in differentiating between radiation necrosis and tumour progression. The generation of FAP PET imaging agents has allowed for the monitoring of regions with increased stromal activity (121). Radio-labelled anti-FAPα mAbs and variant derivatives are also being developed for imaging FAP-positive tissue in tumours and inflammatory diseases. In a mouse model of rheumatoid arthritis, the build-up of anti-FAPα mAb signalling used for PET and SPECT imaging was associated with the severity of inflammation (129). In metastatic colorectal cancer patients, a FAPα targeting radioisotope – ^{131}I-labelled F19 antibody was able to selectively accumulate in liver metastases using SPECT imaging- suggesting a potential diagnostic, especially as it had a reported excellent half-life similar to that of murine antibodies (130).

The use of mAbs conjugated to radioisotopes or toxins presents a promising adjuvant therapy because they have been shown to enhance immune-mediated cell killing on top of disrupting aberrant signalling pathways. Several clinical trials have been carried out with the EGFR targeting ^{125}I-mAb 425 either as a monotherapy or in combination with standard-of-care-treatment. One Phase II trial employing a combination regimen with TMZ and ^{125}I-mAb 425 showed a higher survival benefit -a median survival of 20.4 months, compared to 14.5 months singular treatment of ^{125}I-mAb 425. These trials have shown that intravenous administration of the mAb results in significantly improved median patient survival (131). Radioimmunotherapy presents the advantage of being able to quantitatively image the distribution of the targeted treatment over time post-administration, thus allowing for a more precise analysis of the impact of the administered treatment (132).

The current focus of SNAP-tag based diagnostic research aims at utilizing the SNAP-tag in various imaging systems. The advantages of this antigen-specific labelling system include real-time visualisation of SNAP-tagged proteins, irreversible binding to tumour biopsies and the ability to detect proteins with high sensitivity (133-135). It is therefore potentially suitable for use as a radio-conjugate for *in vivo* detection of tumour masses.

Chapter 2: Study Aims and Objectives

2.1. Aim

Because of their low incidence rates, CNS tumours have a reputation for being rare; however, the incidence rates may be underestimated because not all healthcare systems have the resources or ability to diagnose these malignancies. This is particularly true in the African context. The location of most CNS tumours in the brain adds an additional layer of complexity, making them difficult to treat as well as detect. Therefore, it is now widely acknowledged that it is necessary to increase the precision of these cancers' diagnoses in order to provide improved treatment outcomes as well as gain more accurate epidemiological data.

GBM is the most aggressive CNS cancer, resulting in a median survival time of 14–16 months for patients receiving standard-of-care therapy. Considering that just 5% of patients survive up to 5 years after their clinical diagnosis, it is imperative to change the outcome of this deadly cancer. The significant morbidity and mortality rates linked to GBM are driving the need to investigate additional/novel methods of diagnosing and treating this cancer. Theranostics is one such novel approach - a proposed process which combines diagnosis and therapy in a single molecule. Recently, immune-radiolabelling has been identified as an ideal theranostic strategy in GBM, as it can simultaneously deliver radio-therapeutics and allow for the detection of tumour masses in cancer patients, with great precision. The key to high precision is the use of antibody-based agents that direct the distribution of the radioisotope load. This study will employ the use of a fusion protein format created by genetically linking a recombinant antibody-based protein to the self-labelling SNAP-tag®. Recombinant SNAP fusion proteins have become increasingly useful tools in labelling the TAA profile, which allows for the detection of tumour cell populations.

The overall aim of this research is to generate and characterize GBM-specific SNAP-tag-based (scFv) fusion proteins that target the TAAs EGFR and FAPα. The fusion proteins will be conjugated to BG-modified diagnostic and therapeutic labels, to determine their optimal conjugation efficiencies and demonstrate their site-specific targeted activity.

This work serves as a proof-of-concept study that demonstrates the suitability of SNAP fusion proteins as novel targeted agents that might be further investigated as radio-immunoconjugates that target GBM tumour masses.

2.2. Objectives:

The study aim will be achieved by investigating the following objectives:

A) Transient expression of anti-FAPα (scFv)-SNAP and anti-EGFR (scFv)-SNAP fusion proteins into the supernatant of Human Embryonic Kidney (HEK293T) mammalian cell culture.

B) Extraction, purification and confirmation of full-length protein expression by SDS-PAGE and Western blot analysis.

C) Conjugation of BG-modified fluorophores to the purified SNAP fusion proteins to validate the enzymatic function of the SNAP-tag element and to establish the optimal conjugation ratios of the fusion protein to BG-substrates.

D) Analyzing the cell binding and internalization profiles in FAP+ and EGFR+ cancer cell lines after conjugation to BG-modified fluorophores, thereby, demonstrating their applicability for immunodiagnosis and targeted delivery.

E) Label the generated SNAP fusion proteins with a BG-modified small molecule toxin (BG-AURIF) and optimize the labelling reaction conditions for enhanced conjugation.

F) To test the ability of BG-AURIF labelled SNAP fusion proteins to specifically kill antigen-positive tumour cell lines, thus validating their immunotherapeutic ability.

2.3. Implication of targeting two different receptors in GBM

As explained in the previous chapter, developing molecularly targeted agents for GBM is complex because tumour masses are believed to not arise from a single cell, given the diverse range of cell types in the TME. If glioma genesis follows a multifactorial course, targeting two distinct aspects of the TME might allow researchers to improve the accuracy of diagnosis as well as develop more effective strategies for treatment. In this study, the two TAAs of interest are (A) EGFR, a well-established oncogenic protein in glioblastoma cells and (B) FAPα, a protein universally overexpressed in stromal tissue surrounding malignant cell populations.

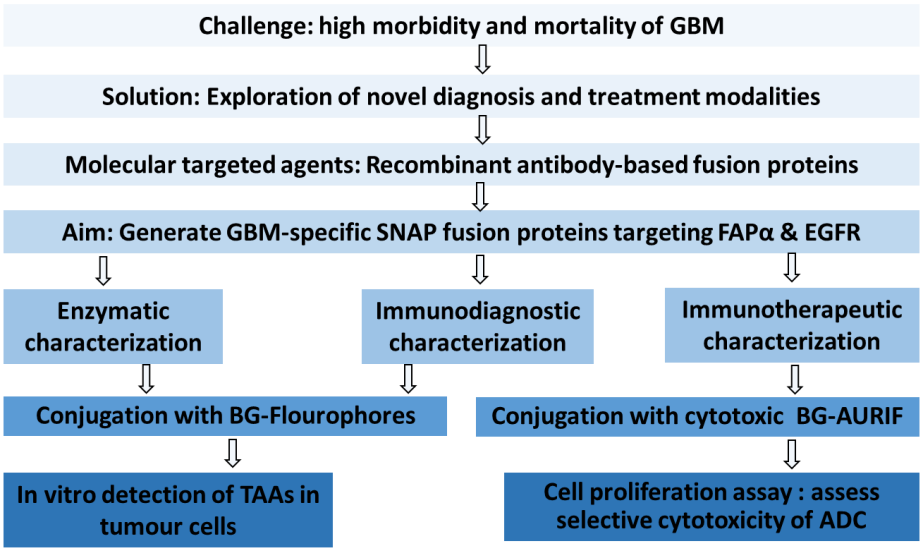

Figure 6. Research workflow. The overall goal of this work is to take a step forward in investigating the applicability of SNAP fusion proteins as TAA targeting tools in the context of GBM.

Chapter 3: Methods

3.1 Antibody format generation

The sequence generation of the anti-FAPα (scFv)-SNAP (originally termed scFv #34) and anti-EGFR (scFv)-SNAP (originally termed scFv #1711) was performed by Fleury Augustin Nsole Biteghe (PhD). The scFv sequences were obtained from 6,235,883 B1 and WO 01/68708A2 patents. To create the antibody format for each fusion protein, the variable heavy chain (V_H) was connected to the complementary variable light chain (V_L) using a specific linker sequence generated by the MB&I Unit.

3.1.1. In silico design of vector construct

SnapGene® software (GSL Biotech, Chicago) was used to design the open reading frame (ORF) encoding the recombinant fusion protein for expression in the pCB vector. The pCB backbone developed at the MB&I Unit is an optimized ThermoFischer Elements expression vector that has been optimized for the mammalian expression of the recombinant SNAP fusion protein. The modification performed on the ThermoFischer Elements expression vector included the removal of the C-terminal histidines, removal of myc tags near the C-terminal *Eco*RI and the introduction of N-terminal His tags and enterokinases. pUC57 commercial vectors containing scFv sequences flanked with *Sfi*I and *Not*I restriction sites were obtained from GenScript (New Jersey, USA). The pUC57 vectors allowed for the excision of the scFv portion and compatible insertion of this portion into the pCB backbone. This resultant construct is transiently expressed in mammalian HEK293T cells, induced by the binding of the SV40 T antigen to the SV40 promoter on the pCB plasmid, allowing for the translation of the recombinant fusion protein. The plasmid has also been engineered in such a way as to allow for the secretion of the recombinant fusion protein into the cell culture supernatant. The other vital elements of the plasmid have been summarized in Table 2.

Table 2. Elements of pCB mammalian vector (203)

Element	Description
(scFv)	Gene of interest encoding N-terminal single-chain variable fragment (82).
Amp(R)	Ampicillin resistance gene, allows selection for successful clone (136).
bGH poly(A) signal	(Bovine growth hormone) polyadenylation signal facilitates transcription termination (137).
$Bleo^R$	Confers Bleomycin resistance selection in mammalian cells (136).
CM7 promoter	Eukaryotic promoter that drives constitutive expression of antibiotic resistance genes and other genes in mammalian cell lines (137).
c-myc	Allows detection of the fusion protein with anti-*myc* antibody (137).
eGFP	A reporter gene used in the identification (through microscopic visualization) of successfully cloned genes (136).
EM7 promoter	Drives the constitutive expression of antibiotic resistance genes in *Escherichia coli* (*E. coli)* (137).
Enteropeptidase (ETK)	Encodes a specific cleavage site which is highly active and specific for cleaving fusion proteins with DDDDK recognition sequence in the inter-domain linker (137).
f1 ori	Bacteriophage derived origin of replication (137).
His_6-tag	Allows protein of interest to bind to the IMAC column during the protein purification procedure (136).
Immunoglobulin Kappa Locus (IgK)	16-20aa leader sequence peptide with an N-terminal secretion signal that instructs cells to release protein into the supernatant. (137).
IRES	Enables the coordinated co-expression of two genes within the same vector. Allows for the steady expression of CSPG4 (scFv) and eGFP using the same promoter (136).
SNAP-tag	Self-labelling protein tag (85).
SV40 poly(A) signal	Simian Virus 40 late polyadenylation allows for cleavage and polyadenylation reactions that produce steady-state mRNA (137).
SV40 promoter	Consists of the SV40 origin of replication and enhancer promoter which facilitates high-level expression and replication in large T antigen expressing cell lines (136).
T7 promoter	Initiates highly specific transcription of gene of interest by T7-phage RNA Polymerase (137).

3.2. Molecular cloning techniques

3.2.1 Transformation of competent bacterial cells competent

Commercially available NEB® 5-alpha *Escherichia coli* competent cells (Catalogue number: C2987I, New England Biolabs, USA), which are calcium competent, were thawed on ice (138). 50µL of competent cells were incubated with 1 µg/µL of plasmid DNA for 30 minutes on ice. The cells were then heat-shocked for 60 seconds at 45 °C. The heat shock disrupts the bacterial membrane, resulting in the formation of pores that allow DNA entry (138). The cells were then treated with 950µL of room temperature Super Optimal Broth with Catabolite Repression (SOC). Each tube was mixed thoroughly and incubated at 37^{o}C for 60 minutes. Each tube was then spun down to pellet the cells, 900µL of the supernatant was discarded and the cells were resuspended in the remaining 100µL and streaked on an ampicillin-supplemented LB agar plate. The streaked plates were incubated overnight at 37^{o}C. The next day, single colonies were selected from each plate and inoculated in 50mL of LB Broth, supplemented with Ampicillin (200ng/µL). The cultures were incubated overnight on a shaking incubator at 37^{o}C.

3.2.2. Bulk Preparation of Plasmid DNA (Phenol-chloroform extraction method)

Phenol-chloroform isolation is a technique for large-scale plasmid DNA extraction and purification (139). 50 mL of overnight transformed *E. coli* culture were extracted by centrifugation at 3901 rcf for 10 minutes (Beckmann Allegra X-22R) at 4°C. After discarding the supernatant, the residual pellet was aspirated into 1mL of Lysis Solution I, a suspension buffer made of glucose, EDTA, and Tris-HCl (Table A1). The glucose raises the osmotic pressure in the extracellular environment of cells, enhancing cellular lysis (140). EDTA assists in the prevention of genomic DNA degradation by chelating Mg^{2+}, an essential cofactor of DNases (141). Tris-HCL is a stabilizing buffer that maintains the optimal pH necessary for DNA isolation (142). Thereafter, 2mL of Solution II, an alkaline solution that ruptures bacterial cells (143), was added and the suspension was mixed by inversion. 1.5mL of Solution III was added and the suspension was mixed by inversion. Solution III is a neutralising buffer that restores normal pH, resulting in the precipitation of both protein and genomic DNA (143). The contents of each vector tube were divided into 800µL aliquots and centrifuged at 15000 rcf for 10 minutes. The supernatant was recovered in a new set of microfuge tubes. 10µL of RNA cleaving RNase A (10mg/mL) was added,

immediately mixed-in by inversion and followed by a 1hr at 37^{o}C. Following this, 700µL of cold isopropanol was added to each microfuge tube, mixed by inversion and incubated for 10 minutes (RT). The DNA was precipitated by centrifugation at 15000 rcf for 30 minutes. The supernatant was discarded, and the pellet was washed with 500µL cold 70 % ethanol, the ethanol was immediately decanted and the tube dab-dried. The pellet was resuspended in 100µL nuclease-free dH_2O, mixed by aspiration and thereafter the tubes were pooled into 1 microfuge tube. 50µL 3M Sodium Acetate (NaOAc) was added, followed by 700µL 3M phenol-chloroform (collected from the bottom phase). The mixture was vortexed until uniformly white in appearance. The DNA was precipitated by centrifugation at 15000 rcf for 10 minutes at room temperature. The top phase on the centrifuged sample was recovered into a new tube. Afterwards, 350µL chloroform isoamyl alcohol (24:1 v/v) was added to each tube followed by mixing by inversion. The DNA was precipitated by centrifugation at 15000 rcf for 10 minutes at room temperature. The top phase on the centrifuged sample was recovered into a new tube. The plasmid DNA solution was precipitated overnight in 1 mL 70 % ethanol at -20^{o}C. The DNA precipitate was pelleted by centrifugation at 13000 rpm for 20 minutes at room temperature. The supernatant was discarded, and the pellet was washed with cold 70 % ethanol, the ethanol was immediately poured off and the tube dab-dried. Thereafter, each tube was dried in the SpeedVac Vacuum (Thermo Fisher Scientific, DE USA). The pellet was resuspended in 30µL nuclease-free dH_2O at 50^{o}C and left to dissolve overnight. The DNA was quantified by spectrometry using the DeNovix® NanoDrop (Thermo Fischer Scientific, DE USA) and thereafter stored at 4^{o}C.

3.2.3. Mini preparation of Plasmid DNA

The Zyppy™ Miniprep Kit (Catalogue number: D4019, Zymo Research, USA) was used for the small-scale isolation of plasmid DNA from *E.coli cells*, according to the manufacturer's protocol. One change was made to the manufacturer's instructions: prewarmed dH_20 (50^{o}C) was used to elute the DNA instead of Zyppy™ Elution Buffer. The DNA was quantified by spectrometry and stored at 4^{o}C.

3.2.4. Restriction Digestion

This was performed in order to cleave the plasmid constructs to generate insert and backbone fragments with compatible DNA ends. A cocktail of reagents was set up consisting of enzyme, buffer, restriction enzymes, water, and 2ug of DNA. The scFv insert fragment was excised out of the commercial pUC57 vector, and the SNAP-tag containing backbone from the pCB-Annexin-SNAP construct, using *Not*I and *Sfi*I REs. The restriction digestion reaction was set up in 1.5ml microfuge tubes, Table A2 indicates the volume of each reagent added to the reaction mixture. Each reaction mixture was initially incubated with *Sfi*I for 3 hours, followed by overnight incubation with *Not*I at 37^{o}C.

3.2.5. Agarose gel electrophoresis (AGE)

Gel electrophoresis was used for the size-dependent separation of digested plasmid constructs. A 1.2 % (w/v) agarose gel recipe was used for all AGE experiments, prepared according to the manufacturer's protocol by dissolving 1.2g agarose powder in 100mL 1x TAE buffer solution. The mixture was boiled till the agarose was completely dissolved and slightly cooled, thereafter 10µL SYBR™ safe DNA gel stain(Thermo Fisher Scientific, SA) was added (1:10000 dilution) and the gel was poured into prepared casting apparatus and allowed to set. The solid gel was placed into a BioRad flat buffer tank and fully submerged in 1x TAE Buffer. DNA samples were stained with 6X Purple Gel Loading Dye (New England BioLabs®, USA) in a 1:10 ratio and 20µL of stained DNA samples were loaded onto the gel. 10µL each of the Generuler 100bp Plus and Quick-Load 1000bp DNA ladder (New England BioLabs®, USA) were added to aid in the determination of DNA band sizes. The buffer tank was connected via positive and negative terminals to the Bio-Rad PowerPac which was set at a voltage of 90V for the Mini Sub-Cell. The gel was run for ~60 minutes at 90V and thereafter visualised on the Dark Reader Trans illuminator (Clare Chemical Research, USA) at 509_{nm}.

3.2.6. Gel Extraction: Isolation of restriction digestion products

The QIAquick Gel Extraction Kit (Catalogue number: 28704, Qiagen, Germany) was used for the retrieval of the DNA from the agarose gel, according to the manufacturer's instructions. DNA

bands were visualized with a UV gel documentation system and band sizes matching the theoretical sizes of the insert and backbone were excised and purified.

3.2.7. T4 DNA Ligation

DNA ligation is the process of joining two linear DNA fragments through the formation of a covalent phosphodiester bond between the 3' hydroxyl group of one fragment and the 5' phosphate group of the other fragment, catalysed by the enzyme DNA ligase (144). In molecular cloning, ligation is performed to incorporate insert DNA into a vector backbone. Purified insert and backbone fragments were ligated with the T4 DNA ligase enzyme (New England Biolabs®, USA) to create the recombinant expression vector, anti-FAPα(scFv)-SNAP. The NEB calculator for ligation, https://nebiocalculator.neb.com/, was used to determine the quantity of insert and backbone DNA to be added for each ligation. The length of the insert DNA and the length and concentration of the backbone (vector) DNA were entered into the online calculator which then determined the concentration of insert DNA required for a range of vector: insert ratios. The ligation reactions were set up in 1.5ml microfuge tubes on ice (Table A4). A bacteria only control were also set up. The ligation reactions were incubated at 16^{o}C O/N, as this is optimal for sticky end ligation. Following this, each ligation reaction was heat-inactivated at 65^{o}C for 10 minutes. Each ligation mixture (containing recombinant clones) was chilled on ice and 5µl was transformed into 50µl DH5α competent cells as mentioned previously.

3.2.8. DNA sequencing

Plasmid DNA was isolated and purified as stated in section 3.2.3. In order to confirm the nucleotide sequence of the cloned anti-FAPα-SNAP construct, dilutions of purified plasmid samples were sent for Sanger DNA sequencing at Inqaba Biotec™ (South Africa). Primer information is listed in Table 3.

Table 3. Sequencing primer information

Primer Name	Primer Description	Sequence (5'-3')
T7	T7 universal forward	AATACGACTCACTATAG
SNAP-tag	SNAP-UNIVERSAL reverse	GAGGCCATCGAGGAGTTCCCTGTG
FAP-Int1	anti-FAPα internal forward	GACTGGAGTCCCATCAAGGTTCAG

3.2.9. Restriction mapping

The previously described restriction digestion protocol was followed for the restriction mapping of pCB-anti-FAPα (scFv)-SNAP vector using *Dra*III and *Hind*III REs.

3.3. Cell culture

Tissue culture was performed in a BS2 Biosafety Level two facility, in a strictly sterile BS2 cabinet. HEK293T cells were cultured in Roswell Park Memorial Institute (RPMI) 1640 medium supplemented with 10% foetal bovine serum (FBS) and 100µL/mL penicillin-streptomycin at 37ºC with 100% humidity and 5% CO_2. Primary human cell lines listed in Table 4 were all cultured in Dulbecco's modified Eagle's medium (DMEM) supplemented as stated above. Cells were passaged at 90% confluency (split 1:20) and the medium changed when required. The ZOE® Fluorescent Cell Imager (Bio-Rad Laboratories, USA) was used to visualize cells and check cell confluence. All reagents used were purchased from Gibco (Life Technologies, USA).

Table 4. Primary cell lines for *in vitro* studies

Cell line	ATCC	Type	Origin
A2058	CRL-11147	Melanoma	Human
A431	CRL-259	Melanoma	Human
HDF	PCS-201	Fibroblast	Human
HS578T	HTB-126	Breast Cancer	Human
MDA-MB-468	HTB-132	Breast Cancer	Human
U87	HTB-14	Glioma	Human

3.4. Transfection with recombinant plasmid DNA

Transfection is the artificial process of introducing DNA into cultured mammalian cells, using chemical or physical means. Chemical-aided transfection was performed with either anti-EGFR (scFv)-SNAP or anti-FAPα (scFv)-SNAP plasmid constructs into HEK293T cells. Transient transfection was performed using the X-tremeGENE HP DNA Transfection Reagent Kit (Sigma-Aldrich, USA) following the manufacturer's instructions with minor adjustments. Two days prior to transfection, 70-80% confluent cultured HEK293T cells were seeded in 35mm x 10mm round cell culture dishes and grown in supplemented RPMI-1640 medium. The X-tremeGENE transfection reagent was added to recombinant DNA in a 3:1 ratio (v/v). The mixture was evenly distributed in the seeded HEK293T culture. The transfected cell culture was incubated at 37^{o}C in 5% $C0_2$ at 100% humidity. Untransfected cells were grown in parallel as a negative control. Plasmid translation was monitored by the level of eGFP. From 2-days post-transfection, the ZOE® Fluorescent Cell Imager (Bio-Rad Laboratories, USA) was used for eGFP detection. Zeocin™ selection pressure was introduced by administering 10 % (v/v) Zeocin™ to positively select for eGFP expressing cells. The cell culture was expanded from the 35mm dish to the T-25 flask, T-75 flask and finally T-175 flask to scale-up protein production. After transfected cell cultures were 90% confluent with enriched eGFP expression, cell culture supernatant was harvested every 3-4 days, centrifuged at 4000 rpm to separate cell debris, and thereafter stored at 4^{o}C.

3.5. Purification and Characterization of SNAP fusion proteins

The ÄKTA Avant system (GE Healthcare, USA) was used for immobilized metal ion affinity chromatography (IMAC), to purify recombinant proteins containing a short poly-histidine affinity tag. IMAC purification relies on the strong interaction of the high-affinity transitional metal ion, Ni^{2+}, immobilized on a matrix with a negatively charged 6x histidine chain (145). This strong interaction keeps the recombinant protein bound to the matrix during washing steps, allowing for the release of unbound proteins. The purified protein is recovered during an elution step using column buffer with a high concentration of imidazole. The ÄKTA Avant system elutes fractions from the column which potentially contain the recombinant protein. In parallel to this, an elution profile is generated which records the absorbance profile (UV= 280nm) of the matrix. Pronounced

peaks in the absorbance profile are indicative of the presence of protein. All of the peak-containing fractions were visualized on a 10% SDS gel to detect the presence of protein in each fraction. Thereafter, protein-containing fractions were pooled and concentrated with a 10 kDa Amicon® Ultra-15 Centrifugal Filter Unit (Sigma-Aldrich, USA). A maximum of 15mL pooled fraction was spun in Amicon filter columns at a time at 4225 rcf for 30 minutes. The flow through was discarded and the spin repeated until all the pooled sample was concentrated until ~500µL was retained. For the final spin, buffer exchange was carried out by adding sterile phosphate buffered saline (PBS) (pH 7.4) into the filter and concentrated to a volume of ~500µL. The pH and salinity of PBS, when compared to that of the elution buffer, are more optimal for correct protein folding and this helps to prevent protein aggregation, thus maintaining protein integrity. The buffer exchange also removes traces of imidazole which interferes with the enzymatic ability of the SNAP-tag. The concentrated protein solution was quantified using spectrometry (Denovix™ Spectrophotometer, $A280_{nm}$). All protein samples were stored at -20^{o}C.

3.5.1. Sodium dodecyl sulphate polyacrylamide gel electrophoresis (SDS-PAGE)

SDS-PAGE was used as the first step for purified protein characterization. This technique employs the use of electrophoresis to separate protein based on the size under reducing conditions (146). The theoretical molecular weight of each SNAP fusion protein was calculated using the conversion calculator available at https://www.aatbio.com/tools/calculate-peptide-and-protein-molecular-weight-mw. Sample loading dye by mixing β-mercaptoethanol to 4x Laemmli sample buffer (Bio-Rad Laboratories, USA) in a 1:9 ratio, and 5µL of the sample buffer was added to 15µL of sample and thereafter incubated at 95^{o}C for 10 minutes. A 10% SDS gel was made and protein samples were loaded and ran at 100V for 20 minutes, followed by 150V for 70 minutes. Next, the gel was incubated with Acqua Stain (Bulldog Bio, USA), following the manufacturer's instructions, to allow for the visualization of protein bands. The Gel Doc XR+ (Gel Doc™ XR System) was used for image capture.

3.5.2. Western Blot (WB) analysis

Western blotting was used to validate purified SNAP fusion protein, by targeting the N-terminal poly-Histidine tag. The purified protein sample was run on a 10% SDS gel. Protein was transferred from the gel to a Polyvinylidene Fluoride (PVDF) membrane (1.3A, 25V, 10min) using the Bio-Rad Trans-Blot Turbo system. The PVDF membrane was blocked in SuperBlock (PBS) Blocking Buffer (Thermo Fisher Scientific, SA) for 1 hour. The membrane was then incubated overnight with 1:1000 primary αHis-rabbit antibody in fat-free milk (Qiagen, Germany) at room temperature, followed by three 5-minute washes with Tris-buffered saline –Tween (TBST). Thereafter, the membrane was incubated with 1:5000 secondary goat-αrabbit-horse radish peroxidase (HRP) antibody conjugate (Bio-Rad Laboratories, USA) in fat-free milk, for 1 hour at room temperature, followed by three 5-minute washes with TBST. For detection of the secondary antibody substrate, the membrane was incubated in 4mL of TMB Blotting Solution (Thermo Fisher Scientific, SA) for 1 minute, followed by a wash with Type I dH_2O to stop the reaction. The Gel Doc XR+ (Gel Doc™ XR System) was used for image capture.

3.5.3. Densitometry

Densitometry is a quantification technique which was used to determine the amount of SNAP fusion protein in the IMAC purified protein sample (147). A stock solution of 5mg/mL Bovine Serum Albumin (BSA) was diluted to generate standard concentrations of 8ug, 4ug, 2ug, 1ug and 0.5ug. The BSA samples and 2ug of purified protein were mixed in a 1:3 ratio with prepared 4X Laemmli sample loading dye and then boiled at 95^{o}C for 10 minutes. These samples were run on a 10% SDS gel as previously described. The gel image was captured using the Gel Doc XR+ (Gel Doc™ XR System). The gel image was further analysed with ImageJ software version 1.53e (https://imagej.net/) to quantify the band intensities of BSA standards and protein samples. Microsoft Excel software was used to plot a standard curve with BSA standards and allowed for the calculation of SNAP fusion protein concentration in each sample.

3.6. Labelling of SNAP-fusion proteins with BG derivatives

Conjugation reactions with benzyl guanine (BG) derivatives were carried out to confirm the functionality of the enzymatic SNAP-tag element of the SNAP fusion proteins. BG-modified fluorophores, SNAP-Surface® Alexa Fluor® 488 (BG-Alexa 488), SNAP-Surface® Alexa Fluor® 647 (BG-Alexa 647), were purchased from New England Biolabs (MA, USA). These are photo-stable fluorescent substrates used to label SNAP-tag fusion proteins in solution or live-cell surfaces and are suitable for standard fluorescein filter sets (148). Naphthalimide-based fluorogenic probes (Table A10), synthesized by Rudolf Dreyer (Stellenbosch University) were also used to label αEGFR (scFv)-SNAP. The micro molar concentrations of the fusion protein were calculated using an online conversion website https://www.bioline.com/media/calculator/0104.html which converts mg/mL to µM. Single and dual conjugation reactions were set up for each fusion protein. Each reaction was set up in a 1.5mL microfuge tube as specified in the Appendix and run under dark conditions. For the dual conjugation, an hour incubation was run with BG-Alexa 488 followed by a second 1-hour incubation with BG-Alexa 647. After incubation, conjugation reactions were run on a 10% SDS polyacrylamide gel (100V for 20 minutes, 150V for 70 minutes). The iBright FL1500 Imaging System (Invitrogen, USA) was used for visualization of the florescent signal.

3.7. Labelling of SNAP-fusion proteins with BG-AURIF

The labelling of SNAP fusion protein to BG-AURIF (provided by Professor Roger Hunter, UCT) was prepared in a 1:2 ratio, set up in 1.5mL microfuge tube with 1mM Dithiothreitol, 20µM BG-AURIF, 10µM αEGFR-SNAP, buffered in 1x PBS (pH7.4) to a final volume of 1000µL. The conjugation reaction was run at 37^{o}C for 2-3 hours followed by 4^{o}C overnight. To remove traces of dimethyl sulfoxide (DMSO) buffer exchange was carried out by centrifuging the conjugation reaction twice in a 10kDa Amicon® Ultra -15 Centrifugal Filter Unit (Sigma-Aldrich, USA) with 14mL phosphate-buffered saline (PBS) (pH 7.4) at 4255 rcf for 25 minutes. The concentration of conjugated protein was quantified using densitometry as previously described. The reaction mixture was filter sterilized (0.22µm) in preparation for tumour cell treatment.

3.8. Live cell imaging

Specific protein binding was visualised with confocal microscopy. $2x10^4$ tumour cells were seeded in live cell viewing dishes and incubated in medium for 48hrs (37°C with 5% CO_2). The SNAP fusion protein was conjugated in a 1:1 ratio with BG-Fluorophore at 37°C for 1 hour (Table A11). Following this, the conjugation reaction was centrifuged at 1500 rcf for 2 minutes using Zeba™ Spin desalting columns 7kDa MWCO (Thermo Fisher Scientific, SA) to remove the unconjugated fluorophore. The conjugation reaction was filter sterilized (0.22µm) and stored at -20°C overnight. Prior to labelling, the conjugation reaction was diluted 1-fold in serum-free culture medium. For the positive treatment, cells were incubated for 20 minutes at room temperature with the labelling medium, followed by two washes with serum-free culture medium. For the negative control, cells were incubated with 1x PBS at room temperature for 20 minutes. After treatment, the labelling medium was decanted, followed by two washes with serum-free culture medium. Hoechst stain (1ng/mL) was added and incubated for 10 minutes at room temperature, followed by washing three times with culture medium. After washing, cells were kept on ice and taken for live cell imaging on the Zeiss LSM880 Airyscan (Oberkochen, Germany) at the Confocal Microscopy Unit (UCT).

3.9. Cytotoxicity studies

The XTT assay is a colourimetric cell assay that quantifies cellular viability by the reduction of the XTT reagent to an orange water-soluble formazan dye that absorbs light at 450nm (149). This assay was used to assess the ability of the SNAP fusion protein to specifically deliver a cytotoxic payload to TAA-positive tumour cells. The cytotoxic payload used in this study is BG-AURIF. In order to determine the optimal incubation time for the conjugation of anti-EGFR (scFv)-SNAP and BG-AURIF, several small-scale conjugation reactions were set up and incubated at 2, 3 and 4 hours. Thereafter, each sample was incubated with BG-Alexa Flour 488 for 1 hour. The fluorescent intensity of unconjugated fusion protein was used to determine the most optimal incubation time.

For the assay, tumour cell lines (A431, A2058, U87, MDA-MB-468) were seeded into a 96-well plate, with 5 $x10^3$ cells in 100µL plated per well. Cells were cultured in supplemented culture

medium (10% FBS, 1% PS) at 37ºC, 5% CO_2. After 24 hours, cells were treated with a range of SNAP fusion protein-BG AURIF concentrations (1000nM-0,0128nM in a final volume of 200µL). After 68 hours of incubation under cytotoxic conditions, XTT and *N*-methyl dibenzopyrazine methyl sulfate (PMS) were mixed in a 50:1 ratio, then 51µL of the mixture was added per well and incubated for 4 hours. The conversion of the XTT reagent to the substrate was measured by spectrophotometry using the iMark™ Microplate Reader (Bio-Rad) and determined as the difference of $OD_{450nm} - OD_{655nm}$. The absorbance readings were analysed with GraphPad Prism version 5(GraphPad Software, La Jolla, USA) and normalized to Zeocin treated (100% killing) control and untreated (0% killing) control. The 50% inhibitory concentration [IC_{50}] of each BG-AURIF-labelled SNAP fusion protein was determined for each treatment group. All treatments were performed in triplicate.

Chapter 4: Results

4.1. In silico design of mammalian vector constructs

The *in silico* design of both pCB_EGFR (scFv)-SNAP and pCB_FAPα (scFv)-SNAP was previously performed by Fluery Biteghe (PhD) (150). SnapGene® software (version 3.1.1, GSL Biotech, Chicago) was used for the *in silico* design of the scFv-containing recombinant SNAP fusion protein vector (section 3.1.1). As a quality control procedure, designed scFv constructs were subject to IgBLAST (https://www.ncbi.nlm.nih.gov/igblast/) to confirm the integrity of the Complementary determining regions (CDRs) and Framework regions (FRs) in the scFvs (illustrated for anti-FAPα(scFv) in Figure 7A). The scFvs were subject to sequence homology analysis with their corresponding parental CDR sequences using the CLC genomic workbench Software (QIAGEN®). The designed scFvs were inserted into a pUC57 vector, flanked with *Not*I and *Sfi*I restriction enzyme cleavage sites to allow for the excision of the scFv portion and compatible insertion of this portion into the pCB backbone. The resultant vector constructs plasmid contains the ORF encoding the recombinant fusion proteins: anti-EGFR (scFv)-SNAP / anti-FAPα (scFv)-SNAP with a 6-histidine element (Figure 7).

A

```
      <--------------------------------FR1-IMGT--------------------------------><-------CDR1-IM
       Q  V  Q  L  Q  Q  S  G  A  E  V  K  K  P  G  S  S  V  K  V  S  C  K  A  S  G  G  T  F  S
1     CAGGTACAGCTGCAGCAGTCAGGGGCTGAGGTGAAGAAGCCTGGGTCCTCGGTGAAGGTCTCCTGCAAGGCTTCTGGAGGCACCTTCAGC  90
1     CAGGTGCAGCTGGTGCAGTCTGGGGCTGAGGTGAAGAAGCCTGGGTCCTCGGTGAAGGTCTCCTGCAAGGCTTCTGGAGGCACCTTCAGC  90
       Q  V  Q  L  V  Q  S  G  A  E  V  K  K  P  G  S  S  V  K  V  S  C  K  A  S  G  G  T  F  S
1     CAGGTCCAGCTGGTGCAGTCTGGGGCTGAGGTGAAGAAGCCTGGGTCCTCGGTGAAGGTCTCCTGCAAGGCTTCTGGAGGCACCTTCAGC  90
1     CAGGTGCAGCTGGTGCAGTCTGGGGCTGAGGTGAAGAAGCCTGGGTCCTCGGTGAAGGTCTCCTGCAAGGCTTCTGGAGGCACCTTCAGC  90

      GT------><--------------------FR2-IMGT--------------------><-------CDR2-IMGT------><-----
       T  H  T  I  N  W  V  R  Q  A  P  G  Q  G  L  E  W  M  G  G  I  A  P  M  F  G  T  A  N  Y
91    ACCCATACTATCAACTGGGTGCGACAGGCCCCTGGACAAGGGCTTGAGTGGATGGGAGGGATCGCCCCTATGTTTGGTACAGCAAACTAC  180
91    AGCTATGCTATCAGCTGGGTGCGACAGGCCCCTGGACAAGGGCTTGAGTGGATGGGAGGGATCATCCCTATCTTTGGTACAGCAAACTAC  180
       S  Y  A  I  S  W  V  R  Q  A  P  G  Q  G  L  E  W  M  G  G  I  I  P  I  F  G  T  A  N  Y
91    AGCTATGCTATCAGCTGGGTGCGACAGGCCCCTGGACAAGGGCTTGAGTGGATGGGAGGGATCATCCCTATCTTTGGTACAGCAAACTAC  180
91    AGCTATGCTATCAGCTGGGTGCGACAGGCCCCTGGACAAGGGCTTGAGTGGATGGGAGGGATCATCCCTATCTTTGGTACAGCAAACTAC  180

      ------------------------------------------------FR3-IMGT---------------------------------
       A  Q  K  F  Q  G  R  V  T  I  T  A  D  K  S  T  S  T  A  Y  M  E  M  S  S  L  R  S  D  D
181   GCACAGAAGTTCCAGGGCAGAGTCACAATTACCGCGGACAAATCCACGAGCACAGCCTACATGGAGATGAGCAGCCTGAGATCTGACGAC  270
181   GCACAGAAGTTCCAGGGCAGAGTCACGATTACCGCGGACAAATCCACGAGCACAGCCTACATGGAGCTGAGCAGCCTGAGATCTGAGGAC  270
       A  Q  K  F  Q  G  R  V  T  I  T  A  D  K  S  T  S  T  A  Y  M  E  L  S  S  L  R  S  E  D
181   GCACAGAAGTTCCAGGGCAGAGTCACGATTACCGCGGACAAATCCACGAGCACAGCCTACATGGAGCTGAGCAGCCTGAGATCTGAGGAC  270
181   GCACAGAAGTTCCAGGGCAGAGTCACGATTACCGCGGACGAATCCACGAGCACAGCCTACATGGAGCTGAGCAGCCTGAGATCTGAGGAC  270
```

B

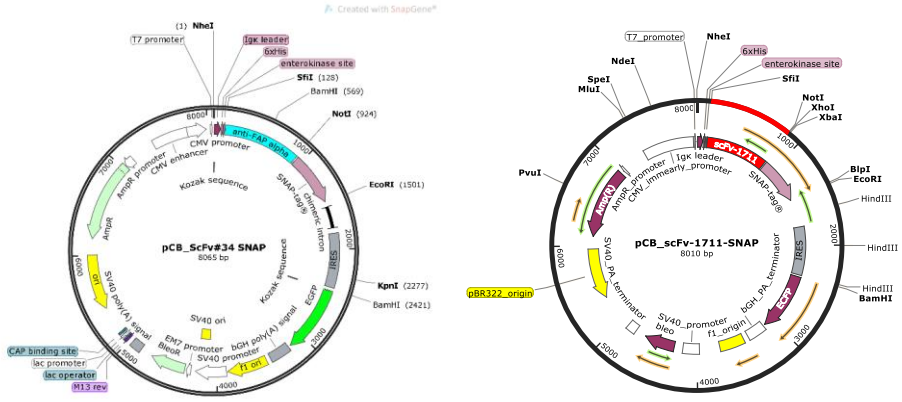

C

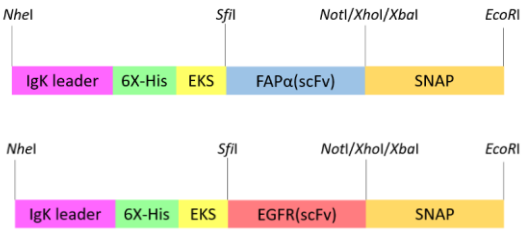

Figure 7. *In silico* design of mammalian vector constructs for FAP*α* and EGFR targeting recombinant SNAP fusion proteins (A) IgBLAST sequence analysis of FAPα(scFv) –DNA comparison of generated scFv sequence to database based immunoglobulin germline sequences. Pink amino acids represent scFv variation from IgG germline sequence. (B) Plasmid map of pCB-scFv#34-SNAP(FAPα targeting) and pCB-scFv-1711-SNAP(EGFR targeting). Image exported from snapGENE® software. (C) Open reading frame (ORF) of pCB-FAPα (scFv)-SNAP6HIS and pCB-EGFR (scFv)-SNAP6HIS, indicating *Sfi*I and *Not*I restriction sites necessary for cloning of scFv region into pCB vector.

4.2. Molecular cloning of FAPα (scFv) into pCB vector

4.2.1. Bulk preparation of pUC57$^{FAPα\ (scFv)}$

pUC57$^{FAPα\ (scFv)}$ was transformed into C2587 competent cells and prepared for bulk DNA isolation by phenol-chloroform extraction. A high concentration of purified pUC57$^{FAPα\ (scFv)}$ plasmid DNA was obtained (Table 5) for downstream cloning.

Table 5. Quantification of purified pUC57_FAPα(scFv) plasmid

pUC57$^{FAPα(scFv)}$	ng/µL	A230/A260	A260/A280
1X dilution	Absorbance too high	-	-
10X dilution	6256.27	2.47	2.13

4.2.2. Restriction digestion of FAPα (scFv) and SNAP containing constructs

A double digest was performed on the plasmid DNA of the pCB-Annexin-SNAP and pUC57$^{FAPα\ (scFv)}$ (Table 6) vector constructs using *NotI* and *SfiI* restriction endonucleases. Figure 8 shows the gel image taken after the completion of the agarose gel electrophoresis run of the RE digestion products. Double digests were run in duplicate to avoid loss of DNA. Both constructs were successfully cleaved and yielded the pCB backbone and observed between 6-8 kb size and FAPα (scFv) insert fragment between 600-800 bp size. The fragment-containing gel sections were excised, purified and quantified for downstream processing.

Table 6. Sizes of DNA fragments from restriction digestion reaction

Vector construct	Total (bp)	Backbone (bp)	Insert (bp)
pCB_AnnexinV-SNAP	8233	7272	961
pUC57$^{FAPα(scFv)}$	3506	2710	796

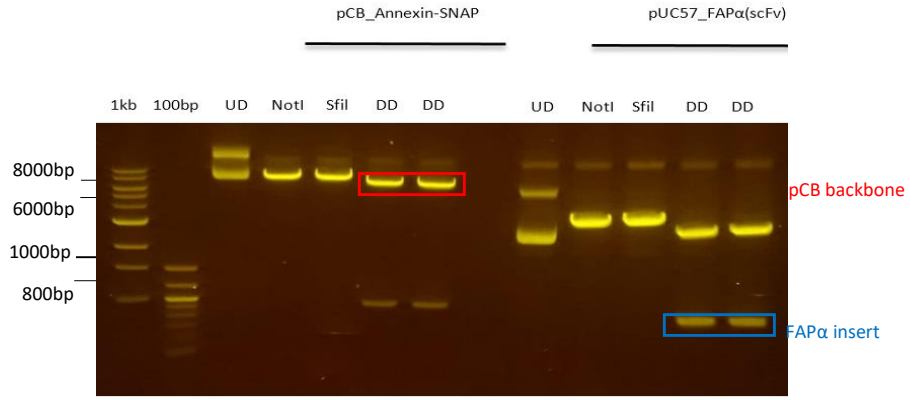

Figure 8. 1.2% Agarose gel of digestion products of pUC57_FAP-alpha (scFv) and pCB_Annexin-SNAP, UD= undigested control, DD = SfiI and NotI double digest

4.2.3. T4 DNA ligation of anti-FAPα (scFv) and pCB_SNAP

Agarose gel derived vector and insert fragments from section 4.2.2. were purified and ligated with T4DNA ligase enzyme. This resulted in the generation of the recombinant expression vector, anti-FAPα (scFv)-SNAP. Three different vector to insert ratios were used to increase the chances of obtaining a successful ligation outcome. Although the transformation of the ligation product into competent *E.coli* cells was successful, the transformation efficiency was low (Table 7). There was no colony growth on the bacterial control plate, which indicates ampicillin selection pressure confirming that observed colonies express the pCB vector. No growth on vector-only control plate indicates that there was auto-ligation of the backbone. Bacterial colonies were selected from the 1:3 and 1:5 ligation plates. These colonies were cultured in LB broth, in order to extract DNA for downstream processing and analysis.

Table 7. Transformation efficiency of T4 DNA Ligation products

Sample	# of colonies	Transformation efficiency(cfu/µg)
0:0(Bacteria)	0	-
1:0(vector control)	0	-
1:1	1	1.46×10^0
1:3	2	1.65×10^0
1:5	3	1.72×10^0

4.2.4. Restriction mapping analysis of pCB-FAPα (scFv) SNAP clones

In order to confirm the successful ligation, of the anti-FAPα (scFv) insert to the pCB vector, restriction mapping was performed on two purified DNA clones and the pCB-AnnexinV-SNAP vector. A theoretical gel was simulated using SnapGene software to identify restriction enzymes that would differentially cut pCB-AnnexinV-SNAP compared to the cloned pCB_FAPα (scFv)-SNAP (Figure 9A). Digestion with *Dra*II-*HF* and *Hind*III-*HF* resulted in the predicted fragmentation pattern (Figure 9B). Thus, we confirmed the production of the desired recombinant plasmid in colonies B and D.

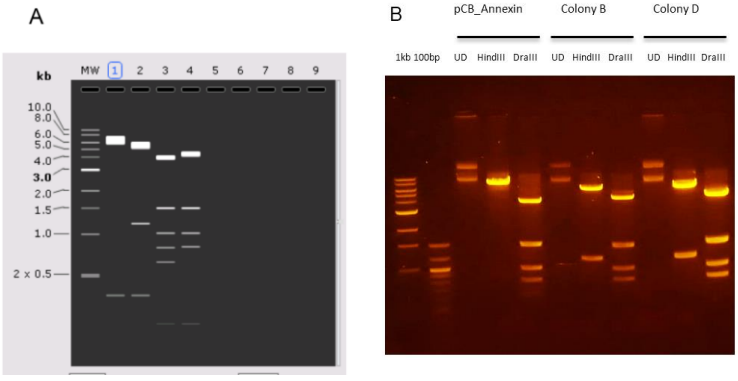

Figure 9. Restriction mapping of pCB_FAPα (scFv)-SNAP clones (A) Theoretical restriction mapping gel simulation with fragmentation patterns of DraII-HF and HindIII-HF on plasmid constructs, created in SnapGene™ software(B)1.2% Agarose gel of digested and undigested plasmid DNA of pCB_AnnexinV-SNAP and pCB_FAPα (scFv)-SNAP. Lane 1 =1 kb DNA ladder, lane 2 = 100bp DNA ladder, lanes 3, 6 &9 = undigested controls, lanes 47&10 =HindIII digest, lanes 5, 8 & 12=DraIII digest

4.2.5. Sequencing of isolated recombinant clones

Sanger sequenced DNA files of two selected plasmid clones (B and D) were aligned to the *in silico* sequence of pCB-FAPα (scFv)-SNAP. The sequence alignment analysis showed > 95% identity with minimal base alterations and gaps – with no signs of any frame shifts, insertions or deletions in the fusion protein ORF (Figure 10A&B).

A

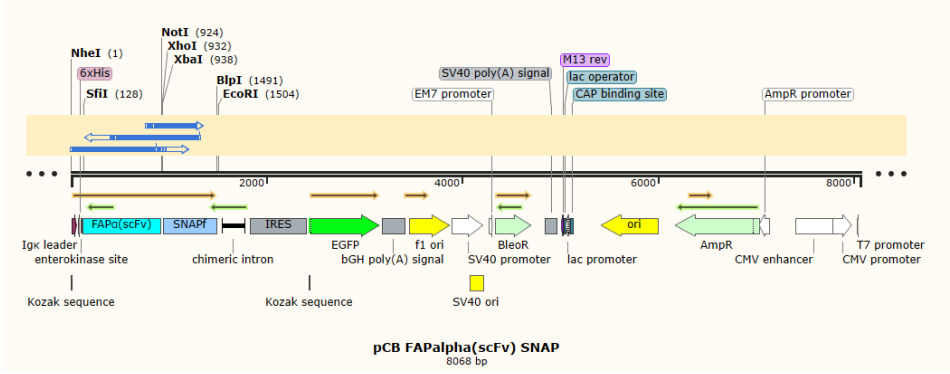

B

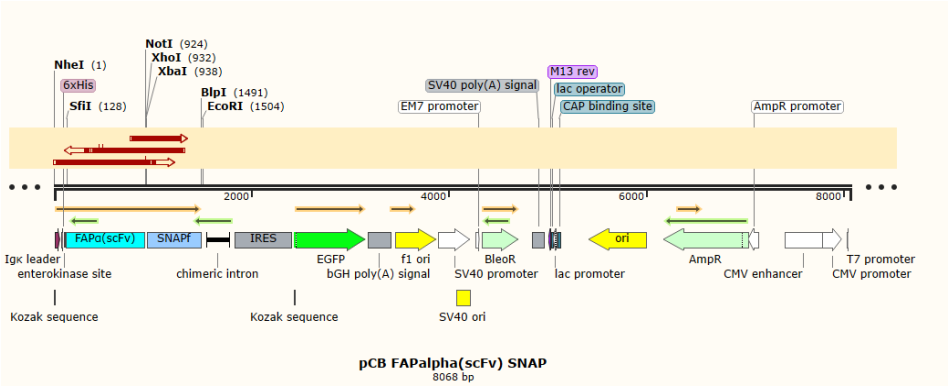

Figure 10. Linear Plasmid alignment with sequencing primers. Arrows represent T7 universal forward, SNAP-UNIVERSAL reverse and anti-FAPα internal forward primers which are complimentary to the anti-FAPα (scFv)-SNAP fusion protein ORF (A) Clone B (B) Clone D

To this point, the presented findings illustrated the principle behind the genetic engineering methodology used to generate recombinant SNAP fusion proteins. Further work with the plasmid created in this study was discontinued, and the transfection stage was omitted because the work with pCB_FAPα (scFv)-SNAP had been previously completed to the level of protein expression.

4.3. Mammalian culture and production of anti-FAPα (scFv)-SNAP

4.3.1. Expression of pCB_FAPα(scFv)-SNAP

Fluery Biteghe (PhD) donated the frozen positive HEK293T cultures (-80ºC, 10% DMSO) that were successfully transfected with pCB_FAPα(scFv)-SNAP. The cultures were thawed and seeded in flat bottom culture flasks. Figures 11 shows images taken with the ZOE™ Fluorescent Cell Imager under the bright field and green fluorescent channel. The strong intensity in the green channel indicates eGFP expression which can be interpreted as the transient expression of the plasmid and translation of the anti-FAPα (scFv)-SNAP fusion protein. Figure 11A was captured 7 days post-seeding, Figure 11B was captured 3 months post-seeding, and after Zeocin selection pressure was applied to enrich for anti-FAPα (scFv)-SNAP expressing cells. This, therefore, indicates that 12-15 weeks were required to establish this mammalian transient expression culture. Once cells reached a confluency of ~90% with high eGFP expression, cell culture supernatant (CCSN) was harvested every 2-3 days over 3 months. The harvested CCSN was collected in 50mL sterile conical tubes, and centrifuged at 4400 rpm for 8 minutes. The centrifuged supernatant was stored at 4^{o}C before further processing. A total of 1.5L of supernatant was harvested from the culture.

A - One week post seeding

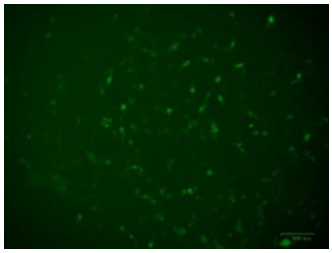

B - 3 months post seeding

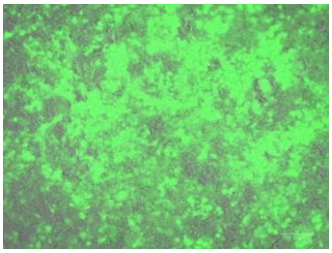

Figure 11. eGFP expression from anti-FAPα (scFv)-SNAP positive HEK293T cells. Expression viewed in bright field and green fluorescence channel. Merged image was generated with the ZOE™ Fluorescent Cell Imager**.** A) Thawed cells, 7 days post seeding in RPMI medium B) Cell confluency versus eGFP expression three months post seeding.

4.3.2. Purification of anti-FAPα (scFv)-SNAP

Harvested CCSN was purified by the IMAC method using the ÄKTA Avant system, as stated in section 3.5. The chromatogram in Figure 12A shows two absorbance peaks which indicates that the fractions covering these peaks contain prominent levels of protein compared to the other fractions. It has been observed that both peaks usually represent the protein of interest, with the second peak having a much lower concentration of total protein. The peak covering fractions were pooled and concentrated using a 10 kDa Amicon® filter column. The total amount of protein harvested was 3.985mg from 1.5L of CCSN. The total yield of anti-FAPα (scFv)-SNAP protein as a percentage of total protein was 33%(Figure 12C).

A

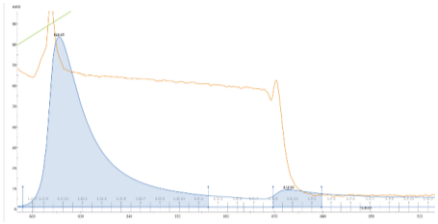

B

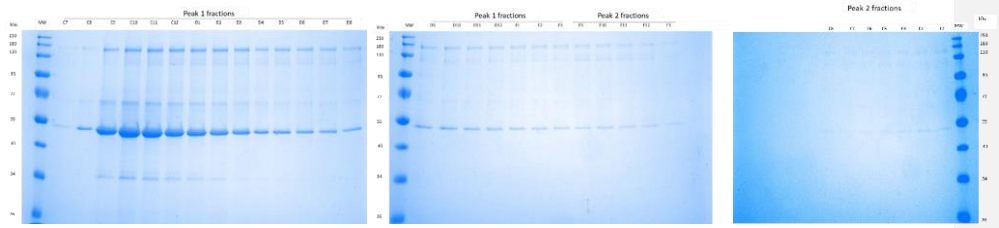

C

Sample	Area	Amount(ug)	Volume loaded(uL)	Densitometry (ug/uL)	DeNovix (mg/mL)	% fusion protein in total IMAC purified protein
anti-FAPα(scFv)-SNAP Peak 1	**8695.116**	**6.546780392**	**1.81**	**3.620696896**	**11.061**	**33%**
anti-FAPα(scFv)-SNAP Peak 2	**1845.184**	**-**	**10.2**	**-**	**0.981**	**-**

Figure 12. Protein purification of anti-FAPα (scFv)-SNAP(A) Absorbance profile (UV 280nm) of eluate from IMAC purified cell culture supernatant (CCSN) containing secreted anti-FAPα (scFv) SNAP (B) Purified IMAC eluate fractions on 10% SDS-PAGE gel(C) Summary of protein quantification

4.3.3. SDS PAGE and Immunoblotting of anti-FAPα (scFv)-SNAP

On a 10% SDS gel, we were able to visualize a characteristic banding pattern observed in previously concentrated samples of other SNAP fusion constructs which shows some level of BSA contamination and thicker bands between the 48-55 kDa regions (Figure 13A). The theoretical size of anti-FAPα (scFv)-SNAP, 52.39 kDa, was determined using the AAT Bioquest Peptide and Protein Molecular Weight Calculator, the bands observed between 48-55 kDa of the 10% SDS gel correspond to the theoretical size.

Purified protein run on a 10% SDS gel was transferred onto a PVDF membrane for Western blot analysis as described in section 3.5.2. The immunoblot (Figure 13B) confirmed the identity of the fusion protein by detecting the N-terminal 6-Histidine tag in both Peak 1 and Peak 2.

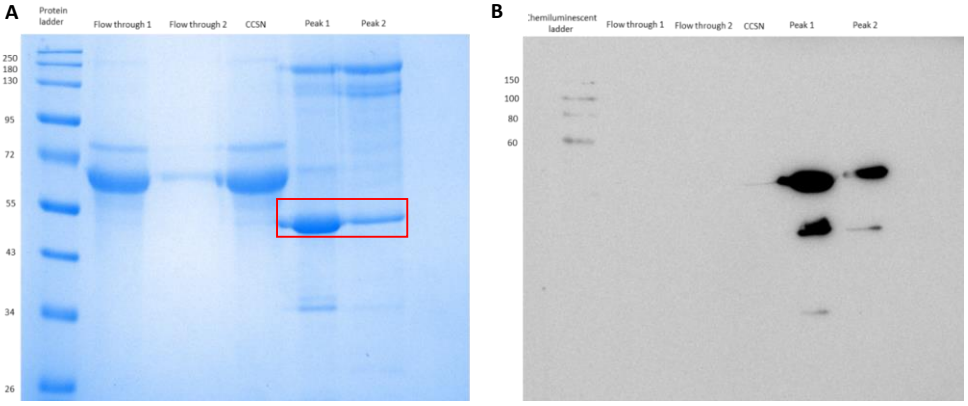

Figure 13. Characterization of anti-FAPα (scFv)-SNAP by SDS-PAGE and Immunoblotting (A) SDS-PAGE analysis of concentrated anti-FAPα (scFv)-SNAP peaks (B) Western Blot analysis of concentrated anti-FAPα (scFv)-SNAP. Primary αHis-rabbit antibody (1:1000) was used, followed by secondary goat-αrabbit-HRP antibody conjugate (1:5000).

4.3.4. Conjugation of anti-FAPα (scFv)-SNAP with BG-Alexa 488 & BG-Alexa 647

To confirm the functionality of anti-FAPα (scFv)-SNAP, we performed conjugation experiments with BG-modified fluorophores. The SNAP-tag element reacts with a 1:1 stoichiometry with BG-substrates and therefore BG-modified fluorophores are ideal markers that indicate the functionality of the SNAP-tag in the fusion protein. Anti-FAPα(scFv)-SNAP was conjugated to BG-Alexa Fluor 488 and BG-Alexa Fluor 647 in different ratios (Figure 14A&B). It was observed that there were

different intensities of fluorescence observed at each ratio. Higher intensities were not observed in the presence of an excess of fluorophores (ratios 4:1 and 2:1), however, for both fluorophores, a ratio of 1:1 gave off the highest fluorescence intensity - thus suggesting that this ratio is ideal for reactions with BG-modified substrates. Notably, there were excess unconjugated fluorophores present at all ratios. We performed a dual conjugation reaction with both fluorophores and observed that the fusion protein was saturated only in the presence of excess fluorophores. At the 1:1 and 1:2 ratio, there was still some unconjugated protein which was able to show binding in the second labelling reaction (Figure 14C).

A

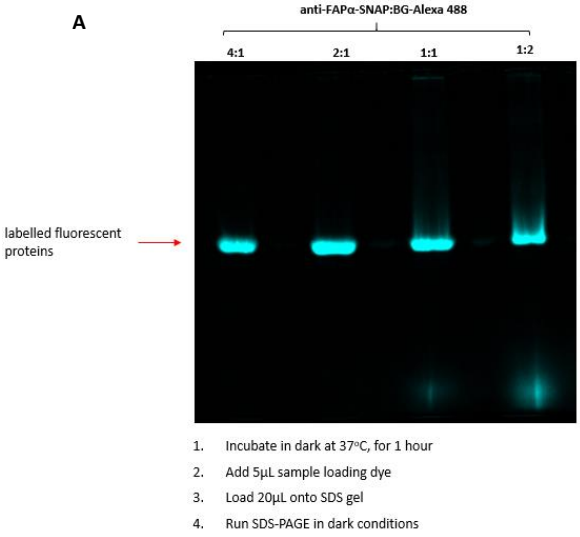

1. Incubate in dark at 37°C, for 1 hour
2. Add 5µL sample loading dye
3. Load 20µL onto SDS gel
4. Run SDS-PAGE in dark conditions

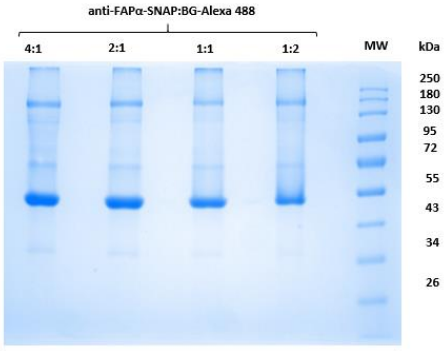

Ratio	Intensity	Bound: unbound
4:1	8168.669	-
2:1	10478.861	-
1:1	12209.903	3.0
1:2	12251.974	1.0

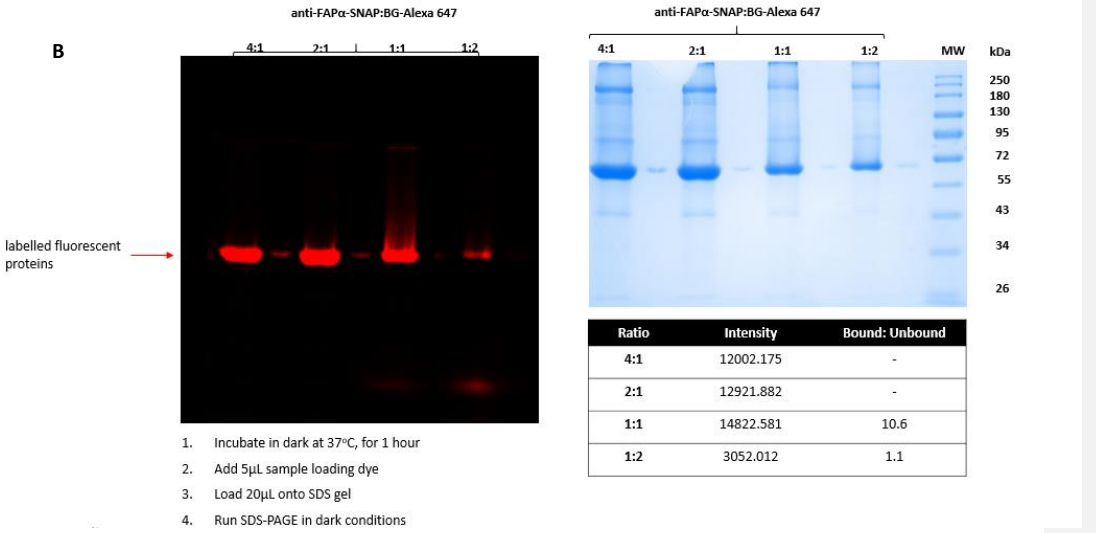

Ratio	Intensity	Bound: Unbound
4:1	12002.175	-
2:1	12921.882	-
1:1	14822.581	10.6
1:2	3052.012	1.1

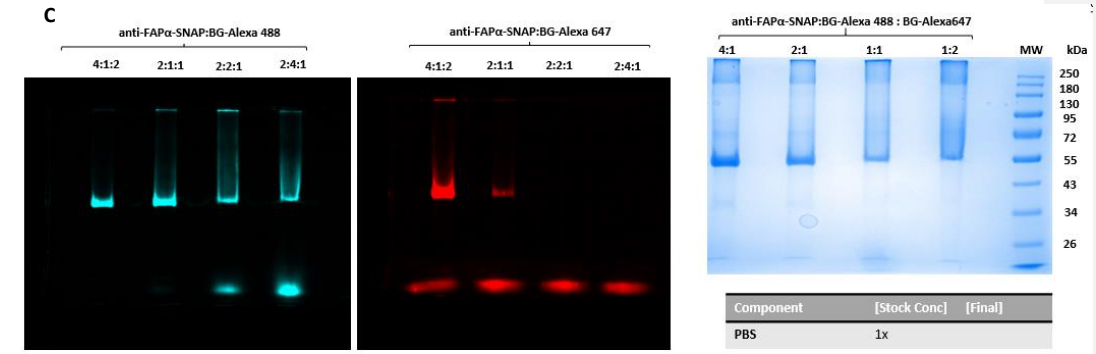

Component	[Stock Conc]	[Final]
PBS	1x	
DTT	10mM	1mM
BG-Alexa 488	25µM	*determine*
BG-Alexa 647	25µM	2.5µM
SNAP fusion protein	50µM	5µM
TOTAL		20µL

Figure 14. Conjugation of BG-Modified fluorophores with anti-FAPα (scFv)-SNAP. (A) Fluorescent blot and 10%SDS gel of anti-FAPα (scFv)-SNAP conjugated with BG Alexa 488 (B) Fluorescent blot and 10%SDS gel of anti-FAPα (scFv)-SNAP conjugated with BG Alexa 647 (C) Fluorescent blot and 10%SDS gel of dual anti-FAPα (scFv)-SNAP conjugated with BG Alexa 488 & 647. Florescent blots captured with the iBright Imaging System.

4.3.5. Binding analysis with anti-FAPα (scFv) SNAP

Commented [MK8]: Consider preparing your imaging and cytotoxicity figures in PowerPoint and pasting them as pictures in Word. That way, when things are edited and inevitably move in your word document, it won't affect the figures and labels. Similar to what you did with the conjugation gel images.

Living cell imaging analysis was conducted to validate the recombinant SNAP fusion protein's biological activity. This enables the visualisation of the particular binding ability of the antibody binding scFv to FAPα on the surface of cancer cells expressing the TAA. A 1:1 conjugation reaction of anti-FAPα (scFv)-SNAP to BG-Alexa Fluor 488 was prepared and hereafter treated with tumour cell lines. A faint fluorescence signal was visible in the HDF cell line, which is known to express FAPα, however, it was not clearly localized on the cell surface and appears to have been internalised (Figure 15A). The U87 brain tumour cell line showed no signs of membrane binding. (Figure 15B). As expected, the FAPα-negative MDA-MB-468 and A431 cell lines showed no binding (Fig15C&D).

Commented [MK9]: It looks like it had internalised already

(A) HDF (B) U87

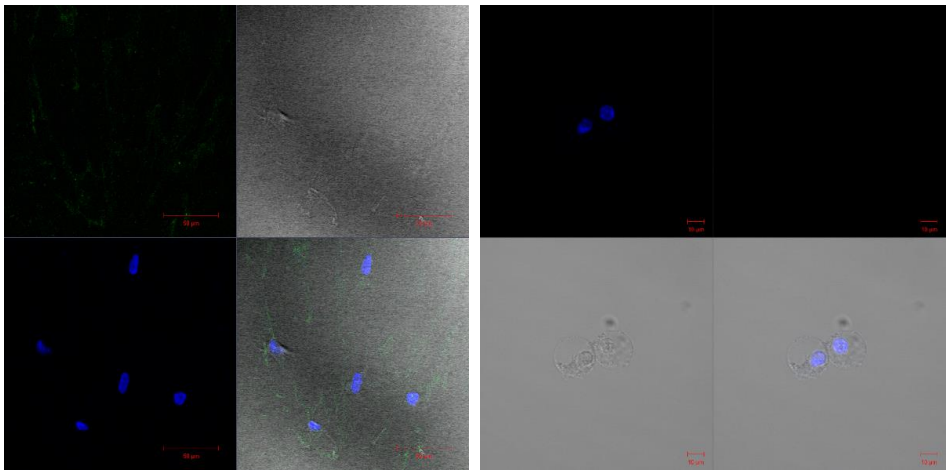

(C)MDA-MB-468 (D)A431

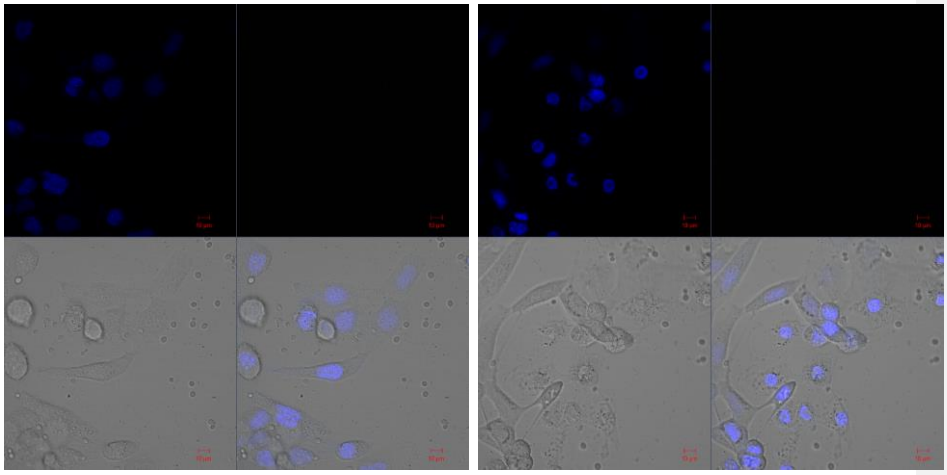

Figure 15. Live cell imaging of tumour cell lines with anti-FAPα (scFv)-SNAP-Alexa Fluor 488. Images were captured at 40x magnification, visualizing nuclear staining (blue), and surface labelling (red) and cell morphology. (A) HDF fibroblast c ell line (B) U87 malignant glioma cell line. (C) MDA-MB-468 triple negative breast cancer cell line-negative control (D) A431 melanoma cell line – negative control.

4.4. Mammalian culture and production of anti-EGFR (scFv)-SNAP

4.4.1. Expression of pCB_EGFR (scFv)-SNAP

Anti-EGFR (scFv)-SNAP positive HEK293T cells were donated by Mr Sanele Cingo and cultured as described in section 3.4. A total of 2.25L of supernatant was collected.

4.4.2. Purification and of anti-EGFR (scFv)-SNAP

Harvested CCSN was purified by the IMAC method (section 3.5.). The chromatogram in Figure 16 shows two absorbance peaks, as observed in the anti-FAPα (scFv)-SNAP purification. Each fraction collected during IMAC purification was run on a 10% SDS gel to identify the protein of interest before pooling and concentrating these fractions. There was evidence of BSA contamination in fraction B10, however with the loss of our protein of interest. Consequently, fraction B10 was excluded from further processing. The peak covering fractions (A1-B9, B11-D9)

were pooled and concentrated using a 10 kDa Amicon® filter column. The total amount of protein harvested was 5.87mg from 2.25L of CCSN as determined by densitometry analysis. The estimated total yield of anti-EGFR (scFv)-SNAP protein as a percentage of total protein was 38%.

A

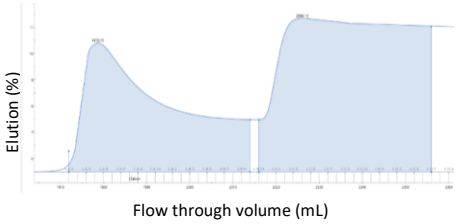

B

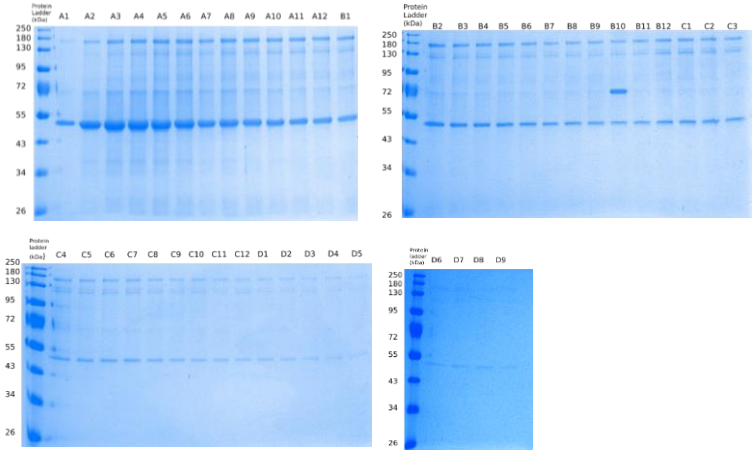

C

Sample	Area	Amount(ug)	Volume loaded(uL)	Densitometry(ug/uL)	Denovix (mg/mL)	% fusion protein in total IMAC purified protein
anti-EGFR-SNAP Peak 1	4718.00	6.55	1.35	3.89	14.90	26%
anti-EGFR-SNAP Peak 2	2796.10	2.42	6.20	0.39	3.21	12%

Figure 16. Protein purification of anti-EGFR (scFv)-SNAP (A) Absorbance profile (UV 280nm) of eluate from IMAC purified cell culture supernatant (CCSN) containing secreted anti-EGFR (scFv)-SNAP (B) Purified IMAC eluate fractions on 10% SDS-PAGE gel(C) Summary of protein quantification

4.4.3. SDS PAGE and Immunoblotting of anti-EGFR (scFv)-SNAP

The purified protein sample was run on a 10% SDS gel to identify protein bands corresponding to the theoretical size of anti-EGFR (scFv)SNAP (50.35 kDa). The thick bands observed between 48-55 kDa of the 10% SDS gel were predicted to be our protein of interest (Figure 17A). Purified protein run on a 10% SDS gel was transferred onto a PVDF membrane for western blot analysis. The membrane was incubated with an anti-His primary antibody and detected by chemiluminescence with an HRP conjugated secondary antibody. The immunoblot (Figure 17B) confirmed the identity of the recombinant fusion protein by detecting the N-terminal 6-Histidine tag in both Peak 1 and Peak 2 samples. Notably, there was observed loss of the fusion protein during the IMAC purification process. There was also noticeable enrichment of the fusion protein from the CCSN after purification and concentration.

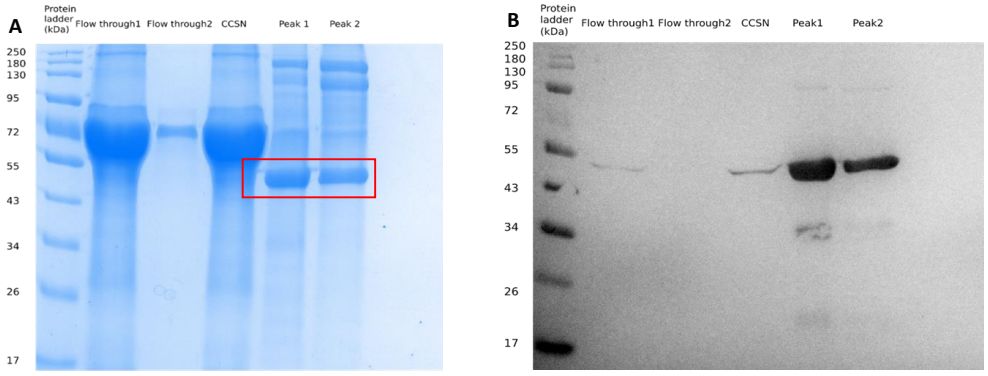

Figure 17. Characterization of anti-EGFR (scFv)-SNAP by SDS-PAGE and Immunoblotting (A) SDS-PAGE analysis of concentrated anti-EGFR (scFv)-SNAP peaks (red rectangle) (B) Western Blot analysis of concentrated anti-EGFR (scFv)-SNAP. Primary αHis-rabbit antibody (1:1000) was used, followed by secondary goat-αrabbit-HRP antibody conjugate (1:5000). CCSN= cell culture supernatant

4.4.4. Conjugation of anti-EGFR (scFv)-SNAP with BG-Fluorophores and BG-Napthalamide substrates

To confirm the functionality of anti-EGFR (scFv)-SNAP, we performed conjugation experiments with BG-modified fluorophores. The SNAP-tag element reacts with a 1:1 stoichiometry with BG-

substrates and therefore BG-modified fluorophores are ideal markers that indicate the functionality of the SNAP-Tag in the fusion protein. Anti-EGFR (scFv)-SNAP was conjugated to BG-Alexa Fluor 488 in different ratios (Figure 18A). It was observed that there were different intensities of fluorescence observed at each ratio. Higher intensities were not observed in the presence of an excess of fluorophores (ratios 4:1 and 2:1), however, for both fluorophores, a ratio of 1:1 gave off the highest fluorescence intensity - thus suggesting that this ratio is ideal for reactions with BG-modified substrates. Notably, there were excess unconjugated fluorophores present at all ratios. We performed a dual conjugation reaction with both fluorophores and observed that the fusion protein was saturated only in the presence of excess fluorophores. At the 1:1 and 1:2 ratio, there was still some unconjugated protein which was able to show binding in the second labelling reaction (Figure 18A).

Napthalamide based BG substrates were synthesized by Mr. Rudolf Dreyer (Stellenbosch University). These compounds represent alternative BG-fluorescent probes for research purposes which exhibit similar labelling rates when compared to commercially available BG substrates (151). The BG-based Napthalamides were conjugated to anti-EGFR (scFv)-SNAP in a 1:1 ratio, run on an SDS gel and visualised (Figure 18C). Notably, the Napthalamide-based probes produced weaker fluorescent signals compared to the positive control (BG-Alexa Fluor 488).

A

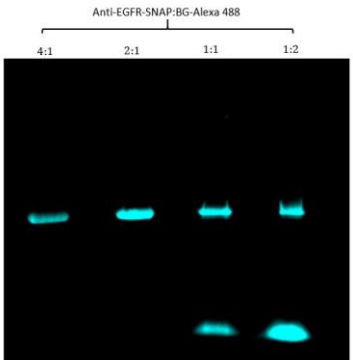

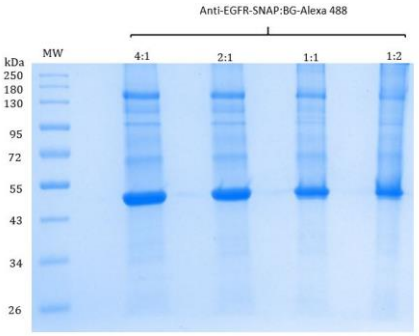

Ratio	Intensity	Bound: Unbound
4:1	4427.163	-
2:1	7431.113	-
1:1	5958.891	1
1:2	5101.134	2.5

B

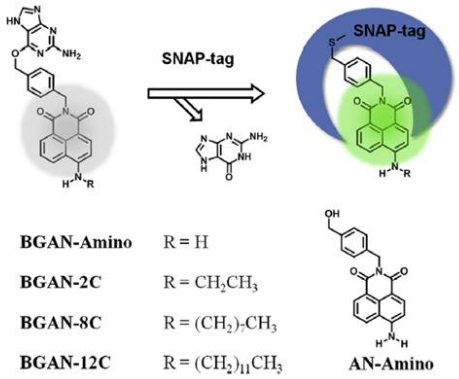

C

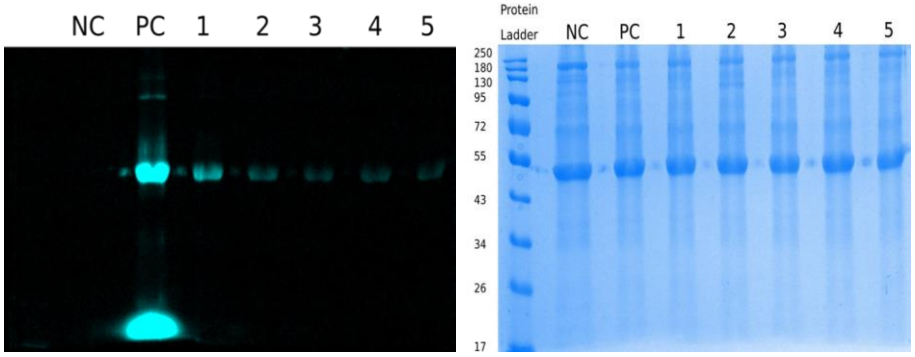

Figure 18. Conjugation of anti-EGFR (scFv)-SNAP with BG-fluorophores. (A) Fluorescent blot and corresponding 10% SDS gel of anti-EGFR (scFv)-SNAP conjugated with BG Alexa 488 at different ratios (B) Schematic adopted from Qiao *et al*. (2017) of reaction of BG-linked napthalamide fluorogenic probes with the SNAP-Tag. 1,8-naphthalimide shows enhanced fluorescence after covalently bonding to the SNAP-tag , due to its localization within the hydrophobic binding region of the SNAP-tag and the release of guanine, the fluorescence quencher. (C) Fluorescent blot and corresponding 10% SDS gel of anti-EGFR (scFv)-SNAP conjugated to BG-napthalamides. Lane 2(NC) = negative control, lane 3 (PC) = positive control, lanes 4-8 = BGAN-Amino, BGAN-Azido, BGAN-X-R, α-BGAN-PVP_{10}, α-BGAN-PVP_{20}

4.4.5. Live cell imaging analysis of anti-EGFR (scFv)-SNAP with tumour cell lines

Live cell imaging analysis with confocal microscopy was carried out to validate the biological activity of the recombinant anti-EGFR (scFv)-SNAP fusion protein by qualitatively assessing its binding to the EGFR TAA is tumour cell lines. The EGFR over-expressing A431 and MDA-MB-468 cell lines showed prominent cell surface binding activity (Figure 19A&B). Notably, there was the internalization of the probe in the cytoplasm in these cell lines, indicating receptor-mediated endocytosis as previously characterized with SNAP fusion proteins. We also observed lower levels of specific binding in the brain tumour cell line, U87 (Figure 19C). As expected, the negative control (A2058) had no binding activity (Figure 19D). These qualitative results confirm the full-length integrity of the fusion protein as both the enzymatic activity and biological activity have been exhibited. Moreover, the observed specific binding ability of anti-EGFR (scFv)-SNAP presents this recombinant protein as an ideal diagnostic and therapeutic tool.

Commented [MK10]: See Figure 19: Labels and images are shifted and no longer easy to interpret. Use PPT to generate figures like these instead

(A)A431

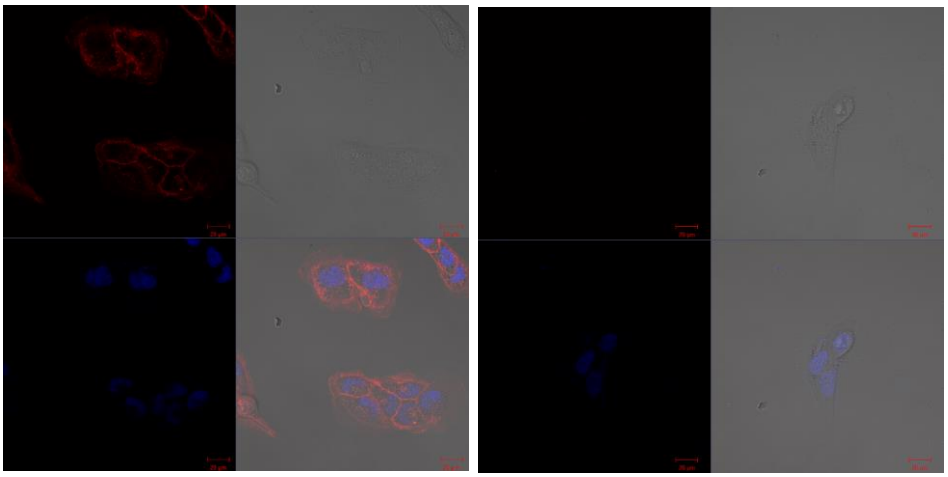

(B)MDA-MB-468

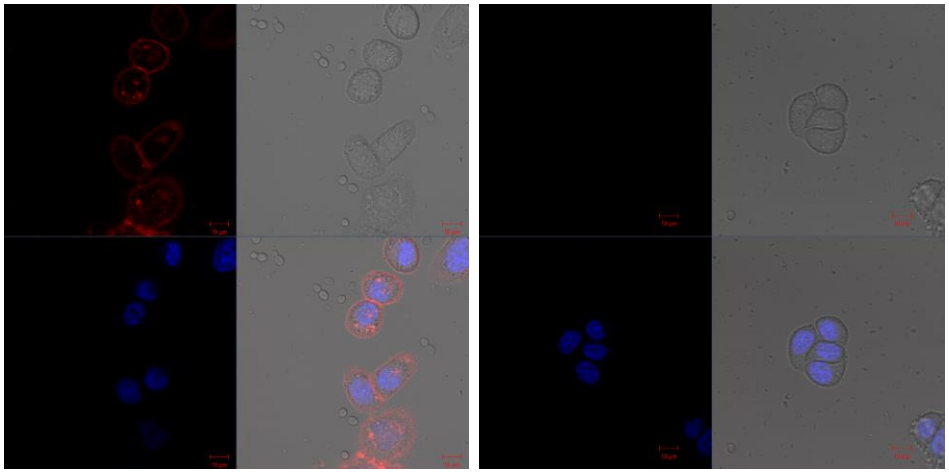

(C) U87

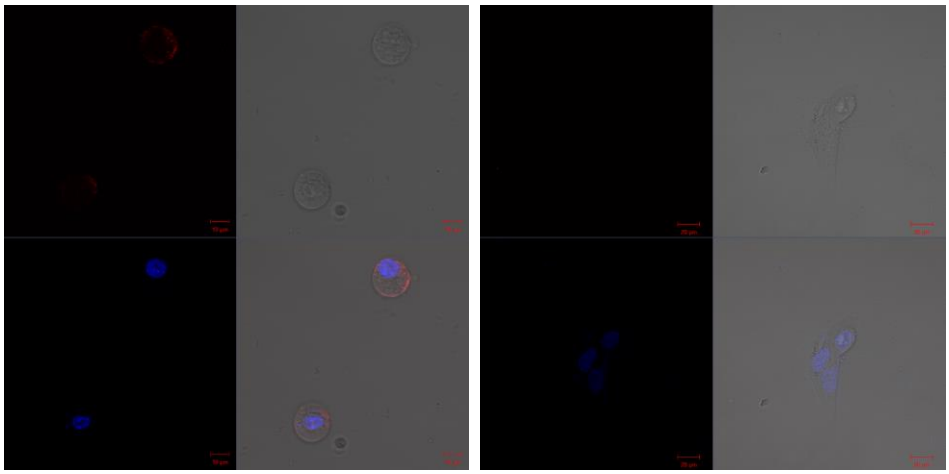

(D)A2058

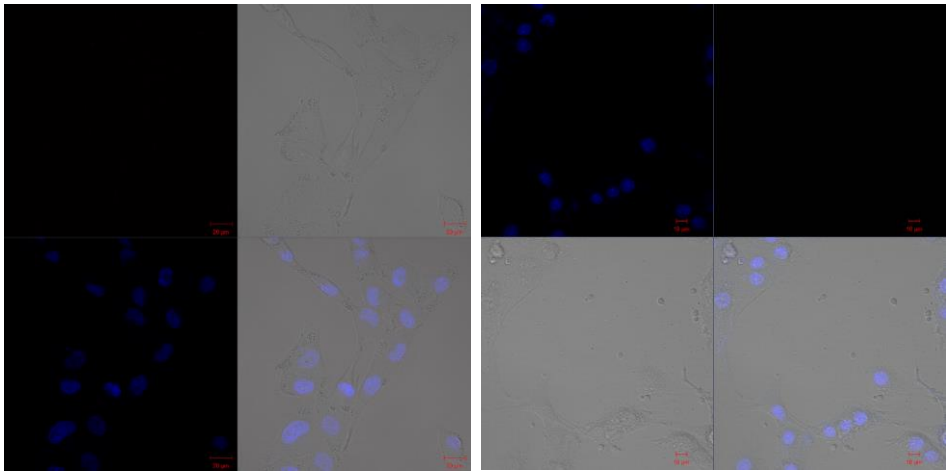

Figure 19. Live cell imaging of tumour cell lines with anti-EGFR (scFv)-SNAP-Alexa Fluor 647. Left = anti-EGFR (scFv)-SNAP-Alexa Fluor 647, right = PBS treated auto-florescence control. Images were captured at 40x magnification, visualizing nuclear staining (blue), surface labelling (red) and cell morphology. (A) A431 melanoma cell line. (B) MDA-MB-468 triple negative breast cancer cell line. (C) U87 malignant glioma cell line. (D) A2058 melanoma cell line – negative control.

4.5.6. Cytotoxicity studies with anti-EGFR (scFv)-SNAP

The XTT viability assay was used to assess the ability of anti-EGFR (scFv)-SNAP to specifically deliver a cytotoxic payload, BG-AURIF, to EGFR-positive tumour cells. Unconjugated BG-AURIF exhibited cell killing in both TAA-negative and -positive cell lines in a dose-dependent manner (Figure 20). To experimentally optimize the conjugation of BG-AURIF to the fusion protein, different incubation times were tested. Notably, improved conjugation at 3 hours and 4 hours incubation times as compared to 2 hours (Figure 21A). There was a dose-dependent response to anti-EGFR (scFv)-SNAP-BG-AURIF in A431, MDA-MB-468 and U87 (Figure 22A-C). The AURIF-based ADC did not affect the EGFR-negative A2058 control cells, as expected (Figure 22D). In addition to the live cell imaging analysis, these findings confirm the specific targeting functionality of the fusion protein.

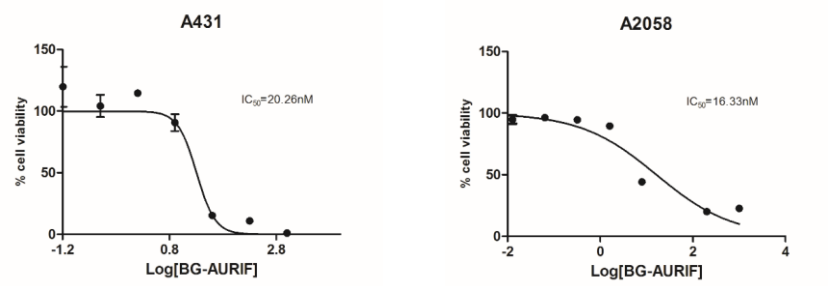

Figure 20. BG-AURIF dose response curves in EGFR $^{+/-}$ cell lines. The XTT viability assay was used to assess the cell killing activity of decreasing concentrations of unconjugated BG-AURIF after 72 hour incubation with A431 (EGFR^{+}) and A2058(EGFR^{-}) tumour cells. GraphPad Prism version 5 was used to calculate the IC_{50} values in comparison to untreated and Zeocin controls. The data are presented as means and standard deviations for each measurement.

A

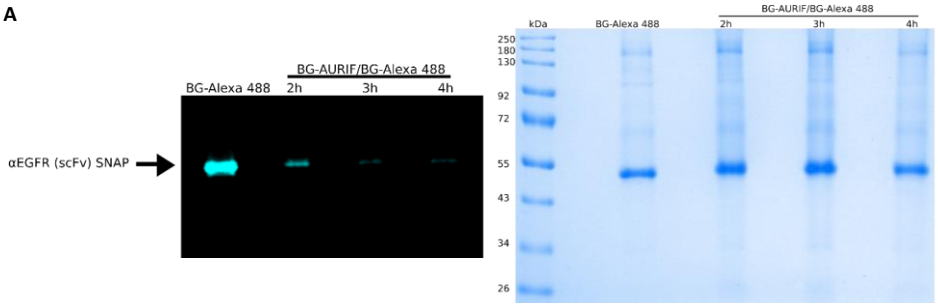

B

Sample	SDS band intensity(B)	Fluorescent intensity(F)	F/B ratio
PC	6018.104	12135.246	2.016
2h	6742.782	4485.497	0.665
3h	7246.56	1850.456	0.255
4h	6268.004	1753.698	0.280

Figure 21. Efficiency of conjugation with BG-AURIF at different incubation periods. (A) Fluorescent blot and corresponding 10% SDS gel anti-EGFR (scFv)-SNAP-AURIF conjugated with BG Alexa 488. PC (positive control) = anti-EGFR (scFv)-SNAP conjugated with Alexa Fluor 488. 2h =2 hour incubation at 37ºC. (B) Quantification of SDS protein band intensity and fluorescent signal, generated with ImageJ Software.

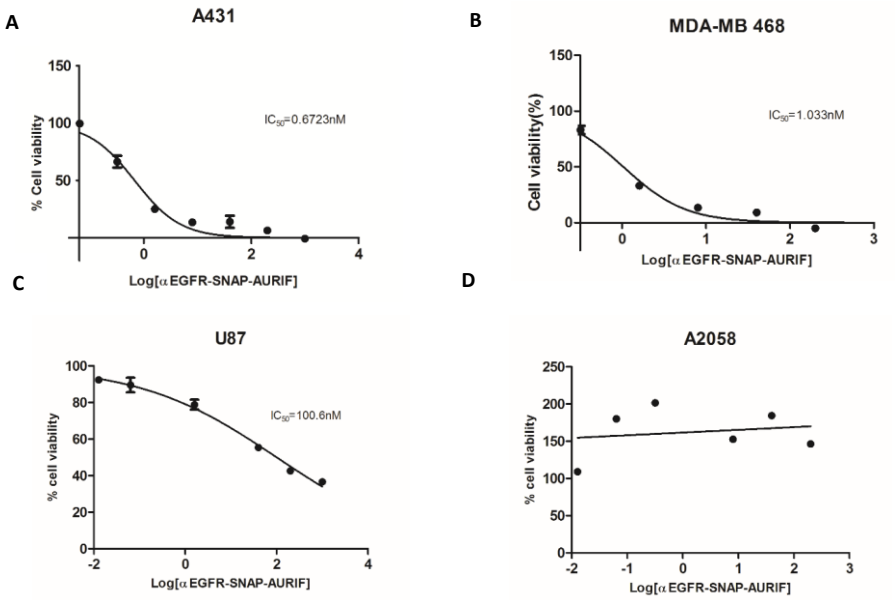

Figure 22. Cytotoxicity of Anti-EGFR-SNAP-AURIF against EGFR-expressing cells. After 72 hours of incubation, cytotoxicity was determined using an XTT viability assay. AURIF-conjugated scFv-SNAP fusion protein was incubated with MDA-MB-468 (A), A2058 (B), A431 (C), and U87 (D) cells in decreasing concentrations. GraphPad Prism was used to calculate the IC50 values in comparison to untreated cells and Zeocin control. Measurements were taken at least three times in duplicate. The data are presented as means and standard deviations for each measurement.

Chapter 5: Discussion

5.1. Glioblastoma Multiforme: an unresolved clinical need

GBM has been described as the most lethal CNS cancer, with less than 5% patient survival living up to 5 years post-diagnosis (152). Globally, it has been hypothesized that GBM affects more people than is thought to be the case because not all regions have access to enough specialists or technological resources to identify it and gather the relevant epidemiological information (2). This is especially important to consider in the African context, where the prevalence of various malignancies has sharply grown over the past twenty years, straining health care systems (153). With the exception of temozolomide chemotherapy paired with radiotherapy, which exhibited a

slight prolongation of survival, there have been no substantial improvements in the treatment of GBM over the past 25 years (34). The infiltrative nature of tumour cells, heterogeneity of antigen expression, and a highly metastatic character - which makes tumour cells resistant to chemotherapy - are all key treatment limitations in GBM. Finding and creating novel, effective treatments for GBM patients, as well as having the best methods possible for testing and developing these treatments, are essential to improving their quality of life.

5.2. Recombinant SNAP fusion proteins: a targeted approach

SNAP-tag is a 20 kDa modified form of the human DNA repair enzyme O^6-alkylguanine-DNA-alkyltransferase (hAGT) that undergoes covalent self-labelling reactions with benzyl guanine (BG) modified substrates such as fluorophores and reporter molecules (78). Because SNAP-tag labelling is both irreversible and quantitative, it is ideal for reliable detection and quantification application (79). SNAP-tag technology presents a potent and versatile tool that, when incorporated in a TAA targeting fusion protein construct, can be applied in the development of more efficacious, safer, and affordable diagnostic and treatment options for GBM. A fusion protein is created by combining two or more distinct protein domains into a single protein molecule employing genetic engineering. Fusion protein technology seeks to improve performance by integrating the properties of different proteins (154). This study focused on the generation and characterization of recombinant SNAP fusion proteins, for simultaneous targeting and labelling of EGFR, an established TAA overexpressed in 60% of GBMs, and FAPα, a versatile protease recently found to contribute to invasiveness in GBM.

It has been proven that glioma genesis is caused by the dysregulation of multiple processes rather than a single factor or pathway. This demonstrates the necessity of using a multi-targeted strategy to combat this disease. Moreover, the heterogeneous nature of GBM discourages a single-target approach. As previously mentioned, there are over 206 genetic alterations linked to GBM, providing a large repertoire of TAAs that can be researched and targeted using SNAP-tag technology to create a panel of recombinant SNAP fusion proteins tailored specifically for GBM (155).

It would also be rational to investigate the development of SNAP-tag fusion proteins to target more TAAs associated with GSCs, as this cell population has been shown to play a crucial role in glioma genesis as well as therapeutic resistance to current therapies (156). Some of the GSC-related TAAs that have already been identified are given in Table 8.

Table 8. Examples of TAAs associated with GSCs

GSC TAA	Antigen type	Role in GSCs	Reference
CD133	Pentaspan transmembrane glycoprotein	• Cause of radiation therapy resistance and proliferation of GBM tumour cells • Promotes Epithelial to mesenchymal transition (EMT) in GSCs	(157)
Nestin	Class VI intermediate filament protein	• Drives the proliferation, cell migration, and self-renewal ability of GSCs.	(158)
Leucine-rich repeat-containing G protein-coupled receptor 5 (LGR5)	G protein-coupled receptor	• Promotes EMT in GSCs through triggering the Wnt/B-catenin pathway • Valid indicator of GBM prognosis	(159)
Nucleophosmin (NPM1)	Nucleolar protein	• Drives GSC proliferation and maintenance, promoting GBM progression	(160)
Glycerol-3-Phosphate Dehydrogenase 1 (GPD1)	Isoenzyme	• Plays a key role in GBM maintenance and proliferation pathways	(161)

5.3. Transient expression of recombinant SNAP fusion proteins

Genetic engineering has revolutionized the biopharmaceutical industry by allowing for the generation of recombinant proteins with desired features in diverse biological expression systems. Mammalian cells have been identified as ideal expression systems for recombinant protein biopharmaceuticals that require post-translational modifications to produce active and functional proteins (162). The mammalian expression host of choice in this study was the HEK293T cell

tissue culture. This culture is easily transfected with plasmid DNA and has been described as an efficient system for generating recombinant antibody fusion proteins (163).

In this study, the anti-FAPα (scFv) SNAP and anti-EGFR (scFv) SNAP fusion proteins were successfully cultured from thawed stocks of previously transfected HEK293T cells. Notably, the levels of protein expression were low upon resuscitating the cultures, but the application of plasmid selection pressure with Zeocin allowed for the enrichment of eGFP-expressing cells, indicative of cells actively translating the pCB plasmid. After the downstream processing and purification of the cell culture supernatant, there was confirmation of the generation of our protein of interest through SDS-PAGE and Western Blot Analysis (Figures 13&17). However, the recovered yield of the fusion protein in IMAC purified samples was poor, being less than 50% for both constructs. There seem to be apparent bands of what are possible aggregates of unwanted proteins from the CCSN (130-250 kDa), and also possible products of the degraded recombinant fusion protein with the N-terminal Histidine residues (as these are apparent in the Immunoblot). There is therefore a need to improve the processing of the CCSN and further downstream purification of IMAC protein samples to remove contaminants, by Size Exclusion Chromatography (SEC) (164). In a study by Sandeep *et al.*, SEC was able to produce purity of up to 98% in the processing of recombinant human granulocyte colony-stimulating factor (165). It has also been noted that the incorporation of protease inhibitors in the CCSN storage as well as purified protein samples is a solution to the issue of possible protein degradation (166).

Recombinant protein purity must be emphasized because it affects subsequent experiments and is crucial for *in vitro* and *in vivo* research because contaminants are very likely to affect the experimental outcome (167). This could consequently result in misinterpretation of fusion protein functionality.

IMAC purified samples were subjected to a densitometry analysis in order to calculate the fusion protein's absolute concentration (Figures 12&16). In the production of recombinant proteins in mammalian systems, the ideal yield for transient expression expected is 50-80 mg/L (168). In this study, the absolute amount of fusion protein was determined to be 2.61 to 2.67 mg per 1 Litre of supernatant. The transient mammalian expression of recombinant SNAP fusion proteins is not fully optimised; there remains a need to design methods that would enable an increase in protein

yield under resource-conscious conditions. This can be achieved by either optimizing the culture conditions or testing alternative production cell lines.

5.4. Validation of the SNAP-tag enzymatic function and conjugation optimization

It has been described in literature that SNAP-tag is able to theoretically react in a 1:1 stoichiometry, which has been validated by various studies (84). In order to confirm that this was also still the case with the SNAP-tag element in the recombinant fusion proteins generated in this study, a series of conjugation reactions were carried out. Each SNAP fusion protein was conjugated to commercially BG-fluorophores, and the different conjugation ratios were set up, in order to determine which was the most optimal for a 1-hour conjugation reaction. According to the findings of this study, for both fusion protein constructs, the 1:1 ratio was decided to be the most optimal as this had relatively the highest fluorescent signal (Figure 14).

5.5. Recombinant SNAP fusion proteins: immunodiagnostic potential in GBM

The scFv portion of the recombinant fusion protein retains the antigen-binding ability of a full-length mAb (169). This study was able to confirm the binding ability of the scFv in one of the two constructs. The speculations as to why no binding was detectable with confocal microscopy for the anti-FAPα (scFv) SNAP construct might include: (i) low levels of FAPα expression in tested cell lines, or (ii) translation of a non-functional scFv portion of the fusion protein (170). The former speculation would need to be confirmed by quantifying the level of FAPα expression in each tested cell by a receptor quantifying technique such as flow cytometry (171). However, the doctoral thesis of former MB&I member, Fleury Biteghe (PhD), reported the expression levels of FAPα in four different tumour cell lines, including the U87 glioma cell line used in this study. However, no subsequent imaging analyses were carried out on these cell lines (150). It is also important to note that most studies that have studied FAPα expression work with cell lines genetically engineered to produce the antigen, whilst this study focused on detecting endogenous expression. Given that the integrity of the plasmid was previously confirmed by pairwise sequencing analysis, it is highly unlikely that DNA mutation resulted in a non-functional scFv (150). This could possibly be a

consequence or erroneous protein translation (172). This second speculation can be investigated by carrying out mass spectrometry analysis to confirm if the actual peptide sequences are identical to theoretical data and in line with the patented humanized scFv #34 from which the FAPα (scFv) was derived (173).

Nevertheless, we were able to demonstrate the binding ability of the scFv in EGFR+ cells at the microscopic level. The use of fluorophore labelled recombinant SNAP fusion protein was distinctly able to define the plasma membrane of the cells as well as indicate internalization – which also gives some insight into the downstream processing of the fusion proteins upon binding and the implications this has in delivering therapeutic payloads.

5.6. Optimization of conjugation of small molecule toxin BG-AURIF with Recombinant SNAP fusion proteins

The introduction of ADCs has transformed the chemotherapy landscape in oncology. The success of this cancer cell targeting drug format has led to there being 10 FDA-approved drugs such as Kadcyla® (2013) for breast cancer, Adcetris® (2011) for haematological cancers, and most recently, Zynlonta™ (2021) for B-cell lymphoma (174). Currently, over 80 ADCs are being investigated in more than 150 clinical trials (174,175).

However, a major challenge associated with developing ADCs has been variable DARs, during the chemical conjugation of cytotoxic payload to antigen targeting moiety (176). This has implications such as reduced efficacy and off-target effects of prematurely dissociated toxic payload (177), To aid in overcoming the challenge of variable DARs (leading to heterogeneous ADCs), novel formats of ADCs now employ the use of site-specific conjugation through different strategies, including enzymatic linkage, which allows for more stable and controlled DARs (178). The recombinant SNAP fusion protein investigated in this study, anti-EGFR(scFv)-SNAP presents a next-generation ADC which allows for the chemo-enzymatic site-specific conjugation of BG labelled small molecular toxin, AURIF, to the SNAP-tag. Mono-methyl auristatin F (MMAF also known as AURIF) is a synthetic anti-mitotic agent that inhibits the polymerization of tubulin in cells, derived from the natural compound dolastatin-10 (179,180). Because MMAF is exceedingly toxic, it cannot be directly used as a chemotherapeutic agent. When coupled to a monoclonal

antibody, however, its activity is targeted, resulting in an effective therapeutic payload (181). In 2020, the MMAF-based ADC, Blenrep®, was FDA approved for the treatment of relapsed or refractory multiple myeloma in adult patients who were unresponsive to at least four previous therapies (182). This ADC combines B-cell maturation antigen (BCMA) binding activity and the microtubule disrupting cytotoxic attached via a maleimidocaproyl linker (182).

The linker element of ADCs acts as a tether between the scFv and cytotoxic payload. The chemistry of the linker affects ADC pharmacodynamics, pharmacokinetics and hydrophobicity (175). Hydrophobicity of linkers has been associated with the non-covalent aggregation of ADCs (183). This issue can be addressed by using hydrophilic linkers with negatively charged pyrophosphate, sulfonate, or polyethene glycol (PEG) groups (184). This study worked with a format of BG-AURIF, containing the non-cleavable linker, PEG_3-NH_2, synthesised by Allan Huysamen (Hunter group, Chemistry department, UCT). This spacer format gives more distance between AURIF and the enzymatic domain of the SNAP-tag, thus making the ADC more hydrophilic (185).

Previous studies have opted for three-fold molar excess BG-AURIF to recombinant SNAP fusion protein (73). This study sought to optimise the reaction conditions of conjugation to the recombinant SNAP fusion proteins, working with a two-fold molar excess of BG-AURIF. The findings demonstrated that a 3-hour incubation time, increased the amount of BG-AURIF bound to the fusion protein, although not reaching saturation, thus there is a need for further optimization.

5.7. Recombinant SNAP fusion proteins: immunotherapeutic potential in GBM

Recombinant SNAP fusion proteins conjugated to toxic payloads have been demonstrated as a novel format of ADCs, which is promising for the treatment of solid tumours. A study by Woitok *et al.* was able to generate a next-generation ADC that could specifically eliminate TNBC tumour cells within nanomolar concentrations (186).

Commented [MK11]: Insert reference for the study

The mechanism of action of scFv-SNAP-AURIF is as follows: (i) the scFv binds to the TAA in target tumour cells; (ii) the ADC is internalized by receptor-mediated endocytosis, and then processed in cellular lysosomes; (iii) the antigen targeting moiety is degraded in the lysosome, releasing the cytotoxic payload into the cytosol in an activated form within the tumour cells,

activating cytotoxic effect by microtubule disruption which results in cell death by apoptosis (186,187).

This study was able to create a next-generation ADC format that can deliver a toxic payload via the TAA EGFR. A dose-dependent response to anti-EGFR(scFv)-SNAP-AURIF was observed in TAA positive cells whilst no such response was present in TAA negative cell line, thus giving a validation on the specific binding ability of the scFv as well as an early indication of the safety of this ADC, as there is no off-target activity. Notably, the cytotoxicity analysis generated a nanomolar range of IC50 values, indicating the efficacy of this ADC format, and further supporting its future investigation *in vivo* as an immunotherapeutic agent.

5.8. Future outlook: Radio-labelled SNAP fusion proteins as theranostic agents in GBM

For more than a half-century, radiation has been used to treat cancer patients. The basis for radiotherapy is the ability of radioactive atoms, commonly referred to as radionuclides, to induce ionization, or the production of electrons and free radicals, when ingested by biological matter. These extremely reactive chemical species interfere with important components in cells (e.g. DNA) and eventually cause cell death (188). This kind of treatment is extremely potent and continues to be improved to achieve more effective therapeutic outcomes. By coupling a radionuclide to an antibody, it is now possible to apply this format for targeted therapeutic applications with the aim of specifically irradiating tumour cells (189).

For the purpose of non-invasive imaging of TAA-positive tissue in GBM tumours, several radio-labelled mAbs and variant derivatives are being developed. This has made it possible to circumvent the morbidity linked to the surgical methods used to gather biopsy samples (190). Besides that, immune-radiolabelling offers a tool to track how well a patient is responding to treatment as it simultaneously delivers radiotherapies and allows for highly accurate tumour mass detection in cancer patients (189,191). This combined treatment and monitoring strategy is the foundation of what is known as ‘theranostics’. Theranostics is a term that describes the use of a diagnostic agent to guide therapy options for patients, in the field of oncology (192). At present imaging with potential radionuclide-based theranostic agents is carried out with PET. The drugs incorporated in

this PET are labelled with beta (**β**) and alpha (**α**) emitting radionuclides that produce a high linear energy transfer and necessary localized absorbed radiation dosage for therapeutic effectiveness (193). The radionuclide-based theranostics first tested out with sodium iodide in the 1950s (131^{I}) were used in the imaging and treatment of advanced thyroid cancers (194). Antibodies and their derivatives have been employed as delivery vehicles for theranostic development. A mAb against EGFR 125^{I}-labelled mouse antibody (mAb 425) was used in a 20-year long phase II clinical trial study as adjuvant treatment of Gliomas through intravenous administration as a monotherapy or in combination with TMZ. The study showed improved survival by several months with the combination treatment, reporting limited off-target effects. The combination group was able to exhibit improved median survival of 20.2 months, qualifying the ADC for further phase III clinical investigation (131). More studies using radionuclide-based theranostics are being investigated for GBM and other CNS tumours, holding promise for better clinical outcomes (195-197).

Commented [MK12]: Average?

Through coupling with BG-modified radionuclides, the recombinant SNAP fusion protein used in this study can be explored as a non-invasive TAA targeting tool for immunoradio-theranostic application. Due to the high site specificity for chemical conjugation, precise stoichiometry, and great stability demonstrated by SNAP fusion protein technology, this promises to be an efficacious tool (79).

At present, no study has investigated the development of immunoradio-theranostic SNAP fusion proteins, but other forms of SNAP-tag based theranostics that employ photodynamic therapy have been extensively investigated. For example, studies by von Felbert *et al*. and Amoury *et al.*, developed SNAP-tag based photoimmuno-theranostics which were able to demonstrate selective specificity and cytotoxicity of these agents both *in vitro and ex vivo,* at a nano-molar ranges (87,135). This suggests that SNAP-tag based immunoradio-theranostics could produce comparable experimental results. Conducting this study marks an early stage but important advancement toward immunoradio-conjugation and preclinical validation of *in vivo* radio-imaging and radio-immunotherapy in GBM.

5.8.1. Transporting radio-labelled SNAP fusion proteins across BBB

To efficiently deliver any payload to the brain, the restrictive BBB must be bypassed. As aforementioned, RMT is an important transport pathway across the BBB. RMT begins with endocytosis triggered by receptor interaction, followed by intracellular trafficking and exocytosis into the brain parenchyma (198).

TfR is one of the known RMT receptors in brain endothelial cells that have been researched in BBB drug delivery, at both *in vitro* and *in vivo* levels (199). Several studies have demonstrated increased brain exposure with the use of TfR peptide ligands or anti-TfR antibodies (200).

Protein engineering has made it possible to create TfR antibody derivatives with less affinity for the natural ligand Transferrin (Tf), improving the detachment of the antigen-antibody complex in the basolateral (brain) area of the BBB(199). Furthermore, additional research has compared the brain penetration of monovalent and divalent antibody derivatives; giving evidence that monovalent derivative exhibits increased transcytosis (201,202).

A study by Niewoehner *et al*. described how to create a BBB shuttle format by fusing a TfR-targeting single antibody fragment (sFab) to the payload, an Alzheimer's targeting mAb (202). Potentially, this kind of engineering can be used to target GBM masses with SNAP fusion proteins by genetically attaching to a TfR-targeting scFv. This will enable effective shuttling across the BBB (Figure 23).

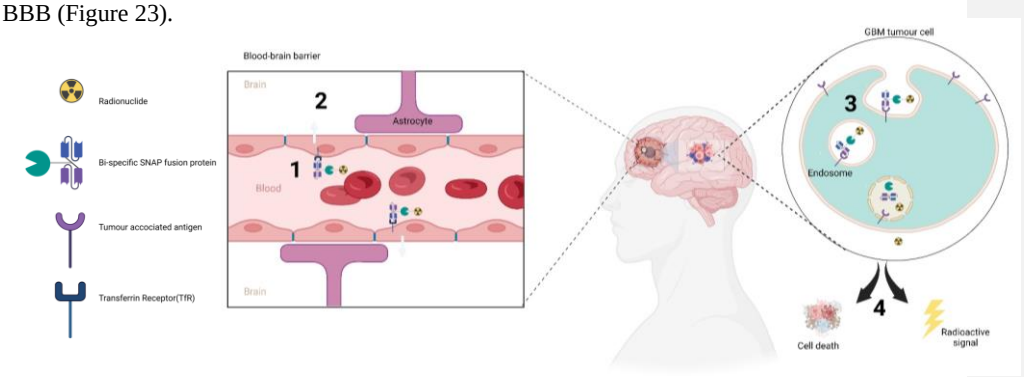

Figure 23. A hypothesized strategy for delivery of bi-specific radiolabelled SNAP fusion proteins to GBM cells after intravenous administration. (1) Interaction of anti-TfR scFv element of fusion protein with TfR will trigger (2) transcytosis of fusion protein across brain endothelial cell into the brain parenchyma. (3) Receptor mediated endocytosis of fusion proteins is induced by interaction with receptor on target GBM cell. (4)After lysosomal degradation of fusion protein, radionuclide payload is released and elicits desired effect. Image created in BioRender.com.

Conclusion

In summary, this study was able to generate and characterize an antibody fusion protein format that can be modified into a radoimmuno-conjugate for therapeutic and diagnostic use in GBM and other malignancies. SNAP-tag activity in the fusion protein displayed excellent labeling ability with a range of BG-substrates – thus indicating its suitability to be further tested with BG-modified radionuclides.

Next, the optimal conjugation ratios and reaction conditions of the fusion protein to BG-substrates were also reported. This provides valuable guidance to improve the conjugation outcomes in further studies with SNAP fusion proteins.

The findings in this work also show the fusion protein's potential for clinical application. Firstly, when labelled with a flourescent payload, the fusion protein exhibited specific binding activity *in vitro*, showing its ability for immunodiagnostic use. Secondly, the ability of toxin-labelled SNAP fusion proteins to specifically kill antigen-positive tumour cells was shown, indicating targeted therapeutic potential.

Presumably, the fusion proteins investigated in this study will be used in neuro-radiological practice in the future to reach GBM tumours in non-invasive yet targeted approaches for the best clinical outcome.

References

(1) statista. 2021; Available at: (https://www.statista.com/statistics/288580/number-of-cancer-deaths-worldwide-by-type/. Accessed 07 June, 2022.

(2) Patel AP, Fisher JL, Nichols E, Abd-Allah F, Abdela J, Abdelalim A, et al. Global, regional, and national burden of brain and other CNS cancer, 1990–2016: a systematic analysis for the Global Burden of Disease Study 2016. Lancet neurology 2019 Apr;18(4):376-393.

(3) Louis DN, Perry A, Wesseling P, Brat DJ, Cree IA, Figarella-Branger D, et al. The 2021 WHO Classification of Tumors of the Central Nervous System: a summary. Neuro Oncol 2021 Aug 2;23(8):1231-1251.

(4) DeAngelis LM. Global consequences of malignant CNS tumours: a call to action. The Lancet Neurology 2019;18(4):324-325.

(5) GBD 2016 Brain and Other CNS Cancer Collaborators. Global, regional, and national burden of brain and other CNS cancer, 1990-2016: a systematic analysis for the Global Burden of Disease Study 2016. Lancet Neurol 2019 Apr;18(4):376-393.

(6) Alomar SA, MD. Clinical manifestation of central nervous system tumor. Seminars in diagnostic pathology 2010;27(2):97-104.

(7) THE GLOBAL CANCER OBSERVATORY. CANCER TOMORROW. 2020; Available at: https://gco.iarc.fr/tomorrow/en. Accessed 18 August, 2022.

(8) Tucker F. MicroHealth - Top 10 Deadliest Cancers. 2017; Available at: https://www.microhealthllc.com/top-ten-deadliest-cancers/. Accessed 7 June, 2022.

(9) Woodworth GF, Dunn GP, Nance EA, Hanes J, Brem H. Emerging Insights into Barriers to Effective Brain Tumor Therapeutics. Frontiers in Oncology 2014;4.

(10) Ebert LM, Yu W, Gargett T, Toubia J, Kollis PM, Tea MN, et al. Endothelial, pericyte and tumor cell expression in glioblastoma identifies fibroblast activation protein (FAP) as an excellent target for immunotherapy. Clin Transl Immunology 2020 Oct 14;9(10):e1191.

(11) krebsdaten.de. 2020; Available at: https://www.krebsdaten.de/Krebs/EN/Content/Cancer_sites/Central_nervous_system_cancer/central_nervous_system_cancer_node.html.

(12) Wang H, Xu T, Jiang Y, Xu H, Yan Y, Fu D, et al. The challenges and the promise of molecular targeted therapy in malignant gliomas. Neoplasia 2015;17(3):239-255.

(13) Mentlein R, Hattermann K, Hemion C, Jungbluth AA, Held-Feindt J. Expression and role of the cell surface protease seprase/fibroblast activation protein-α (FAP-α) in astroglial tumors. Biol Chem 2011 Mar;392(3):199-207.

(14) McLendon R, Friedman A, Bigner D, Van Meir EG, Brat DJ, Mastrogianakis G,M., et al. Comprehensive genomic characterization defines human glioblastoma genes and core pathways. Nature 2008;455(7216):1061-1068.

(15) Liang Y, Diehn M, Watson N, Bollen AW, Aldape KD, Nicholas MK, et al. Gene expression profiling reveals molecularly and clinically distinct subtypes of glioblastoma multiforme. Proc Natl Acad Sci U S A 2005 Apr 19;102(16):5814-5819.

(16) Diehn M, Nardini C, Wang DS, McGovern S, Jayaraman M, Liang Y, et al. Identification of noninvasive imaging surrogates for brain tumor gene-expression modules. Proc Natl Acad Sci U S A 2008 Apr 1;105(13):5213-5218.

(17) Busek P, Mateu R, Zubal M, Kotackova L, Sedo A. Targeting fibroblast activation protein in cancer - Prospects and caveats. Frontiers in bioscience 2018 Jun 1,;23:1933.

(18) Pesenti C, Navone SE, Guarnaccia L, Terrasi A, Costanza J, Silipigni R, et al. The Genetic Landscape of Human Glioblastoma and Matched Primary Cancer Stem Cells Reveals

Intratumour Similarity and Intertumour Heterogeneity. Stem Cells International 2019;2019:2617030.

(19) Shergalis A, Bankhead A, Luesakul U, Muangsin N, Neamati N. Current Challenges and Opportunities in Treating Glioblastoma. Pharmacol Rev 2018 July 01;70(3):412-445.

(20) Kan LK, Drummond K, Hunn M, Williams D, O'Brien TJ, Monif M. Potential biomarkers and challenges in glioma diagnosis, therapy and prognosis. BMJ Neurol Open 2020 August 24;2(2):e000069-000069. eCollection 2020.

(21) Neska-Matuszewska M, Bladowska J, Sąsiadek M, Zimny A. Differentiation of glioblastoma multiforme, metastases and primary central nervous system lymphomas using multiparametric perfusion and diffusion MR imaging of a tumor core and a peritumoral zone-Searching for a practical approach. PLoS One 2018 Jan 17;13(1):e0191341.

(22) Wesseling P, Capper D. WHO 2016 Classification of gliomas. Neuropathol Appl Neurobiol 2018;44(2):139-150.

(23) Wee P, Wang Z. Epidermal Growth Factor Receptor Cell Proliferation Signaling Pathways. Cancers (Basel) 2017 May 17;9(5):52. doi: 10.3390/cancers9050052.

(24) Verhaak RG, Hoadley KA, Purdom E, Wang V, Qi Y, Wilkerson MD, et al. Integrated genomic analysis identifies clinically relevant subtypes of glioblastoma characterized by abnormalities in PDGFRA, IDH1, EGFR, and NF1. Cancer Cell 2010 January 19;17(1):98-110.

(25) Sottoriva A, Spiteri I, Piccirillo SG, Touloumis A, Collins VP, Marioni JC, et al. Intratumor heterogeneity in human glioblastoma reflects cancer evolutionary dynamics. Proc Natl Acad Sci U S A 2013 March 05;110(10):4009-4014.

(26) Walker MD, Green SB, Byar DP, Alexander E, Batzdorf U, Brooks WH, et al. Randomized comparisons of radiotherapy and nitrosoureas for the treatment of malignant glioma after surgery. N Engl J Med 1980 December 04;303(23):1323-1329.

(27) Montemurro N, Fanelli GN, Scatena C, Ortenzi V, Pasqualetti F, Mazzanti CM, et al. Surgical outcome and molecular pattern characterization of recurrent glioblastoma multiforme: A single-center retrospective series. Clin Neurol Neurosurg 2021 August 01;207:106735.

(28) Kitange GJ, Carlson BL, Schroeder MA, Grogan PT, Lamont JD, Decker PA, et al. Induction of MGMT expression is associated with temozolomide resistance in glioblastoma xenografts. Neuro Oncol 2009 Jun;11(3):281-291.

(29) Stewart LA. Chemotherapy in adult high-grade glioma: a systematic review and meta-analysis of individual patient data from 12 randomised trials. Lancet 2002 Mar 23;359(9311):1011-1018.

(30) Wang HC, Lin YT, Lin WC, Ho RW, Lin YJ, Tsai NW, et al. Tumor Volume Changes During and After Temozolomide Treatment for Newly Diagnosed Higher-Grade Glioma (III and IV). World Neurosurg 2018 June 01;114:e766-e774.

(31) Onishi R, Sawaya R, Tsuji K, Arihara N, Ohki A, Ueda J, et al. Evaluation of Temozolomide Treatment for Glioblastoma Using Amide Proton Transfer Imaging and Diffusion MRI. Cancers (Basel) 2022 April 10;14(8):10.3390/cancers14081907.

(32) O'Reilly SM, Newlands ES, Glaser MG, Brampton M, Rice-Edwards JM, Illingworth RD, et al. Temozolomide: a new oral cytotoxic chemotherapeutic agent with promising activity against primary brain tumours. Eur J Cancer 1993;29A(7):940-942.

(33) Stupp R, Mason WP, van den Bent, Martin J., Weller M, Fisher B, Taphoorn MJB, et al. Radiotherapy plus Concomitant and Adjuvant Temozolomide for Glioblastoma. N Engl J Med 2005;352(10):987-996.

(34) O'Rourke DM, Nasrallah MP, Desai A, Melenhorst JJ, Mansfield K, Morrissette JJD, et al. A single dose of peripherally infused EGFRvIII-directed CAR T cells mediates antigen loss and induces adaptive resistance in patients with recurrent glioblastoma. Sci Transl Med 2017 Jul 19;9(399):eaaa0984. doi: 10.1126/scitranslmed.aaa0984.

(35) Bae SH, Park MJ, Lee MM, Kim TM, Lee SH, Cho SY, et al. Toxicity profile of temozolomide in the treatment of 300 malignant glioma patients in Korea. J Korean Med Sci 2014 July 01;29(7):980-984.

(36) Fang C, Wang K, Stephen ZR, Mu Q, Kievit FM, Chiu DT, et al. Temozolomide nanoparticles for targeted glioblastoma therapy. ACS Appl Mater Interfaces 2015 April 01;7(12):6674-6682.

(37) Vanderbeek AM, Rahman R, Fell G, Ventz S, Chen T, Redd R, et al. The clinical trials landscape for glioblastoma: is it adequate to develop new treatments? Neuro Oncol 2018 Jul 5;20(8):1034-1043.

(38) McComb RD, Burger PC. Pathologic analysis of primary brain tumors. Neurol Clin 1985 Nov;3(4):711-728.

(39) Ravanpay AC, Gust J, Johnson AJ, Rolczynski LS, Cecchini M, Chang CA, et al. EGFR806-CAR T cells selectively target a tumor-restricted EGFR epitope in glioblastoma. Oncotarget 2019 Dec 17;10(66):7080-7095.

(40) Busek P, Balaziova E, Matrasova I, Hilser M, Tomas R, Syrucek M, et al. Fibroblast activation protein alpha is expressed by transformed and stromal cells and is associated with mesenchymal features in glioblastoma. Tumor Biol 2016 Oct;37(10):13961-13971.

(41) Prager BC, Bhargava S, Mahadev V, Hubert CG, Rich JN. Glioblastoma Stem Cells: Driving Resilience through Chaos. Trends Cancer 2020 Mar;6(3):223-235.

(42) Vorbrodt AW, Dobrogowska DH. Molecular anatomy of intercellular junctions in brain endothelial and epithelial barriers: electron microscopist's view. Brain Res Rev 2003;42(3):221-242.

(43) Al-Azzawi S, Masheta D, Guildford A, Phillips G, Santin M. A Peptide-Based Nanocarrier for an Enhanced Delivery and Targeting of Flurbiprofen into the Brain for the Treatment of

Alzheimer's Disease: An In Vitro Study. Nanomaterials (Basel) 2020 Aug 13;10(8):1590. doi: 10.3390/nano10081590.

(44) Gabathuler R. Approaches to transport therapeutic drugs across the blood–brain barrier to treat brain diseases. Neurobiol Dis 2010;37(1):48-57.

(45) Vlieghe P, Khrestchatisky M. Peptide-based vectors for blood–brain barrier targeting and delivery of drugs to the central nervous system. Therapeutic Delivery 2010;1(4):489-494.

(46) Pardridge WM. The blood-brain barrier: Bottleneck in brain drug development. NeuroRX 2005;2(1):3-14.

(47) de Boer AG, Gaillard PJ. Drug Targeting to the Brain. Annu Rev Pharmacol Toxicol 2007;47(1):323-355.

(48) Stylli SS. Novel Treatment Strategies for Glioblastoma. Cancers (Basel) 2020 Oct 8;12(10):2883. doi: 10.3390/cancers12102883.

(49) Karpov OA, Fearnley GW, Smith GA, Kankanala J, McPherson MJ, Tomlinson DC, et al. Receptor tyrosine kinase structure and function in health and disease. AIMS Biophysics 2015;2(4):476-502.

(50) Hubbard SR, Miller WT. Receptor tyrosine kinases: mechanisms of activation and signaling. Curr Opin Cell Biol 2007 Apr;19(2):117-123.

(51) Schlessinger J. Cell signaling by receptor tyrosine kinases. Cell 2000 Oct 13;103(2):211-225.

(52) Ostman A, Böhmer FD. Regulation of receptor tyrosine kinase signaling by protein tyrosine phosphatases. Trends Cell Biol 2001 Jun;11(6):258-266.

(53) Pottier C, Fresnais M, Gilon M, Jerusalem G, Longuespee R, Sounni NE. Tyrosine Kinase Inhibitors in Cancer: Breakthrough and Challenges of Targeted Therapy. Cancers (Basel) 2020 March 20;12(3):10.3390/cancers12030731.

(54) Thomson RJ, Moshirfar M, Ronquillo Y. Tyrosine Kinase Inhibitors. StatPearls Treasure Island (FL); 2022.

(55) Kim G, Ko YT. Small molecule tyrosine kinase inhibitors in glioblastoma. Arch Pharm Res 2020;43(4):385-394.

(56) Roskoski R. Properties of FDA-approved small molecule protein kinase inhibitors: A 2021 update. Pharmacol Res 2021 March 01;165:105463.

(57) List of clinically approved kinase inhibitors | MRC PPU. Available at: https://www.ppu.mrc.ac.uk. Accessed Aug 25, 2022.

(58) Fujita KI, Ishida H, Kubota Y, Sasaki Y. Toxicities of Receptor Tyrosine Kinase Inhibitors in Cancer Pharmacotherapy: Management with Clinical Pharmacology. Curr Drug Metab 2017;18(3):186-198.

(59) Smith EL, Zamarin D, Lesokhin AM. Harnessing the immune system for cancer therapy. Curr Opin Oncol 2014;26(6).

(60) Luke JJ, Flaherty KT, Ribas A, Long GV. Targeted agents and immunotherapies: optimizing outcomes in melanoma. Nat Rev Clin Oncol 2017 Aug;14(8):463-482.

(61) Johnson LA, Scholler J, Ohkuri T, Kosaka A, Patel PR, McGettigan SE, et al. Rational development and characterization of humanized anti-EGFR variant III chimeric antigen receptor T cells for glioblastoma. Sci Transl Med 2015 February 18;7(275):275ra22.

(62) Feins S, Kong W, Williams EF, Milone MC, Fraietta JA. An introduction to chimeric antigen receptor (CAR) T-cell immunotherapy for human cancer. Am J Hematol 2019 May;94(S1):S3-S9.

(63) Newick K, O'Brien S, Moon E, Albelda SM. CAR T Cell Therapy for Solid Tumors. Annu Rev Med 2017 January 14;68:139-152.

(64) Maggs L, Cattaneo G, Dal AE, Moghaddam AS, Ferrone S. CAR T Cell-Based Immunotherapy for the Treatment of Glioblastoma. Front Neurosci 2021;0.

(65) Kim YK. RNA Therapy: Current Status and Future Potential. Chonnam Med J 2020 May 01;56(2):87-93.

(66) Bahreyni A, Luo H. Advances in Targeting Cancer-Associated Genes by Designed siRNA in Prostate Cancer. Cancers (Basel) 2020 Dec 3;12(12):3619. doi: 10.3390/cancers12123619.

(67) Zhu Y, Ma K, Ye Y, Tang J, Zhu J. Long non-coding RNA LINRIS is upregulated in non-small cell lung cancer and its silencing inhibits cell proliferation by suppressing microRNA-10a maturation. null 2022;13(2):4340-4346.

(68) Padfield E, Ellis HP, Kurian KM. Current Therapeutic Advances Targeting EGFR and EGFRvIII in Glioblastoma. Front Oncol 2015 Jan 29;5:5.

(69) Lee YT, Tan YJ, Oon CE. Molecular targeted therapy: Treating cancer with specificity. Eur J Pharmacol 2018 Sep 5;834:188-196.

(70) Cohen MH, Shen YL, Keegan P, Pazdur R. FDA drug approval summary: bevacizumab (Avastin) as treatment of recurrent glioblastoma multiforme. Oncologist 2009 Nov;14(11):1131-1138.

(71) Gilbert MR, Dignam JJ, Armstrong TS, Wefel JS, Blumenthal DT, Vogelbaum MA, et al. A randomized trial of bevacizumab for newly diagnosed glioblastoma. N Engl J Med 2014 Feb 20;370(8):699-708.

(72) Reth M. Matching cellular dimensions with molecular sizes. Nat Immunol 2013 August 01;14(8):765-767.

(73) Woitok M, Klose D, Di Fiore S, Richter W, Stein C, Gresch G, et al. Comparison of a mouse and a novel human scFv-SNAP-auristatin F drug conjugate with potent activity against EGFR-overexpressing human solid tumor cells. Onco Targets Ther 2017 Jul 6;10:3313-3327.

(74) Padayachee ER, Biteghe FAN, Malindi Z, Bauerschlag D, Barth S. Human Antibody Fusion Proteins/Antibody Drug Conjugates in Breast and Ovarian Cancer. Transfusion medicine and hemotherapy 2017 Sep;44(5):303-310.

(75) Perez HL, Cardarelli PM, Deshpande S, Gangwar S, Schroeder GM, Vite GD, et al. Antibody–drug conjugates: current status and future directions. Drug Discov Today 2014;19(7):869-881.

(76) Hussain AF, Kampmeier F, von Felbert V, Merk HF, Tur MK, Barth S. SNAP-tag technology mediates site specific conjugation of antibody fragments with a photosensitizer and improves target specific phototoxicity in tumor cells. Bioconjug Chem 2011 Dec 21;22(12):2487-2495.

(77) Rong L, Li N, Zhang Z. Emerging therapies for glioblastoma: current state and future directions. J Exp Clin Cancer Res 2022 Apr 15;41(1):142-7.

(78) Keppler A, Gendreizig S, Gronemeyer T, Pick H, Vogel H, Johnsson K. A general method for the covalent labeling of fusion proteins with small molecules in vivo. Nature biotechnology 2002;21(1):86-89.

(79) Padayachee ER, Adeola HA, Van Wyk JC, Nsole Biteghe FA, Chetty S, Khumalo NP, et al. Applications of SNAP-tag technology in skin cancer therapy. Health Sci Rep 2019 Jan 8;2(2):e103.

(80) Choudhary S, Barth S, Verma RS. SNAP-Tag Technology: A Promising Tool for Ex Vivo Immunophenotyping. Mol Diagn Ther 2017 Jun;21(3):315-326.

(81) Kampmeier F, Ribbert M, Nachreiner T, Dembski S, Beaufils F, Brecht A, et al. Site-Specific, Covalent Labeling of Recombinant Antibody Fragments via Fusion to an Engineered Version of 6-O-Alkylguanine DNA Alkyltransferase. Bioconjugate chemistry 2009 May 20,;20(5):1010-1015.

(82) Nelson AL. Antibody fragments: hope and hype. MAbs 2010 February 01;2(1):77-83.

(83) Li Z, Qiu Y, Lu W, Jiang Y, Wang J. Immunotherapeutic interventions of Triple Negative Breast Cancer. J Transl Med 2018 May 30;16(1):147-7.

(84) Kampmeier F, Ribbert M, Nachreiner T, Dembski S, Beaufils F, Brecht A, et al. Site-Specific, Covalent Labeling of Recombinant Antibody Fragments via Fusion to an Engineered Version of 6-O-Alkylguanine DNA Alkyltransferase. Bioconjugate chemistry 2009 May 20,;20(5):1010-1015.

(85) Gong H, Kovar JL, Baker B, Zhang A, Cheung L, Draney DR, et al. Near-Infrared Fluorescence Imaging of Mammalian Cells and Xenograft Tumors with SNAP-Tag. PLOS ONE 2012;7(3):e34003.

(86) Bauerschlag D, Meinhold-Heerlein I, Maass N, Bleilevens A, Bräutigam K, Al Rawashdeh W, et al. Detection and Specific Elimination of EGFR+ Ovarian Cancer Cells Using a Near Infrared Photoimmunotheranostic Approach. Pharm Res 2017 -04;34(4):696-703.

(87) von Felbert V, Bauerschlag D, Maass N, Bräutigam K, Meinhold-Heerlein I, Woitok M, et al. A specific photoimmunotheranostics agent to detect and eliminate skin cancer cells expressing EGFR. J Cancer Res Clin Oncol 2016 -05;142(5):1003-1011.

(88) Bosch PJ, Corrêa IR,Jr, Sonntag MH, Ibach J, Brunsveld L, Kanger JS, et al. Evaluation of fluorophores to label SNAP-tag fused proteins for multicolor single-molecule tracking microscopy in live cells. Biophys J 2014 Aug 19;107(4):803-814.

(89) Hsu PC, Jablons DM, Yang CT, You L. Epidermal Growth Factor Receptor (EGFR) Pathway, Yes-Associated Protein (YAP) and the Regulation of Programmed Death-Ligand 1 (PD-L1) in Non-Small Cell Lung Cancer (NSCLC). Int J Mol Sci 2019 Aug 5;20(15):3821. doi: 10.3390/ijms20153821.

(90) Dawson JP, Berger MB, Lin CC, Schlessinger J, Lemmon MA, Ferguson KM. Epidermal growth factor receptor dimerization and activation require ligand-induced conformational changes in the dimer interface. Mol Cell Biol 2005 Sep;25(17):7734-7742.

(91) Chakravarti A, Zhai G, Suzuki Y, Sarkesh S, Black PM, Muzikansky A, et al. The prognostic significance of phosphatidylinositol 3-kinase pathway activation in human gliomas. J Clin Oncol 2004 May 15;22(10):1926-1933.

(92) Sibilia M, Kroismayr R, Lichtenberger BM, Natarajan A, Hecking M, Holcmann M. The epidermal growth factor receptor: from development to tumorigenesis. Differentiation 2007 Nov;75(9):770-787.

(93) Aguirre A, Rubio ME, Gallo V. Notch and EGFR pathway interaction regulates neural stem cell number and self-renewal. Nature 2010 September 16;467(7313):323-327.

(94) Tebbutt N, Pedersen MW, Johns TG. Targeting the ERBB family in cancer: couples therapy. Nat Rev Cancer 2013 -09;13(9):663-673.

(95) Miller, MD, PhD,C.Ryan, Buchsbaum D, Reynolds P, Douglas J, Gillespie G, Mayo M, et al. Differential Susceptibility of Primary and Established Human Glioma Cells to Adenovirus Infection: Targeting via the Epidermal Growth Factor Receptor Achieves Fiber Receptor-independent Gene Transfer. Cancer Res 1999;58:5738-5748.

(96) Heimberger AB, Hlatky R, Suki D, Yang D, Weinberg J, Gilbert M, et al. Prognostic effect of epidermal growth factor receptor and EGFRvIII in glioblastoma multiforme patients. Clin Cancer Res 2005 Feb 15;11(4):1462-1466.

(97) Cancer Genome Atlas Research Network. Comprehensive genomic characterization defines human glioblastoma genes and core pathways. Nature 2008 October 23;455(7216):1061-1068.

(98) Karpel-Massler G, Schmidt U, Unterberg A, Halatsch ME. Therapeutic inhibition of the epidermal growth factor receptor in high-grade gliomas: where do we stand? Mol Cancer Res 2009 July 01;7(7):1000-1012.

(99) Yamaoka T, Ohba M, Ohmori T. Molecular-Targeted Therapies for Epidermal Growth Factor Receptor and Its Resistance Mechanisms. Int J Mol Sci 2017 Nov 15;18(11):2420. doi: 10.3390/ijms18112420.

(100) Argyriou AA, Kalofonos HP. Molecularly targeted therapies for malignant gliomas. Mol Med 2009;15(3-4):115-122.

(101) de Vries NA, Buckle T, Zhao J, Beijnen JH, Schellens JH, van Tellingen O. Restricted brain penetration of the tyrosine kinase inhibitor erlotinib due to the drug transporters P-gp and BCRP. Invest New Drugs 2012 April 01;30(2):443-449.

(102) Agarwal S, Sane R, Gallardo JL, Ohlfest JR, Elmquist WF. Distribution of gefitinib to the brain is limited by P-glycoprotein (ABCB1) and breast cancer resistance protein (ABCG2)-mediated active efflux. J Pharmacol Exp Ther 2010 Jul;334(1):147-155.

(103) Rosenthal M, Curry R, Reardon DA, Rasmussen E, Upreti VV, Damore MA, et al. Safety, tolerability, and pharmacokinetics of anti-EGFRvIII antibody-drug conjugate AMG 595 in patients with recurrent malignant glioma expressing EGFRvIII. Cancer Chemother Pharmacol 2019 Aug;84(2):327-336.

(104) Parrozzani R, Lombardi G, Midena E, Londei D, Padovan M, Marchione G, et al. Ocular Side Effects of EGFR-Inhibitor ABT-414 in Recurrent Glioblastoma: A Long-Term Safety Study. Front Oncol 2020 Oct 14;10:593461.

(105) van den Bent M, Gan HK, Lassman AB, Kumthekar P, Merrell R, Butowski N, et al. Efficacy of depatuxizumab mafodotin (ABT-414) monotherapy in patients with EGFR-amplified, recurrent glioblastoma: results from a multi-center, international study. Cancer Chemother Pharmacol 2017 Dec;80(6):1209-1217.

(106) Eshraghi H, Mantopoulos D, Suh LH, Zaldana F, Fine HF. Corneal Toxicity Induced by ABT-414 Therapy for Glioblastoma Multiforme: A Case Report. Case Rep Ophthalmol 2018;9(3):479-483.

(107) Goss GD, Vokes EE, Gordon MS, Gandhi L, Papadopoulos KP, Rasco DW, et al. Efficacy and safety results of depatuxizumab mafodotin (ABT-414) in patients with advanced solid tumors likely to overexpress epidermal growth factor receptor. Cancer 2018;124(10):2174-2183.

(108) Lo A, Li CP, Buza EL, Blomberg R, Govindaraju P, Avery D, et al. Fibroblast activation protein augments progression and metastasis of pancreatic ductal adenocarcinoma. JCI Insight 2017 Oct 5;2(19):e92232. doi: 10.1172/jci.insight.92232.

(109) Baghban R, Roshangar L, Jahanban-Esfahlan R, Seidi K, Ebrahimi-Kalan A, Jaymand M, et al. Tumor microenvironment complexity and therapeutic implications at a glance. Cell Commun Signal 2020 Apr 7;18(1):59-4.

(110) Zhou J, Wang X, Zhao Y, Chen C, Xu X, sun Q, et al. Cancer-Associated Fibroblasts Correlate with Tumor-Associated Macrophages Infiltration and Lymphatic Metastasis in Triple Negative Breast Cancer Patients. Journal of Cancer 2018;9(24):4635-4641.

(111) Erdogan B, Ao M, White LM, Means AL, Brewer BM, Yang L, et al. Cancer-associated fibroblasts promote directional cancer cell migration by aligning fibronectin. J Cell Biol 2017 Nov 6;216(11):3799-3816.

(112) Goldstein LA, Chen WT. Identification of an alternatively spliced seprase mRNA that encodes a novel intracellular isoform. J Biol Chem 2000 Jan 28;275(4):2554-2559.

(113) Koczorowska MM, Tholen S, Bucher F, Lutz L, Kizhakkedathu JN, De Wever O, et al. Fibroblast activation protein-α, a stromal cell surface protease, shapes key features of cancer associated fibroblasts through proteome and degradome alterations. Mol Oncol 2016 Jan;10(1):40-58.

(114) Park JE, Lenter MC, Zimmermann RN, Garin-Chesa P, Old LJ, Rettig WJ. Fibroblast activation protein, a dual specificity serine protease expressed in reactive human tumor stromal fibroblasts. J Biol Chem 1999 Dec 17;274(51):36505-36512.

(115) Hofheinz R-, al-Batran S-, Hartmann F, Hartung G, Jäger D, Renner C, et al. Stromal Antigen Targeting by a Humanised Monoclonal Antibody: An Early Phase II Trial of Sibrotuzumab in Patients with Metastatic Colorectal Cancer. Oncology Research and Treatment 2003 Feb;26(1):44-48.

(116) Krepela E, Vanickova Z, Hrabal P, Zubal M, Chmielova B, Balaziova E, et al. Regulation of Fibroblast Activation Protein by Transforming Growth Factor Beta-1 in Glioblastoma Microenvironment. Int J Mol Sci 2021 January 21;22(3):10.3390/ijms22031046.

(117) Santos AM, Jung J, Aziz N, Kissil JL, Puré E. Targeting fibroblast activation protein inhibits tumor stromagenesis and growth in mice. J Clin Invest 2009 Dec;119(12):3613-3625.

(118) Liu F, Qi L, Liu B, Liu J, Zhang H, Che D, et al. Fibroblast activation protein overexpression and clinical implications in solid tumors: a meta-analysis. PLoS One 2015 Mar 16;10(3):e0116683.

(119) Yang J, Shi Z, Liu R, Wu Y, Zhang X. Combined-therapeutic strategies synergistically potentiate glioblastoma multiforme treatment via nanotechnology. Theranostics 2020 Feb 10;10(7):3223-3239.

(120) Simkova A, Busek P, Sedo A, Konvalinka J. Molecular recognition of fibroblast activation protein for diagnostic and therapeutic applications. Biochim Biophys Acta Proteins Proteom 2020 July 01;1868(7):140409.

(121) Röhrich M, Loktev A, Wefers AK, Altmann A, Paech D, Adeberg S, et al. IDH-wildtype glioblastomas and grade III/IV IDH-mutant gliomas show elevated tracer uptake in fibroblast activation protein-specific PET/CT. Eur J Nucl Med Mol Imaging 2019 Nov;46(12):2569-2580.

(122) Tchou J, Zhang PJ, Bi Y, Satija C, Marjumdar R, Stephen TL, et al. Fibroblast activation protein expression by stromal cells and tumor-associated macrophages in human breast cancer. Human Pathology 2013;44(11):2549-2557.

(123) Fischer E, Chaitanya K, Wuest T, Wadle A, Scott AM, van den Broek M, et al. Radioimmunotherapy of fibroblast activation protein positive tumors by rapidly internalizing antibodies. Clin Cancer Res 2012 November 15;18(22):6208-6218.

(124) Cremasco V, Astarita JL, Grauel AL, Keerthivasan S, MacIsaac K, Woodruff MC, et al. FAP Delineates Heterogeneous and Functionally Divergent Stromal Cells in Immune-Excluded Breast Tumors. Cancer immunology research 2018;6(12):1472-1485.

(125) Lyons SK. Advances in imaging mouse tumour models in vivo. The Journal of Pathology 2005 Jan;205(2):194-205.

(126) Kessler C, Pardo A, Tur MK, Gattenlöhner S, Fischer R, Kolberg K, et al. Novel PSCA targeting scFv-fusion proteins for diagnosis and immunotherapy of prostate cancer. J Cancer Res Clin Oncol 2017 Oct;143(10):2025-2038.

(127) Kratochwil C, Flechsig P, Lindner T, Abderrahim L, Altmann A, Mier W, et al. (68)Ga-FAPI PET/CT: Tracer Uptake in 28 Different Kinds of Cancer. J Nucl Med 2019 Jun;60(6):801-805.

(128) Barbet J, Bardiès M, Bourgeois M, Chatal J, Chérel M, Davodeau F, et al. Radiolabeled Antibodies for Cancer Imaging and Therapy. In: Chames P, editor. Antibody Engineering: Methods and Protocols, Second Edition Totowa, NJ: Humana Press; 2012. p. 681-697.

(129) Dorst DN, Rijpkema M, Buitinga M, Walgreen B, Helsen MMA, Brennan E, et al. Targeting of fibroblast activation protein in rheumatoid arthritis patients: imaging and ex vivo photodynamic therapy. Rheumatology (Oxford) 2022 July 06;61(7):2999-3009.

(130) Tanswell P, Garin-Chesa P, Rettig WJ, Welt S, Divgi CR, Casper ES, et al. Population pharmacokinetics of antifibroblast activation protein monoclonal antibody F19 in cancer patients. Br J Clin Pharmacol 2001 Feb;51(2):177-180.

(131) Li L, Quang TS, Gracely EJ, Kim JH, Emrich JG, Yaeger TE, et al. A Phase II study of anti-epidermal growth factor receptor radioimmunotherapy in the treatment of glioblastoma multiforme. J Neurosurg 2010 Aug;113(2):192-198.

(132) Welt S, Divgi CR, Scott AM, Garin-Chesa P, Finn RD, Graham M, et al. Antibody targeting in metastatic colon cancer: a phase I study of monoclonal antibody F19 against a cell-surface protein of reactive tumor stromal fibroblasts. JCO 1994;12(6):1193-1203.

(133) Cole NB. Site-specific protein labeling with SNAP-tags. Current protocols in protein science 2013;73:30.1.1-30.1.16.

(134) Sun X, Zhang A, Baker B, Sun L, Howard A, Buswell J, et al. Development of SNAP-tag fluorogenic probes for wash-free fluorescence imaging. Chembiochem 2011 Sep 19;12(14):2217-2226.

(135) Amoury M, Bauerschlag D, Zeppernick F, von Felbert V, Berges N, Di Fiore S, et al. Photoimmunotheranostic agents for triple-negative breast cancer diagnosis and therapy that can be activated on demand. Oncotarget 2016 Aug 23;7(34):54925-54936.

(136) Makrides SC. Components of Vectors for Gene Transfer and Expression in Mammalian Cells. Protein Expr Purif 1999;17(2):183-202.

(137) Clark D, Pazdernik N. Cloning Genes for Analysis. In: Clark DP, Pazdernik NJ, editors. Molecular Biology (Second Edition) Boston: Academic Press; 2013. p. vii-viii.

(138) Martin, Natalia ,Van Alst, Andrew J., LeVeque, Rhiannon, DiRita VJ. Transformation of E. coli: Adapted Calcium Chloride Procedure | Microbiology | JoVE. Available at: https://www.jove.com/v/10515/transformation-e-coli-cells-using-an-adapted-calcium-chloride. Accessed Aug 29, 2022.

(139) Chauhan DT. Phenol Chloroform DNA Extraction: Basics, Preparation of Chemicals and Protocol. 2018; Available at: https://geneticeducation.co.in/phenol-chloroform-dna-extraction-basics-preparation-of-chemicals-and-protocol/. Accessed Sep 3, 2022.

(140) Brennan J. Components of Lysis Buffers. 2018; Available at: https://sciencing.com/components-lysis-buffers-8148370.html. Accessed Sep 3, 2022.

(141) Yagi N, Satonaka K, Horio M, Shimogaki H, Tokuda Y, Maeda S. The Role of DNase and EDTA on DNA Degradation in Formaldehyde Fixed Tissues. null 1996;71(3):123-129.

(142) Tan A. What Is the Function of a Tris Buffer in DNA Extraction? 2018; Available at: https://sciencing.com/function-tris-buffer-dna-extraction-6370973.html. Accessed 3rd September, 2022.

(143) Oswald Nick. Alkaline Lysis: How it Works in 5 Simple Steps. 2021; Available at: https://bitesizebio.com/180/the-basics-how-alkaline-lysis-works/. Accessed Sep 4, 2022.

(144) Engler, M. J., Richardson, C. C. DNA ligases, in The Enzymes XV Part B In P. D. Boyer (Ed.). New York: Academic Press; 1982. p. 3-29.

(145) Wong JW, Albright RL, Wang NL. Immobilized Metal Ion Affinity Chromatography (IMAC) Chemistry and Bioseparation Applications. Sep Purif Methods 1991;20(1):49-106.

(146) Manns JM. SDS-Polyacrylamide Gel Electrophoresis (SDS-PAGE) of Proteins. Current Protocols in Microbiology 2011;22(1):A.3M.1-A.3M.13.

(147) Alonso Villela SM, Kraïem H, Bouhaouala-Zahar B, Bideaux C, Aceves Lara CA, Fillaudeau L. A protocol for recombinant protein quantification by densitometry. Microbiologyopen 2020 Jun;9(6):1175-1182.

(148) New England Biolabs. SNAP-Surface® Alexa Fluor® 488. 2022; Available at: https://international.neb.com/products/s9129-snap-surface-alexa-fluor-488#Product%20Information_Product%20Notes. Accessed 4th September, 2022.

(149) Özlem Sultan Aslantürk ED1 - Marcelo L Larramendy ED2, - Sonia Soloneski. In Vitro Cytotoxicity and Cell Viability Assays: Principles, Advantages, and Disadvantages. Genotoxicity Rijeka: IntechOpen; 2017. p. Ch. 1.

(150) Biteghe, Fleury. Comparison of the therapeutic efficacy of SNAP-tag fusion protein and the synergistic actions of chemotherapy and photodynamic therapy in killing resistant melanomaUniversity of Cape Town; 2018.

(151) Qiao Q, Liu W, Chen J, Zhou W, Yin W, Miao L, et al. A naphthalimide-derived fluorogenic probe for SNAP-tag with a fast record labeling rate. Dyes and Pigments 2017;147:327-333.

(152) Tamimi AF, Juweid M. Epidemiology and Outcome of Glioblastoma. In: De Vleeschouwer S, editor. Glioblastoma Brisbane (AU); 2017.

(153) Hamdi Y, Abdeljaoued-Tej I, Zatchi AA, Abdelhak S, Boubaker S, Brown JS, et al. Cancer in Africa: The Untold Story. Frontiers in Oncology 2021;11.

(154) Keppler A, Gendreizig S, Gronemeyer T, Pick H, Vogel H, Johnsson K. A general method for the covalent labeling of fusion proteins with small molecules in vivo. Nat Biotechnol 2003 Jan;21(1):86-89.

(155) McLendon R, Friedman A, Bigner D, Van Meir EG, Brat DJ, Mastrogianakis G,M., et al. Comprehensive genomic characterization defines human glioblastoma genes and core pathways. Nature 2008;455(7216):1061-1068.

(156) Tang X, Zuo C, Fang P, Liu G, Qiu Y, Huang Y, et al. Targeting Glioblastoma Stem Cells: A Review on Biomarkers, Signal Pathways and Targeted Therapy. Front Oncol 2021 -7-08;11.

(157) Ruiz-Garcia H, Alvarado-Estrada K, Schiapparelli P, Quinones-Hinojosa A, Trifiletti DM. Engineering Three-Dimensional Tumor Models to Study Glioma Cancer Stem Cells and Tumor Microenvironment. Front Cell Neurosci 2020;0.

(158) Ehrmann J, Kolář Z, Mokrý J. Nestin as a diagnostic and prognostic marker: immunohistochemical analysis of its expression in different tumours. J Clin Pathol 2005;58(2):222-223.

(159) Zhang J, Cai H, Sun L, Zhan P, Chen M, Zhang F, et al. LGR5, a novel functional glioma stem cell marker, promotes EMT by activating the Wnt/β-catenin pathway and predicts poor survival of glioma patients. Journal of Experimental & Clinical Cancer Research 2018;37(1):225.

(160) Cela I, Di Matteo A, Federici L. Nucleophosmin in Its Interaction with Ligands. Int J Mol Sci 2020 -7-10;21(14).

(161) Rusu P, Shao C, Neuerburg A, Acikgöz AA, Wu Y, Zou P, et al. GPD1 Specifically Marks Dormant Glioma Stem Cells with a Distinct Metabolic Profile. Cell Stem Cell 2019 -08-01;25(2):241-257.e8.

(162) Barnes LM, Dickson AJ. Mammalian cell factories for efficient and stable protein expression. Curr Opin Biotechnol 2006 Aug;17(4):381-386.

(163) Jäger V, Büssow K, Wagner A, Weber S, Hust M, Frenzel A, et al. High level transient production of recombinant antibodies and antibody fusion proteins in HEK293 cells. BMC Biotechnology 2013;13(1):52.

(164) Saraswat M, Musante L, Ravidá A, Shortt B, Byrne B, Holthofer H. Preparative purification of recombinant proteins: current status and future trends. BioMed research international 2013;2013:312709.

(165) Vemula S, Thunuguntla R, Dedaniya A, Kokkiligadda S, Palle C, Ronda SR. Improved Production and Characterization of Recombinant Human Granulocyte Colony Stimulating Factor from E. coli under Optimized Downstream Processes. Protein Expr Purif 2015;108.

(166) Ryan BJ, Henehan GT. Overview of approaches to preventing and avoiding proteolysis during expression and purification of proteins. Curr Protoc Protein Sci 2013 Feb;Chapter 5:Unit5.25.

(167) Wang W, Ignatius AA, Thakkar SV. Impact of residual impurities and contaminants on protein stability. J Pharm Sci 2014 May 01;103(5):1315-1330.

(168) Liu C, Dalby B, Chen W, Kilzer JM, Chiou HC. Transient transfection factors for high-level recombinant protein production in suspension cultured mammalian cells. Mol Biotechnol 2008 Jun;39(2):141-153.

(169) Bird RE, Hardman KD, Jacobson JW, Johnson S, Kaufman BM, Shwu-Maan Lee, et al. Single-Chain Antigen-Binding Proteins. Science 1988;242(4877):423-426.

(170) Suzuki, Y. (Tokyo Univ. (Japan)), Ito S, Otsuka K, Iwasawa E, Nakajima M, Yamaguchi I. Preparation of functional single-chain antibodies against bioactive gibberellins by utilizing randomly mutagenized phage-display libraries. Bioscience, biotechnology, and biochemistry 2005 Mar;69(3):610-619.

(171) Wang L, Degheidy H, Abbasi F, Mostowski H, Marti G, Bauer S, et al. Quantitative Flow Cytometry Measurements in Antibodies Bound per Cell Based on a CD4 Reference. Current Protocols in Cytometry 2016 Jan;75(1):1.29.1-1.29.14.

(172) Liu Y, Sharp JS, Do DH, Kahn RA, Schwalbe H, Buhr F, et al. Mistakes in translation: Reflections on mechanism. PLoS One 2017 Jun 29;12(6):e0180566.

(173) Coon JJ, Syka JEP, Shabanowitz J, Hunt DF. Tandem Mass Spectrometry for Peptide and Protein Sequence Analysis. BioTechniques 2005;38(4):519-523.

(174) Dean AQ, Luo S, Twomey JD, Zhang B. Targeting cancer with antibody-drug conjugates: Promises and challenges. null 2021;13(1):1951427.

(175) Tsuchikama K, An Z. Antibody-drug conjugates: recent advances in conjugation and linker chemistries. Protein Cell 2018 Jan;9(1):33-46.

(176) Hughes B. Antibody–drug conjugates for cancer: poised to deliver? Nature Reviews Drug Discovery 2010;9(9):665-667.

(177) Chalouni C, Doll S. Fate of Antibody-Drug Conjugates in Cancer Cells. Journal of Experimental & Clinical Cancer Research 2018;37(1):20.

(178) Shen B, Xu K, Liu L, Raab H, Bhakta S, Kenrick M, et al. Conjugation site modulates the in vivo stability and therapeutic activity of antibody-drug conjugates. Nat Biotechnol 2012;30(2):184-189.

(179) Doronina SO, Mendelsohn BA, Bovee TD, Cerveny CG, Alley SC, Meyer DL, et al. Enhanced activity of monomethylauristatin F through monoclonal antibody delivery: effects of linker technology on efficacy and toxicity. Bioconjug Chem 2006;17(1):114-124.

(180) Pettit GR. The dolastatins. Fortschr Chem Org Naturst 1997;70:1-79.

(181) Nilsson R, Mårtensson L, Eriksson SE, Sjögren H, Tennvall J. Toxicity-reducing potential of extracorporeal affinity adsorption treatment in combination with the auristatin-conjugated monoclonal antibody BR96 in a syngeneic rat tumor model. Cancer 2010;116:1033-1042.

(182) Tzogani K, Penttilä K, Lähteenvuo J, Lapveteläinen T, Lopez Anglada L, Prieto C, et al. EMA Review of Belantamab Mafodotin (Blenrep) for the Treatment of Adult Patients with Relapsed/Refractory Multiple Myeloma. Oncologist 2021;26(1):70-76.

(183) King HD, Dubowchik GM, Mastalerz H, Willner D, Hofstead SJ, Firestone RA, et al. Monoclonal antibody conjugates of doxorubicin prepared with branched peptide linkers: inhibition of aggregation by methoxytriethyleneglycol chains. J Med Chem 2002 Sep 12;45(19):4336-4343.

(184) Zhao RY, Wilhelm SD, Audette C, Jones G, Leece BA, Lazar AC, et al. Synthesis and evaluation of hydrophilic linkers for antibody-maytansinoid conjugates. J Med Chem 2011 May 26;54(10):3606-3623.

(185) Hermanson GT. Chapter 20 - Antibody Modification and Conjugation. In: Hermanson GT, editor. Bioconjugate Techniques (Third Edition) Boston: Academic Press; 2013. p. 867-920.

(186) Woitok M, Klose D, Niesen J, Richter W, Abbas M, Stein C, et al. The efficient elimination of solid tumor cells by EGFR-specific and HER2-specific scFv-SNAP fusion proteins conjugated to benzylguanine-modified auristatin F. Cancer Lett 2016;381(2):323-330.

(187) Peters C, Brown S. Antibody–drug conjugates as novel anti-cancer chemotherapeutics. Biosci Rep 2015;35(4):e00225.

(188) Koh W, Sales LR. Principles of Radiation Therapy. 2019 July 7,.

(189) Bailly C, Vidal A, Bonnemaire C, Kraeber-Bodéré F, Chérel M, Pallardy A, et al. Potential for Nuclear Medicine Therapy for Glioblastoma Treatment. Frontiers in Pharmacology 2019;10.

(190) Chaddad A, Kucharczyk MJ, Daniel P, Sabri S, Jean-Claude BJ, Niazi T, et al. Radiomics in Glioblastoma: Current Status and Challenges Facing Clinical Implementation. Front Oncol 2019 -5-21;9.

(191) Bolcaen J, Kleynhans J, Nair S, Verhoeven J, Goethals I, Sathekge M, et al. A perspective on the radiopharmaceutical requirements for imaging and therapy of glioblastoma. Theranostics 2021 -7-6;11(16):7911-7947.

(192) Zaccagna F, Grist JT, Quartuccio N, Riemer F, Fraioli F, Caracò C, et al. Imaging and treatment of brain tumors through molecular targeting: Recent clinical advances. Eur J Radiol 2021;142.

(193) Prados MD, Schold SC, Jr., Fine HA, Jaeckle K, Hochberg F, Mechtler L, et al. A randomized, double-blind, placebo-controlled, phase 2 study of RMP-7 in combination with carboplatin administered intravenously for the treatment of recurrent malignant glioma. Neuro Oncol 2003;5(2):96-103.

(194) Sonenberg M, Rall JE. The Use of Radioactive Iodine in Cancer of the Thyroid. Med Clin North Am 1956;40(3):821-836.

(195) Suh M, Lee DS. Brain Theranostics and Radiotheranostics: Exosomes and Graphenes In Vivo as Novel Brain Theranostics. Nucl Med Mol Imaging 2018 Dec;52(6):407-419.

(196) Nemati R, Rekabpour SJ, Jokar N, Ahmadzadehfar H, Shooli H, Jafari E, et al. RADI-15. Radiotheranostic Approach in Brain Tumor. Neuro Oncol Adv 2021;3(Supplement_3):iii21.

(197) Shooli H, Nemati R, Ahmadzadehfar H, Aboian M, Jafari E, Jokar N, et al. Theranostics in Brain Tumors. PET Clinics 2021;16(3):397-418.

(198) Stewart PA. Endothelial vesicles in the blood–brain barrier: are they related to permeability? Cell Mol Neurobiol 2000;20(2):149-163.

(199) Pulgar VM. Transcytosis to Cross the Blood Brain Barrier, New Advancements and Challenges. Front Neurosci 2019;0.

(200) Qian ZM, Li H, Sun H, Ho K. Targeted drug delivery via the transferrin receptor-mediated endocytosis pathway. Pharmacol Rev 2002;54(4):561-587.

(201) Johnsen KB, Bak M, Kempen PJ, Melander F, Burkhart A, Thomsen MS, et al. Antibody affinity and valency impact brain uptake of transferrin receptor-targeted gold nanoparticles. Theranostics 2018;8(12):3416-3436.

(202) Niewoehner J, Bohrmann B, Collin L, Urich E, Sade H, Maier P, et al. Increased brain penetration and potency of a therapeutic antibody using a monovalent molecular shuttle. Neuron 2014 -01-08;81(1):49-60.

(203) Grace Mayuni. Optimizing the expression of anti-CSPG4 (scFv)-SNAP fusion protein in mammalian cells through hyperosmotic stress and compatible solutes buffering University of Cape Town; 2019.

Appendix- Materials/ Buffer Recipes and Reaction Tables

Phenol/chloroform extraction

Materials needed:

5mL overnight bacterial culture

1.5mL microfuge tubes

7X Lysis Buffer

Neutralization buffer

Collection tubes and Zymo-Spin IIN column

Endo-wash buffer

Materials needed:

50mL overnight bacterial culture

Luria-Bertani (LB) broth

DH5α Calcium competent cells (*E. coli)*

Ice

Incubator with shaker

Super Optimal Broth with Catabolite repression (SOC) at RT

Heating block

Plasmid DNA

Microfuge

Nuclease free dH_2O

LB agar plates

Glycerol (50%)

1.5mL microfuge tubes

Solution I, II and III

RNase A

Phenol/Chloroform

Chroloform: isoamyl alcohol

15mL culture tubes

100% ethanol

3M sodium acetate (NaOAc)

50mL centrifuge tubes

Isopropanol

Ampicillin

70% ethanol

Pipette

Pipette tips

SpeedVac vacuum

Spectrophotometer (Denovix NanoDrop™)

Table A1. Buffer recipes and composition for Phenol Chloroform DNA extraction

Buffer/Reagent	Description	Composition
LB Broth (1L, pH 7)	Bacterial culture media	
LB Agar (20mL in 100 mm x 15 mm plate)		35g LB agar powder dH_2O- top up to 1L
70% Ethanol (100mL)		
Ampicillin (100mg/mL)	Antibiotic - selection for plasmids containing ampicillin resistance gene (AMP^R)	1g ampicillin 10mL dH_2O
50% Glycerol(100mL)	Freezing down of bacterial culture	50mL 100% Glycerol 50mL dH_2O
Solution I (store at 4ºC)	Resuspension buffer	10ml 0.5M Glucose [50 mM] 2.5ml 1M Tris-HCl (pH 8) [25 mM] 2ml 0.5M EDTA [10 mM] 85.5ml sterile nuclease free dH_2O Store at 4°C
Solution II	Denaturation buffer	20ml 10% SDS [1%] 4ml 10M NaOH [1.2M] 176 ml sterile nuclease free dH_2O Autoclave for 10 minutes and store at room temperature
Solution III (store at 4ºC)	Renaturation buffer (Aqueous potassium acetate)	60 mL 5M Potassium Acetate 11.5 mL acetic acid 28.5 mL of dH_2O **Do not autoclave**
RNase A	RNA digestion	
Phenol/chloroform solution (store at 4ºC)		
Chloroform: Isoamyl alcohol (store at RT)		

Table A2. Restriction digestion reaction components with *Not*I and *Sfi*I

Component	50 µl reaction
DNA	2)µg
CutSmart Buffer	5µl
***Not*I-HF (to be added after 3hr *Sfi*I incubation)**	1µl
***Sfi*I**	1µl
Nuclease-free water (make up to 50µl)	

Table A3. Buffer recipes and composition for Agarose Gel Electrophoresis

Reagent/Buffer	Composition
10x TAE buffer(1L)	48.5g Tris Base 20mL 0.5M EDTA (pH8.00) 11.4mL glacial acetic acid H_2O - top up to 1L
1x TAE buffer(1L)	100mL 10x TAE buffer 900mL dH_2O
Agarose gel	1.2g agarose 100mL 1x TAE buffer 10µL SYBR™safe (after cooling)

Agarose Gel Electrophoresis

Materials needed:

Agarose powder

1x TAE buffer

SYBR™ safe

Microwave

250mL beaker

Weighboat, scale, spatula

dH_20

BioRad buffer tank

Gel casting tray

Gel comb

6X purple loading dye

Pipette

Pipette tips

100bp+and/or 1000bp DNA ladder

UV gel documentation system

DNA Ligation

Materials needed:

Insert DNA

Backbone DNA

Ice

Zyppy Miniprep purification kit

T4 DNA Ligase

T4 DNA Ligase Buffer

Nuclease free dH_20

Heating block

SOC at RT

LB broth

1L flask

15mL culture tubes

1.5mL microfuge tubes

LB agar plates

Ampicillin (100mg/mL)

Pipette

Pipette tips

Incubator with shaker

Table A4. Reagents for T4DNA Ligation

Reagent	**1:0(vector only control)**	**1:1**	**1:3**	**1:5**
T4 Ligase Buffer	2µL	2µL	2µL	2µL
Vector(50ng)	3µL	3µL	3µL	3µL
Insert	0	0.5µL(5.5ng)	1.6µL(16.4ng)	2.6µL(27.3ng)
T4 DNA Ligase	1	1	1	1
H_20(make up to 20µL)	14µL	13.5µL	12.4µL	11.4µL

Protein purification

Materials needed:

ÄKTA Avant

Cell culture supernatant

Incubation buffer

Equilibration buffer

Elution buffer

96-deep well plate

PVDF membrane

5mL HisTrap™ excel

10kDa Amicon® Ultra 15ml Centrifugal Filter

Table A5. Buffer compositions for protein purification of SNAP fusion proteins

Buffer	Composition
4X Incubation Buffer (pH8)	200mM NaH_2PO_4 1.2M NaCl 40mM Imidazole Sterile dH_2O (fill up to desired final volume)
Equilibration buffer (pH8)	50mM NaH_2PO_4 300mM NaCl Sterile dH_2O (fill up to desired final volume)
Elution Buffer(pH8)	50mM NaH_2PO_4 300M NaCl 500mM Imidazole Sterile dH_2O (fill up to desired final volume)
1X PBS (pH7.4)	8.1mM Na_2HPO_4 8.1mM KH_2PO_4 137mM NaCl 2.7mM KCL Sterile dH_2O (fill up to desired final volume)

SDS-PAGE & WB

Materials needed:

Mini-PROTEAN® system (Bio-Rad)

Micropipettes and tips

Microfuge tubes

Acrylamide

10% SDS solution

10%APS solution

TEMED

TRIS-HCl buffer (0.5M, pH 6.8)

TRIS-HCl buffer (1.5M, pH 8.8)

dH_2O

1X Running Buffer

4X Laemmli sample loading dye (1:9 ratio, 2-mercaptoethanol: Laemmli sample buffer)

Protein Ladder

Acqua Stain Protein Gel Stain (Vacutec, South Africa)

Tween® 20

1X Transfer Buffer

1X Tris-buffered saline, 0.1% (w/v) Tween®20(TBST)

Table A6. Buffer recipes and composition for SDS and Western Blot Analysis

Buffer	Composition
10% Ammonium per sulphate (APS)	Ammonium per sulphate powder (5g) dH_2O (50mL)
10% SDS	SDS powder(10g) dH_2O(100mL)
10X Running Buffer	Tris Base (30.3g) SDS (10g) Glycine (144g) dH_2O (fill up to 1L)
1X Running Buffer	10X Running Buffer: dH_2O (1:9)
10 X Transfer Buffer	Tris Base (30g) Glycine(144g)
1X Transfer Buffer	10X Transfer Buffer: 100% Methanol: dH_2O (1:2:7)
10X Tris-buffered saline (TBS)	Tris Base(200mM) NaCl (1.5M) dH_2O
1X TBS-Tween(TBST)	TBS: dH_2O (1:9) 1mL Tween®20

Conjugation

Materials needed:

Dimethyl sulfoxide (DMSO)

1X PBS

BG- Alexa 488

BG- Alexa 647

Heating block

Dithiothreitol (DTT)

SNAP fusion protein

SDS-PAGE apparatus

Table A7. Conjugation reaction composition

Component	**[Stock Conc]**	**[Final]**	**4:1**	**2:1**	**1:1**	**1:2**
PBS	1x					
Dithiothreitol DTT	10mM	1mM				
BG-Alexa 488/BG-Alexa 647	25µM	*determine*	1.25µM	2.5µM	5µM	10µM
SNAP fusion protein	50µM	5µM				
TOTAL VOLUME (+ loading dye)		20µL				

Table A8. Dual conjugation reaction composition

Component	**[Stock Conc]**	**[Final]**	**4:1:2**	**2:1:1**	**2:2:1**	**2:4:1**
PBS	1x					
Dithiothreitol DTT	10mM	1mM				
BG-Alexa 488	25µM	*determine*	1.25µM	2.5µM	5µM	10µM
BG-Alexa 647	25µM	2.5µM	2.5µM	2.5µM	2.5µM	2.5µM
SNAP fusion protein	50µM	5µM				
TOTAL VOLUME (+ loading dye)		20µL				

Table A9. Conjugation reaction with BG-AURIF

Component	[Stock Conc]	[Final]
PBS	1x	
Dithiothreitol DTT	10mM	1mM
BG-AURIF	5mM	20µM
SNAP fusion protein	50µM	10µM
TOTAL VOLUME		1000µL

Table A10. BG-functional napthalamide based fluorogenic probes

BG-functional probe	Molar mass(g.mol^{-1})	Excitation maximum (nm)	Emission maximum (nm)
BGAN-Amino	465.47	440	530
BGAN-Azido	491.47	440	530
BGAN-X-R	665.75	440	530
α-BGAN-PVP_{10}	1700	440	530
α-BGAN-PVP_{20}	2800	440	530
α-BG-ω-Alexa488-PVP_{35}	5000	496	520

Live cell imaging

Table A11. SNAP labelling reaction (αEGFR(scFv)-SNAP : BG-Alexa 647 = 1 : 1)

Component	[initial]	[final]	volume(µL)
PBS(fill up to 200µL)	1x		172
Dithiothreitol (DTT)	50mM	1mM	4
BG-Alexa 647/488	250µM	5µM	4
SNAP fusion protein	50µM	5µM	20
Final			200